The Hong Kong Polytechnic University

Department of Mechanical Engineering

香港理工大學 機械工程學系

Analysis and Control of Computer Cooling Fan Noise

By

Kam Wong

Ph.D.

The Hong Kong Polytechnic University

September 2005

DECLARATION OF ORIGINALITY

I hereby declare that this thesis is my own work and that, to the best of my knowledge and belief, it reproduces no material previously published or written, nor material that has been accepted for the award of any other degree or diploma, except where due acknowledgement has been made in the text.

_____ (Signed)

Kam WONG

Table of contents

Acknowledgements

I would like to express my sincere gratitude towards my supervisor, Dr. Lixi Huang, for his professional guidance and patience throughout the research project. I am also grateful to my co-supervisor Professor Li Cheng for his technical support, and to Dr. Yu Zhou for his encouragement. The project will not be successful without their support and enlightenment.

I would like to thank my family and my friends for their love and care during my study. I would also like to thank all the staff and technicians in the laboratories and offices for their support.

Abstract

The problem of noise radiation from large turbomachines in aerospace applications has received a lot of attention, but the same is not true for small ventilation fans. The noise from the small fans shares many features with that of the large turbomachines, but there are important differences. For example, Gutin noise can be ignored for the small fan, but it may be significant for the turbo-fan of aircraft engine. The other reason for the difference is that technical measures allowed for large fans may not be feasible for small fans due to the cost. The main objective of this study is to find feasible techniques to reduce small fan noise through a thorough understanding of the noise mechanisms which are previously lacking.

This thesis is divided into three parts: the study of the source mechanisms and their separation, passive noise control, and active noise control. The mechanisms of noise radiated by a typical computer cooling fan is investigated both theoretically and experimentally focusing on the dominant rotor-stator interaction. The unsteady force generated by the aerodynamic interaction between the rotor blades and struts is phase locked with the blade rotation and radiates tonal noise. Experimentally, synchronous averaging with the rotation signal extracts the tones made by the deterministic part of the rotor-strut interaction mechanism. This averaged signal is called the rotary noise. The difference between the overall noise and rotary noise is defined as random noise which is broadband in the spectrum. The deterministic tonal peaks are certainly more annoying than the broadband, so the suppression of the tones is the focus of this study. Based on the theoretical study of point force formulation, methods are devised to separate the noise radiated by the two components of drag and thrust forces on blades

and struts. The source separation is also extended to the leading and higher order modes of the spinning pressure pattern. By using the original fan rotor and installing it in various casings, the noise sources of the original fan are decomposed into elementary sources through directivity measurements. Details of the acoustical directivity for the original fan and its various modifications are interpreted. For the sample fan, two common features account for most of the tonal noise radiated. The two features are the inlet flow distortion caused by the square fan casing, and the large strut carrying the electric wires for the motor. When the inlet bellmouth is installed and the large strut is trimmed down to size, a significant reduction of 12 dB in tonal sound power is achieved. These structural corrections constitute the passive noise control. However, the end product still features the leading mode drag noise. Further reduction of this noise is left to the active noise control.

The feasibility of the active noise control technique is demonstrated for the cancellation of both thrust and drag noise radiated at their leading modes. An open loop, feed-forward system is used to maximize the simplicity of the rig in order to deliver an appropriate technology for a small ventilation fan. The leading mode configurations are constructed by re-designing the struts. The control rig consists of three components, a miniature electret microphone used as a rotation sensor, ordinary loudspeakers, and a bandpass filter with adjustable amplitude and phase delay. The miniature electret microphone measures the unsteady aerodynamic pressure on the fan casing, and it eliminates the possible acoustic feedback caused by the secondary loudspeaker. Its smooth and rich blade passing frequency content also allows the use of low-order filter. For the thrust noise rig, in which the number of rotor blades is equal to the number of struts, the sound power of the BPF tone is reduced by 14.8 dB,

while the second BPF is reduced by 9.8 dB. For the drag noise rig, which is based on the improved version of the original fan, a 12.7 dB reduction in BPF tone is achieved. Note that the noise reduction for the second rig is on top of the passive noise control which has already reduced the original fan noise by 12 dB. For both rigs, the residual noise is analysed and it is found that the variation of the fan noise radiation from one rotational cycle to the next is the main reason that causes the mismatch between the antisound constructed from the signal input from the past cycle and the actual sound radiated at the present cycle. This variation is believed to be present even though the rotational speed of the fan is held absolutely constant, and the mechanism behind this could be rooted in the turbulent flow through the fan. A single loudspeaker is used for the thrust noise radiation and a mimimum of two loudspeakers are needed for the drag noise control. It is postulated that, for a general case where both drag and thrust noises are present at the leading modes, perhaps at different frequencies for each component, three loudspeakers would be needed to construct the antisound to achieve the global noise control for a small axial flow fan.

Nomenclature

Capital letters

A	Cross section area of the flow passage
B	Number of the rotor blades
C_L	Constant of a lift model for the interaction between a strut with a blade
D	Drag component of the unsteady force on the blades
E	Radial force component of the unsteady force on the blades
F	Unsteady point force in arbitrary motion
F_r	Unsteady force on a blade projected pointing to the receiver
I	Sound intensity
J	Jocobian transformation
$J_\nu(z)$	Bessel function
L	Unsteady lift generated on a blade
M	Mach number, for a mean flow, $M=U/c_0$, or for a source rotation $M = \omega R / c_0$
M_r	Projection of the source movement Mach number towards the observer
P	Aerodynamic power of the fan
Q	Volume flow rate of the fan
R	Radius of the sample fan or a point source
R_{hub}	Hub radius
R_{tip}	Tip radius
S	Number of the struts
$S1$	A configuration of a fan with a single strut
$S13$	A configuration of a fan with one large strut and three small struts
$S4$	A configuration of a fan with four equal struts

$S5$ A configuration of a fan with five equal struts

$S7$ A configuration of a fan with seven equal struts

T Thrust component of the unsteady force on a blade

T_{ij} Lighthill's stress tensor

U Mean flow velocity

V Volume enclosing the acoustic sources

W Sound power

Lowercase letters

c_0 Speed of sound in air

c Complex amplitude of the far field sound

d Strut diameter

i Index of the measuring angular position

j Index of the blade number

k Order of the harmonics of the interaction force with S struts

k_0 Wavenumber, $k_0 = \omega_0 / c_0$

l Characteristic length of the source

m Order of the harmonics of the blade passing frequency (BPF)

n Frequency index of the observed sound, $n=mB$

nW Nano Watt, or 10^{-9} Watt

p Sound pressure

p' Unsteady pressure fluctuation on a blade

r Distance between a source to the receiver

r_0 Distance between the fan center to the receiver

s Index of the strut number

t Sound reception time, $t = \tau + r / c_0$

u Acoustic particle velocity

u^*_r Conjugate of the the acoustic particle velocity in r direction

v Rotational speed of a point source, or blade movement velocity

x, y, z Cartesian coordinates for the fan standing vertically up with origin at the fan, cf. Fig. 2.3(a).

$\vec{x}$ Location vector for the observer

$\vec{y}$ Location vector for the source

z Argument of the Bessel function, $z=nM\sin\alpha$

Greek symbols

Θ Initial angular position of a point source relative to the observer

α Latitudinal angle measured from the $+x$ axis

β Pitching angle of a rotor blade section (airfoil)

γ Latitudinal angle measured from the vertical axis $+z$

ϕ Longitudinal angle measured from the $+x$ axis on the horizontal cross section

λ Wavelength, $\lambda = c_0 / f$, or

the frequency index of the unsteady force, $\lambda = kS$

ν Index of the pressure spinning mode, and order of the Bessle function,

$v = mB - kS$

θ Angular position of a rotating blade, $\theta = \omega\tau$

ρ Density of fluid, $\rho = \rho_0 + \rho'$, where ρ' is the perturbation density

ρ_0 Mean density of fluid (air)

τ Radiation time (retarded time), $\tau = t - r / c_0$

ω Angular frequency of the fan rotation

ω_0 Angular frequency of sound

Subscripts

*D*0 Radiation from the drag component at the mode of ν=0

*D*1 Radiation from the drag component at the mode of ν=1

L Large strut

R Rotor

*R*0 Initial location of rotor blade relative to the observer

*S*0 Initial location of strut relative to the observer

*T*0 Radiation from the thrust component at the mode of ν=0 (coincident mode)

*T*1 Radiation from the thrust component at the mode of ν=0

i index of the measurement position

j blade index

n frequency index of the received sound

r Direction of projection to the observer, or the radial component of the observer sphere

ret Evaluation at the retard time, $\tau=t-r/c_0$

rms Root mean square value

ref Reference value, $W_{ref}=10^{-12}$ watt and $p_{ref}=20$ μPa

y Projection in *y* direction

z Projection in *z* direction

α	Projection in the angular direction of α
γ	Projection in the angular direction of γ
λ	frequency index of the source
1-4	Four quadrants of the measurement horizontal plane

Superscripts

D	Quantity related to the drag component
extra	Effect of the extra size of the cable carrying strut
Gutin	Gutin noise
L	Large strut with 6 mm diameter
T	Quantity related to the thrust component
rotor	Sound radiation from the rotating blades
strut	Sound radiation from the stationary struts
*R*1	Sound radiation from one blade
S	Small strut with 4 mm diameter
*S*1	Sound radiation from one strut
’	Small perturbation

List of figures

Chapter 1 Introduction

The fan noise studies reported in this thesis are divided into three stages: identification of noise mechanisms, passive noise abatement by structural redesign, and active noise control. The first stage focuses on the mechanisms of the noise sources. The noise sources of a general turbomachine is categorized and applied to the typical computer fan. The dominant noise source is identified as the unsteady forces arising from the rotor/stator interactions, and the noise distribution is conveniently characterized by patterns associated with the force components. The measured directivity records the acoustic interference among all the patterns and the knowledge of each pattern allows the separation of the noise sources. The noise abatement is attempted by passive and active noise means. The second stage is the passive noise control. The noticeable noise features of the cooling fan are identified and quantified by experimental studies. The final improved fan has 12 dB sound power reduction in terms of the tonal noise. The third stage is the active noise control studies, which demonstrate the feasibility of globally eliminating the rotation-locked tones by applying a simple destructive acoustic interference. According to the understandings of the fan noise distributions, a secondary source composed by a few point dipoles can accurately match the noise radiated by the fan. Therefore, a simple rotational signal can be used to drive a few secondary sources without using a complex array of detection microphones or loudspeakers. The rig is a simple open-loop feedforward control. No feedback signal is used. It is hoped that the simplicity will be a crucial advantage for eventual practical implementation. The sound power level of the deterministic BPF tone is reduced by 18.5 dB and 12.7 dB for noise radiated by the thrust and drag components of the rotor-strut interactions, respectively.

In the remainder of this chapter, the general theory of the aerodynamic sound is briefly visited. The literature of the classical knowledge of aerodynamic sound is reviewed. The noise source of the turbomachine is categorized, followed by the consideration of noise mechanisms specific to the axial-flow fan, leading to the objectives set for this study.

1.1 Aerodynamic sound

Sound is a longitudinal wave propagating in an elastic media, and the most usual type of sound in our daily life is produced by vibrations, such as the vibration of violin strings and membrane covered loudspeakers. A simple model for vibration induced sound is the sound generation by a piston placed in one end of a uniform duct, moving at a speed of $u=Ae^{i\omega t}$. It can produce a sound pressure of $p=\rho_0 c_0 u$, with a time-mean sound power of $I = \overline{pu} = \frac{1}{2}\rho_0 c_0 A^2$. Here, u, A and ω represent the velocity, velocity amplitude and the frequency of the piston vibration, respectively. ρ_0 is the undisturbed air density and c_0 is the speed of sound propagation in the undisturbed air. When vibration is absent, sound can be radiated by an unsteady flow, and this kind of noise falls in the category of aerodynamic sound. The aerodynamic sounds can be generated by unsteady aerodynamic forces on propellers due to either the instability of turbulent flow or flow-structure interactions. For example, unsteady force can be induced by the vortex shedding from the trailing edge of an airfoil at a large incident angle; the airfoil surface reflects or organizes the sound generation process. In fact, even in the absence of any structural surface or fluid inhomogenity, one part of flow can interact with another in such a way that momentum exchanges (forces) between them forms tightly coupled sound sources and the sound thus generated is another type of aerodynamic sound, mathematically characterized by a quadrupole.

In terms of general aeroacoustics research for rotating machines, Gutin (1936) was among the first to quantify the propeller noise caused by the rotation of the steady loading, later called Gutin noise. An exact statement of "aerodynamic sound" is made by Ligthill's acoustic analogy (1952). This analogy establishes a definite relationship between flow and sound, as shown below:

$$\frac{\partial^2 \rho'}{\partial t^2} - c_0^2 \nabla^2 \rho' = \frac{\partial^2 T_{ij}}{\partial x_i \partial x_j}, \quad T_{ij} = \rho v_i v_j + p_{ij} - c_0^2 \rho' \delta_{ij} \tag{1.1}$$

where ρ' is the density perturbation and T_{ij} is called Lighthill's stress tensor. It was soon extended by Curle (1955) to include the effect of solid boundaries by replacing the surface with distributed dipoles while the explicit effect of acoustic scattering is neglected. A rather elegant extension was given by Ffowcs Williams and Hawkings (1969) to applications with the presence of a solid structure in arbitrary motion. The integral form of the Ffowcs Williams and Hawkings equation is written below,

$$\left.\begin{aligned} 4\pi c_0^2 \left(\rho - \rho_0\right) = \frac{\partial^2}{\partial x_i \partial x_j} \int_V \left[\frac{T_{ij} J}{r\left(1 - M_r\right)}\right] dV - \frac{\partial}{\partial x_i} \int_S \left[\frac{p_{ij}' n_j}{r\left(1 - M_r\right)}\right] dA \\ + \frac{\partial}{\partial t} \int_S \left[\frac{\rho_0 v_n}{r\left(1 - M_r\right)}\right] dA, r = \left|\vec{x} - \vec{y}\right|, \tau = t - \frac{r}{c_0}, M_r = \frac{v_j r_j}{cr} \end{aligned}\right\} \tag{1.2}$$

where J is the Jocobian of the coordinate transformation, V is volume enclosed by the surface of S for the moving body at the retarded time τ, for which all integrand terms in [ ] are to be evaluated, M_r is the Mach number of the sources movement towards the observer, $p_{ij}' n_j$ is the unsteady pressure fluctuation on the normal direction of the surface, r is the distance separating the source from the observer, v_j is the velocity component of the source. The so-called Ffowcs Williams and Hawkings equation has served well the community of turbomachinery noise research although alternative approaches also exist.

Generally, there are three types of sources in a tubomachine or any machine with moving blades, monopole from the blade motion, dipole from fluctuating forces on the blades, and quadrupole emanating from the core of the turbulent jets. The power laws for the three types of sources can be expressed by dimensional scaling of the Eq. (1.2). Assuming that the region where intensive turbulence occurs has a dimension of D, the flow has a Mach number of $M=U/c_0$, where U is characteristic flow velocity in the problem. The dimension of time is D/U, so that the frequency of noise radiated scales with U/D. The wavelength is $\lambda = cD/U = D/M$. Together with these dimensions, we have the scales of $\partial/\partial x \sim \lambda^{-1}, dV \sim D^3, T_{ij} \sim \rho U^2$. The dimensional analysis shows that the sound power radiated by the quadrupole term $\left(T_{ij}\right)$, the dipole and monopole terms are respectively proportional to the 8^{th}, 6^{th} and 4^{th} powers of the Mach number M. Quadrupole term is therefore negligible for most low speed applications, $M<<1$, while the dipole and monopole sources are effective. In fact, Isom (Farassat 1979) demonstrated that the monopole term can be simply grouped with the dipole using a constant surface pressure of $\rho_0 c_0^2$. The final simplified sound radiation is equivalent to the integration of Lowson's (1965, 1970) point force formulations, which will be studied in Chapter 3.

In fact, search for the knowledge of specific fan noise mechanism has never ceased since Gutin's time, and reviews of the topic at large were written by authors such as Sharland (1964) and Morfey (1973). Focusing on the specific mechanisms at work in trubomachines and axial flow fans at subsonic speed, it is found that the dominant noise sources is often the unsteady pressure fluctuation from the interaction between rotating blades and stationary blades, or between rotating blades and steady but non-

uniform incoming flow. Typical noise spectrum consists of a broadband superimposed by a few pure tones, mostly the fundamental and harmonics of the blade passing frequency (BPF). The dominant source for the pure tones is the interaction events. One of the most significant contributions was made by Tyler and Sofrin (1962), who revealed the important role played by the numbers of the rotor and stator blades. The phenomenon of modal cut-off was discovered and shown to be consistent with duct acoustics. The link between this cut-off behavior for the ducted fan was related to that of the unducted fan by Lowson (1970) whose work also demonstrated that the radiation of the mismatched spinning modes cannot be cut off altogether but are rather reduced in acoustic efficiency. These formulations were recently adapted to characterize the specific applications of the computer cooling fan (Huang 2003) where the numbers of rotor and stator blades are small. The emphasis of this thesis is not on the discovery of any entirely new type of aerodynamic noise source, but rather on the acoustic characterization of a small axial-flow fan, and the noise abatement of such a family of fans.

1.2 Mechanisms of axial flow fan noise

The noise of an axial flow fan can generally be characterized in terms of discrete tones and broadband noise. Longhouse (1976) called the tonal noise as rotational noise, and the broadband noise as non-rotational noise. The frequency of the radiated tonal noise is determined by the fan rotation. Even after excluding the quadrupole and Gutin noise, there are still a host of possibilities and sites of unsteady flow dipoles in a cooling fan:

1. Tip leakage flow. Flow past the blade has a pressure difference, which gives lift, between the pressure and suction sides of a blade. The pressure difference causes

flow leakage through the blade tip, i.e., leakage flow. The leakage flow may manifest itself into a jet-like, unstable shear layer which rolls up into vortices in the blade passage. It may even hit a neighboring blade. Details can be found by the work of Fukano *et al.* (1986).

2. Non-uniform inlet flow condition. A non-uniform inlet flow is seen as unsteady flow by rotating blades and unsteady pressure ensues on the blade surfaces. This is perhaps one of the most efficient dipole sources in a fan. The noise thus radiated is often a combination of broadband and tones (Trunzo *et al.* 1981, Majumdar and Peake 1998). Its tonal noise mechanism is similar to the rotor-stator interaction, and is more efficient than the broadband. The motion of vortices from the inlet distortion is not entirely coordinated with a phase locked to the rotation, it should contribute to the broadband noise spectrum.
3. Turbulent and/or separated flow condition on a rotor. Flow separation occurs whenever the incidence angle is large, and most realistic flows through a fan are more or less all turbulent. Large scale flow turbulence, such as that caused by a fan working at a loading much higher than the condition it is designed for, can be very noisy, and most of the noise created is broadband in nature, see, for example, (Sharland 1964) and (Longhouse 1976).
4. Trailing edge noise. The interaction of the turbulent boundary layer flow, or laminar-to-turbulence transitional flow, with the blade trailing edge is a special class of noise source. The convected waves in the boundary layer are scattered by the structural discontinuity, and part of the energy is scattered into sound waves (Ffowcs Williams and Hall 1970). The resulting sound power is proportional to the 5th power of the representative flow speed when the source is non-compact,

and the dependency becomes the 6^{th} power when the source is compact (Howe 1998, Blake 1986).

5. Rotor-stator interaction. When the wake of a rotor impinges on the stator blades, forces on the stator blades fluctuate rapidly. This mechanism mainly generates the tone noise. Empirical models for such interactions (Kemp & Sears 1953, 1955, Wu, 1998) have still served the purpose of noise estimation. This is often the dominant noise source in turbomachinery. In the recent work of Huang (2003), it was speculated that the back reaction towards the upstream blade row could be more important when the downstream stator is a bluff body like a circular strut used in computer cooling fans. Such mechanism of unsteady force generation on an upstream rotor can be thought of as caused by the periodic flow blockage by the downstream struts.

For the small axial-flow fan, there are broadband noise as well as tones generated by the regions of the tip leakage flow and the non-uniform inlet flow. The former is excluded in this thesis, while the later is separated by the experimental method. The result shows that the inlet flow distortion is the most efficient dipole source of a typical computer fan noise (Huang and Wang 2004). However, since this dipole can be eliminated by structural design easily, it is not the focus of this thesis. The next most significant dipole source is the rotor-stator interaction, which induces the deterministic BPF tones. This will be the focus of the thesis. For slow speed fan operating in the design conditions, the BPF noise is found to be more than 20 dB above the broadband floor, such tonal component definitely induces more significant annoyance than the broadband. Therefore, the broadband noise mechanism is only addressed briefly in the thesis.

1.3 Fan noise abatement

The problem of noise is a concern for all types of turbomachinery. One of the most common usages in our daily life is the cooling fan. A quest for a quiet living environment has led to numerous efforts to combat fan noise, and the focus of R&D work in indistry has gradually shifted from aerodynamic performance to acoustic quality of products and machinery. The traditional fan noise reduction is to absorb the sound after it is radiated, but such solution is not practical for the ventilation fan in the electronic device. In order to reduce noise, one has to improve the flow conditions pertinent to noise source mechanisms, such as the inlet flow uniformity, and the wake interaction strength which depends crucially on the distance between the rotor and stator blades. In fact, acoustic performance is becoming one of the major indices differentiating one manufacturer from another for a broad range of consumer products in which fans are used. Take computer cooling fan as an example, the noise radiated by the computer cooling fan is receiving increasing attention as the CPU power increases rapidly and the trend of slim packaging continues.

In the area of noise abatement for small axial flow fans, considerable efforts have also been made. A selected few of them are mentioned here. Fitzgerald and Lauchle (1984) demonstrated the effect of a comprehensive range of corrective measures that can be taken to modify a cooling fan design for better acoustic quality, such as the equalization of downstream strut size, the reduction or elimination of the potential flow interaction with nearby objects, use of bellmouth inlet to minimize inlet flow distortions, and the prevention of possible large scale flow separation on the suction side of blades. Quinlan and Bent (1998) focused on broadband, high frequency noise generated by the tip leakage flow with extensive acoustic and aerodynamic

measurements. Attempts were also made to reduce tonal noise by uneven blades for propellers (Lewy 1992) and small radial fans (Boltezar *et al* 1998). It was concluded that only spectral shifts can be made while the total sound power remains more or less the same. The optimization in terms of stator/vane blade sweep and lean was conducted by Envia and Nallasamy (1999). They showed that a positive sweep angle can reduce the tone level due to the additional cancellation caused by phase differences in the axial direction. Longhouse (1978) attempted to eliminate the tip leakage flow by using a rotating shroud, a feature which may cause structural vibration problem if the shroud is not properly balanced. Brookfield and Waitz (2000) proposed to fill the deficit of the rotor wakes by using trailing-edge blowing. This technique was also demonstrated in the active aerodynamic control to suppress the BPF noise originating from the wake interactions by Nauhaus *et al* (2003), Rao *et al* (2001) and Simonich *et al* (1993). The active noise control (ANC) technique for ducted fan has been successful. Tyler and Sofrin's model (1962) for the ducted fan requires the multiple detection microphones in order to cancel the high order modes sound propogating in a duct and some success is achieved by Gerhold (1997) and Thomas *et al*. (1993, 1994). For unducted fan noise, the model composition in free space is more complex than that in the duct. Lauchle *et al* (1997) and Quinlan (1992) have both achieved significant noise reductions in a baffled fan. Note that the baffle may have altered the acoustic distribution and the result cannot be extrapolated to the natural fan. A new work of the baffled fan is also reported by Gee and Sommerfeldt (2004), which used a model to suggest that a near field error sensor can be used to minimize the far-field sound radiation.

The present study focuses entirely on the tonal noise using an isolated computer cooling fan as an example. The acoustic model composition in free space seems to be a complex problem to solve, which is one of the most crucial issues in the thesis. This represents a first step towards understanding the noise radiation by such cooling fans installed in a computer chassis. If the sounds radiated by different parts of the fan cancel themselves out, it can be expected that the chassis environment may not have much sound wave to scatter about in the first place. In other words, efforts in silencing an isolated cooling fan can be a short cut to achieving the noise reduction for a fan installed in a real computer chassis.

1.4 Objectives and strategy of this project

The small axial-flow cooling fan is an important air-moving device for the computers, it is very important to improve its acoustic qualities to meet the demands of the advancing CPU technology. The noise emitted from the fan is a combination of all possible noise sources. The tone noise at BPF and its harmonics are found to be dominant when the fan operates at a satisfactory design condition. The focus of this study is on the dominant noise components through the studies of the source mechanisms. The knowledge is then applied to improving the acoustical performance of the fan. The study reported by the thesis is organized as follows.

Chapter 2 is an overall experimental study of the noise mechanism and the separation of the rotary (tone) noise from the random (broadband) noise. The general structure of the computer cooling fan has 7 blades with 4 struts, and its inlet is distorted by four sharp edges caused by the intersection of the bellmouth and the square outer frame. This structure includes two aerodynamic interactions. One is the distorted inlet flow with the rotor blades. This feature, however, can be avoided. Another interaction is

the rotor blade with the downstream struts, which is unavoidable and becomes the focus of the following chapters.

Chapter 3 is theoretical study of the interaction noise with focus on the characteristics of the noise from each force component. The unsteady force acting on a blade is divided by the thrust and drag components. The radiated noise is a result of the complex acoustic interference among noises form these two force components on the blades, and noises from all the blades. Noise radiated by each force component has its own distinct features, and the knowledge is used to devise an experimental method for separating noise sources in Chapter 4.

Chapter 4 investigates, experimentally, the contribution of each noise source and the results validate theoretical derivations. On the basis of this, design optimization is conducted. The structure of the fan is modified by redesigning the numbers of the struts to obtain the distributions of the pure thrust noise, the pure drag noise, and the pattern with the combination of the two noise components. Measurements for the improved fan show a 12 dB tonal sound power level reduction compared with the original fan.

Chapters 5 and 6 are active noise control studies on the components of thrust and drag noise, respectively. This is done on top of the structural improvement achieved in Chapter 4. The aim of the active control is to explore the feasibility of a very simple acoustic interference technique for typical computer fans, and the primary motivation is to maximize the simplicity and the global effectiveness of the technique so that it might become economic enough to be applied in practice. A simple open-loop, feed-

forward control scheme is used. For the BPF tone, 14.9 dB and 12.7 dB sound power reductions are achieved for the thrust noise and drag noise components, respectively.

Chapter 7 concludes the study by summarizing findings made in the noise mechanism studies and the achievements made in both passive and active noise controls.

Chapter 2 Overall noise characteristics of a typical fan

A small axial-flow fan working as an air-moving device for the computer is selected for the studies and introduced in this chapter. Similar to most fans, the noise from the computer cooling fan consists of two parts: the broadband noise superimposed by the discrete tones whose amplitudes generally decrease with the harmonic index. The harmonic tones are phase locked with the blade rotation and the others are not. The basic objective of this chapter is to differentiate between the random noise and the tonal noise. In what follows, Sec. 2.1 discusses details of the sample fan, Sec. 2.2 describes the measurement method, and the rest of the chapter is devoted to the study of the sound induced by the inlet flow distortion and the separation of the tonal noise from the random noise.

2.1 The sample computer cooling fan

A typical computer cooling fan of 92 mm in diameter is chosen for the study, and it is manufactured by Delta Electronics, Inc. with the type number of AFB0912HH. The photographs are shown in Figs 2.1(a) and 2.1(b). The fan has 7 rotor blades and 4 downstream struts for holding the motor.

Observing the structure of the fan shown in Figs 2.1 (a) and 2.1(b), three distinct features pertinent to noise generation are noted.

(a) The front view of Fig. 2.1(a) shows that the inlet is distorted by the four sharp edges caused by the intersection of the bellmouth and the square inlet frame.

(b) The back view of Fig. 2.1(b) shows that the rotor blades interact with the four downstream struts.

(c) The four downstream struts are unequal in size. One strut is enlarged for carrying the electrical cable for the motor.

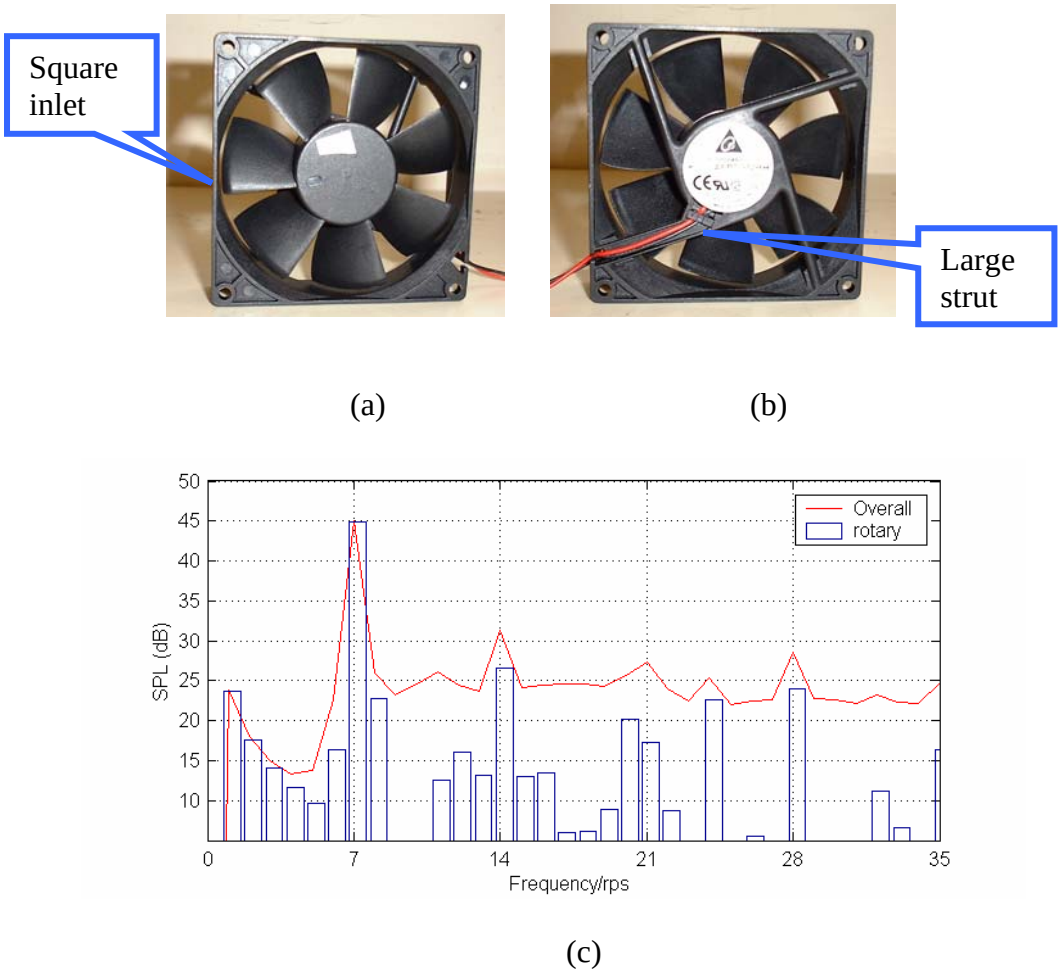

Figure 2.1 A sample computer cooling fan of 92 mm in diameter. (a) Front view. (b) Back view. (c) The spectrum of sound measured on the rotational plane without using the analogure filter.

Figure 2.1(c) shows two spectra from a typical measurement: the overall noise (line), which is calculated according to the raw data acquisition, and the rotary noise (bar chart) based on the synchronous averaging of the raw data (it is also labelled as 'raw' in later figures). The spectra show the dominance of the discrete tonal peaks at the

multiples of the blade passing frequency, *m*BPF, where *m* is an integer, BPF=B rps, and *B* is the number of rotor blades. The tone of the fundamental BPF is more than 20 dB above the broadband floor, while the other harmonics are less distinctive. As is discussed in more details later, the dominant discrete peaks appearing in Fig. 2.1(c) represent the sound radiated by the aerodynamic interaction between the rotor and the sharp edges of the inlet flow distortion, and the rotor with the downstream strut. Apart from the harmonics of BPF, a few noticeable peaks are found in between the BPF harmonics, such as 24 rps. These might be induced by the vibration of the motor. They do not show much change through both passive and active noise control, and are left out of subsequent discussions.

The present study focuses entirely on the tonal noise using an isolated computer cooling fan as an example. Based on the specifications provided by the manufacturer, the normal rotating speed of the cooling fan can be either 3000 or 3200 rpm depending on the electric current rating for the motor. In the experiment, the rotating speed is measured by an optical tachometer and it is observed that, typically, the fan speed varies within a range of ±25 rpm.

The typical aerodynamic performance of the fan is illustrated in Fig. 2.2 for a given rotational speed. The abscissa is the volume flow rate, *Q*, which is varied by controlling the throttle in a testing facility. The solid line is the pressure rise across the fan, Δp, and the dashed line is the efficiency defined as the fluid mechanical power output, $P_{output} = Q \cdot \Delta p$ to the electric power input. In the current study, the fan is isolated from its chassis, and it is similar to the free-delivery condition near the point of B. Point A gives the maximum volume flow rate when the exit pressure, p_{exit}, is

deliberately lowered to the level of the incoming flow pressure, p_{inlet}, which is below the atmospheric pressure, p_{atm}, according to the Bernoulli equation $p_{inlet} = p_{atm} - \frac{1}{2}\rho V^2$ for a potential flow of velocity V originating from a stagnant atmosphere. Point C denotes the maximum efficiency point, for which there is normally some more loading than the free-delivery, such as the flow condition in a chassis. In other words, the acoustic studies conducted in the free delivery condition differs from the design condition, e.g. C, but the flow should be rather similar to that of the real working condition. In the real case of the fan working in a computer chassis, there is aerodynamic loading and the operation point is not at A, probably near the maximum efficiency point C. The flow is expected to be more turbulent than it is the free delivery condition. In order to find the effect of this condition on noise radiation, the fan was installed in an acoustically transperent box (using plastic covers) with an exit throttling valve to simulate the flow condition in the chassis. More broadband noise was found, but no qualitative difference was found with respect to the tonal noise.

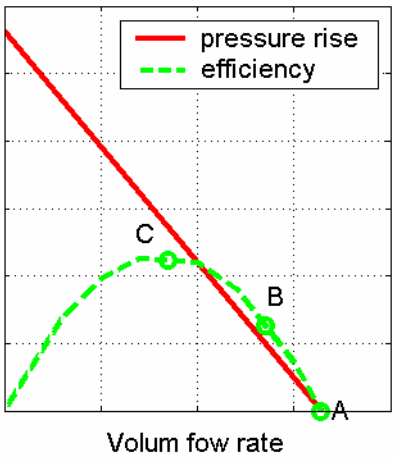

Figure 2.2 The typical fan curve

Acoustically, a fan installed inside a chassis is quiet different from an isolated fan as the chassis acts as confining walls to reflect and scatter sound waves. The study of an isolated fan in free delivery condition represents a first step in the direction for the fan noise abatement. However, it is anticipated that, if the noise from the isolated fan is more or less eliminated by design, the effect of the chassis should also vanish as there is not much sound to scatter in the first place. In other words, efforts in silencing an isolating fan represents an effective method of dealing with the real fan noise in a chassis.

2.2 Acoustic directivity measurement

The noise source separation is the foundation for the studies conducted in this project. It is known that the fluctuation of unsteady force on the blades generates the noise, so the nature of the force and its movement characterize the sound distribution. Therefore, the directivity measurement will be a good method to separate the noise components for a given total noise which is the result of complex acoustic interference in the fan. Details of the source separation method is explained systematically in the next two chapters, but the measurement set-up is described in this chapter. The acoustic surveys were conducted in an anechoic chamber with an internal dimension of 4mx5mx3m. The chamber is classified as anechoic above 80 Hz. When the frequency is above 80Hz, 99% of sound energy is absorbed by the sound-absorbing wedges. For the sound below 80 Hz, the reflected sound from the wall at a distance of more than 2 m is also regarded as trivial in this test since 12 dB is deduced by the dispersive attenuation apart from the wedge absorption. The fundamental BPF of the fan noise is around 350 Hz, so the laboratory environment can simulate a free space.

Before describing the experimental setup, some geometrical definitions are illustrated in Fig. 2.3(a). The axial-flow fan is shown standing vertically up, and the sound radiated by the fan is surveyed by a microphone over a sphere of radius r_0 from the fan centre. The Cartesian coordinate system is also defined in the figure: x is pointing against the inlet flow, y points out of the paper, and z points upwards. When viewed from the upstream, the fan rotates anti-clockwise from the $+y$ axis towards the $+z$ axis. An observer on the sphere is described by two angular coordinates. There are two ways to define the observer, and they are used in the separate occasions for convenience. In the first, the latitudinal angle is measured from the $+x$ axis, and is denoted by $\alpha \in [0, \pi]$, while the longitudinal angle is denoted by $\theta \in [0, 2\pi]$, which is shown in the left-hand side of Fig. 2.3(a) as a projection of the conic section cut out from the sphere. The second method to define the observer position is to use vertical axis as the axis of symmetry, and use a latitudinal angle measured from the $+z$. The corresponding longitudinal angle is then $\phi \in [0, 2\pi]$ measured from the $+x$ axis on the horizontal cross section. The $+x$ axis based coordinates (α,θ) are more convenient to use for theoretical discussions where the thrust force is defined along the x axis, while the latter $+z$ axis based are needed for three dimensional measurements based on horizontal microphone traversing arrangements. The latter is explained in Chapters 5 and 6. Note that, for a single horizontal plane measurement conducted for the central plane of z=0, α overlaps with ϕ for $\phi < \pi$, and the symbol of α is used liberally beyond its limit of π, in which case it can be regarded as ϕ.

The acoustic directivity is measured by a half-inch B&K microphone fixed on the mesh ground of the anechoic chamber at a distance of r_0=0.5 m from the fan center. The fan and a tachometer are fixed on top of a tripod which rotates with an angular

interval of 10^o. The schematic diagram of the test rig is shown in Fig. 2.3(b). Illustrated at the upper-right corner are a 0.5" measurement microphone (B&K type 4187) and a tachometer (B&K type M004) connected to a PC equipped with MATLAB® and A/D card. The pulse signal from the tachometer is sampled together with that of the microphone by a 24 bit analog to digital converter using a sampling rate of 16kHz. A four- channel B&K conditioning amplifier (Nexus type 2693) supplies the power to the microphones and amplifies the signal. Before every

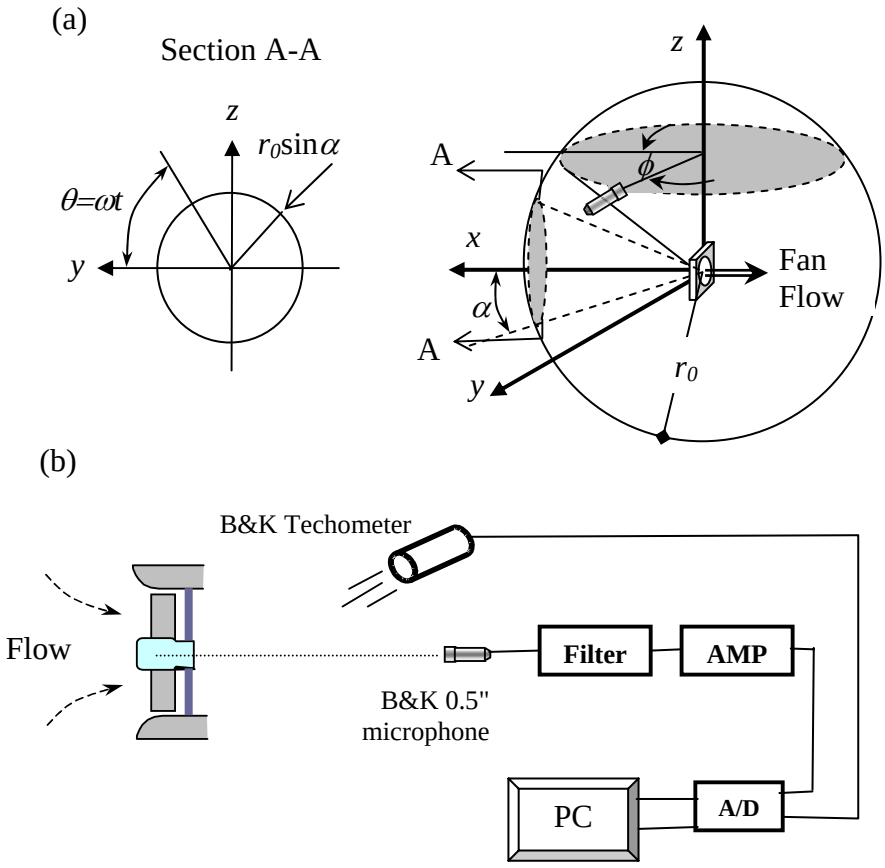

Figure 2.3 Illustrations of (a) the co-ordinate system, and (b) the experimental setup.

directivity measurement, the microphone is calibrated by B&K's calibrator type 4231. The tachometer is powered and digitized by B&K's stroboscope type 4913. Sound signals are segregated by tachometer pulses for each rotating cycle, which typically vary around a target rpm of, say, 3000, by about ±25 rpm from one moment to the

next. The timebase of the signals are stretched to a uniform value of the target rpm, and the stretched signals are then synchronously averaged for all rotational cycles of the fan. Signals averaged this way is called 'rotary' noise in this study, and it should register all sources locked to the fan rotation. The difference between the directly measured signal and the time-domain rotary sound signal is designated as the 'random' noise which does not have phase relation with the rotation.

Due to the substantial electronic noise in the measurement system, a bandpass filter of 20Hz-10kHz was used. Before the filter was adopted, a measurement without the filter was taken, and no significant tonal noise was found below the first blade passing frequency, which was 350 Hz. This means that noise radiation by all blades is basically equal, and the use of the filter does not distort the results.

Figure 2.4(a) demonstrates the effect of such synchronous averaging on the raw (overall) signal. The upper square-pulse train is the tachometer signal. The curve in the middle is the raw data, and the rotary sound waveform is shown at the bottom. Figure 2.4(b) shows the acoustic directivity for the measurement conducted for the original fan. In order to clearly distinguish the noise distribution, the acoustical directivity plotted here uses the sound intensity, $I = p_{rms}^2 /(\rho_0 c_0)$. The use of this quadratic variable amplifies any non-uniformity of the sound pressure. The outer thin line is the total sound intensity distribution obtained by the raw signal, while the rotary and random noises are plotted by the thick and dashed lines, respectively. The directivity patterns of the overall fan noise and the rotary noise are found to be tilted by about 30^o from the rotational plane direction of α=90^o. The sound power is found by the integration over the spherical surface:

$$W = r_0^2 \int_0^{2\pi} d\theta \int_0^{\pi} I(\alpha,\theta)\sin(\alpha)d\alpha\,. \tag{2.1}$$

It is explained in Chapter 3 that the rotary sound intensity does not change with angle θ if the fan structure is symmetrical about the *x* axis. In such case, a measurement on the central plane with an angular interval of $\Delta\phi$=$\Delta\alpha$=10^o gives 36 data points for one directivity. The sound intensity is simply a function of α, and the sound power can be integrated as

$$W = 2\pi r_0^2 \int_0^{\pi} I(\alpha)\left|\sin(\alpha)\right| d\alpha \approx \pi^2 r_0^2 (\Delta\alpha)\sum_{i=1}^{36} I(\alpha_i)\left|\sin(\alpha_i)\right|, \tag{2.2}$$

where, in the last identity, the actual data from the front side of the plane, $\alpha = \phi \propto [0,\pi]$, is allowed to differ from those at the back side, $\phi \propto [\pi, 2\pi]$. This is the reality in any measurement although the acoustic distribution is theoretically assumed to be uniform for the whole range of the longitudinal angle $\theta \propto [0, 2\pi]$. In other words, one recognizes the actual difference between sound at one angular position of $\phi < \pi\ (\theta = 0)$ and another at $2\pi - \phi\ (\theta = \pi)$. The sound power integration in Eq. (2.2) uses the average.

The overall sound power level is calculated by

$$SWL = 10\log_{10}\left(W / W_{ref}\right)\ \text{dB},\ W_{ref} = 10^{-12}\,\text{Watt}\,.$$

The result for this fan is about 50.8 dB including 49.5 dB rotary noise and 44.7dB random noise, as shown below the graph in Fig. 2.4(b). The rotary noise dominates over the random noise by a margin of 5 dB. However, as is shown later, the random noise dominates when the fan design is modified and the rotary noise is significantly reduced. Nevertheless, our attention is still firmly on the rotary noise as pure tones are more annoying than broadband noise.

2.3 Rotary noise

The discrete tonal noise is distributed over the BPF and its harmonics. The sound energy around the narrow frequency bands is induced by a series of aerodynamic interactions experienced by the blades. The three distinct features explained in Sec. 2.1 all radiate significant interaction noise. The interactions are between the rotating blades with the distorted inlet flow and with the downstream struts. The task now is to have a preliminary investigation as to which one is more important.

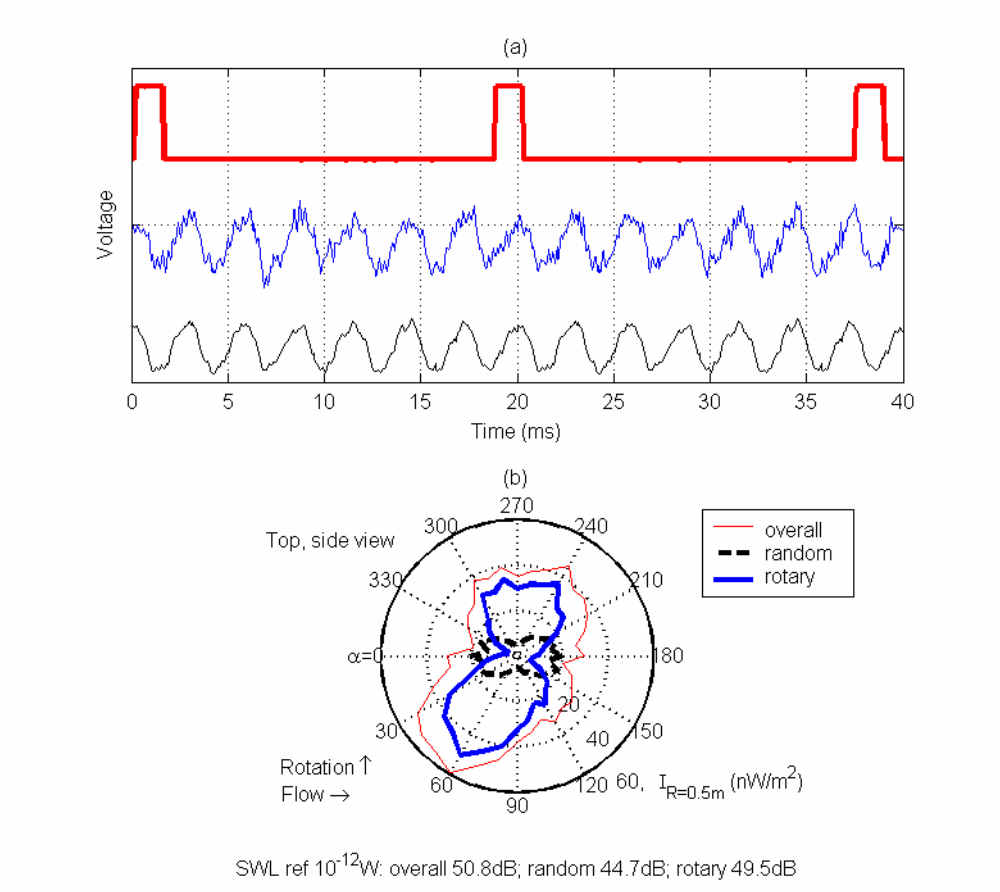

Figure 2.4 Synchronous averaging and the acoustical directivity of the original fan. (a) Synchronization of the two signal of tachometer (top) and raw data of fan noise (meddle) to rotary noise (bottom). (b) Measured directivity of sample fan with all noise components separations.

In most turbomachines, the inlet bellmouth is designed for inlet flow to pass through a contraction smoothly. Even with a smooth inlet, atmospheric flow carries vortices which are ingested by the fan to produce noise. Majumdar and Peake (1998) report the studies on the topic of sound generation by the elongated eddies being chopped by blades for a greater number of times. In our case, the vortices are expected to be generated by the sharp edges of the square bellmouth, and they would generate significant noise. This noise is also expected to be dominant over that from the interaction between the rotor blades with the downstream struts. This occurs because the flow through a distorted (non-uniform) inlet frame will be more turbulent than that of the potential flow blocked from downstream struts. This assertion is now put to test in the experiment as follows. The sole contribution from the inlet flow distortion is measured by installing the rotor in the original square casing frame. The motor is held by a cylindrical rod with four holders located at about 200 mm from the blade trailing edge, which is very far compared with the 3 mm separation distance between the blade trailing edge and the original struts. In the experiment, a check was performed to ensure the far away holder did not produce significant sound. The sound from such a rotor with the square inlet is shown in Fig. 2.5(a). The outer thin solid curve is the overall noise, the thick solid curve is the rotary noise and the dashed line is the random noise. The sound power level of the noise component are labeled below the graph; they are 49.3 dB overall noise, 45.0 dB rotary noise, and 47.3 dB random noise. The rotary noise from the square inlet is compared with other sources as follows.

- Compared with the original noise given in Fig. 2.4(b), the rotary noise from the inlet frame is 49.5-45=4.5 dB below the total. It represents $10^{-0.45} = 35.5\%$ of the total rotary sound power. However, it does not mean that the rotary noise caused

by the other mechanisms in the original fan, i.e. the interaction between the rotor and downstream struts, is definitely the remaining 64.5%. Such division is correct only when the sounds from two mechanisms are uncorrelated or correlated but with 90deg phase difference.

- When a full circle bellmouth with 10 mm flaring radius is used to replace the original square inlet frame, as shown later in Fig. 4.1(a), the flow distortion by the inlet frame is expected to be eliminated. Details of the measurement results are given in Chapter 4 in Fig. 4.6. The rotary noise is found to be 45.2 dB, which is only 0.2 dB above the interaction noise caused by the square inlet frame. If one assumes zero-coupling between the two, the total noise is 48.1 dB, which is not far from the 49.5 dB measured in the original fan. From these results, it seems that the zero-coupling assumption is probably close to reality.
- It is known that the interaction of the four-lobe distorted pattern is equivalent to that of the four equal struts. When the large strut shown in Fig. 2.1(b) is replaced by a regular size struts, the rotary noise from the rotor blade interaction with the four equal struts is found to be 40.4 dB, and the details are given later in Fig. 4.9(d). It is 45-40.4=4.6 dB below that from the inlet distortion. Therefore, the upstream interaction between the inlet flow distortion and the rotor blades is the dominant dipole source in the small sample fan.

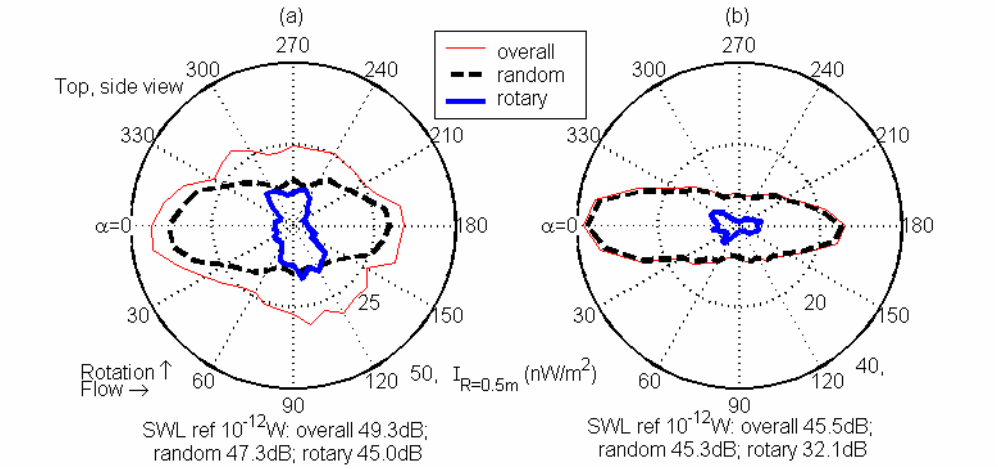

Figure 2.5 The directivity of the fan (a) with square inlet only, and (b) with the bellmouth only (five times amplification of the rotary component).

The interaction of the rotor blade with the downstream struts is a result of both potential flow blockage and the viscous wake interaction. The snapshot during one rotor-strut encounter is illustrated in Fig. 2.6. The unsteady lift experienced by the rotor-stator interaction arises on the rotor blades as well as on the stator blades (it is downstream struts in this case). The lift on the rotor surface is the potential flow blockage by the downstream struts. For *S* downstream struts, the rotating motion gives *S* times blockage on each rotor blade in every rotating cycle. The unsteady force fluctuation has many circumferential harmonics of the fundamental rotating frequency.

The trailing edge wake is formed by the momentum deficit in the flow, and there is velocity discontinuity between the suction and pressure sides of the airfoil surface. Similarly, for *B* rotor blades, the wake interaction with the struts occurs *B* times on each struts per rotating cycle. This unsteady force also contributes to the circumferential harmonics of the fundamental rotating frequency.

The unsteady forces experienced by the struts are normally much smaller than those on the rotor blades which are profiled to generate large lift. Finally, the acoustic interference of the blade rows determines the dominant tonal noise. The mathematical model for a free-space rotor is first derived by Lowson (1965), similar modelling is described in Chapter 3 for further comparison with experiment in Chapter 4.

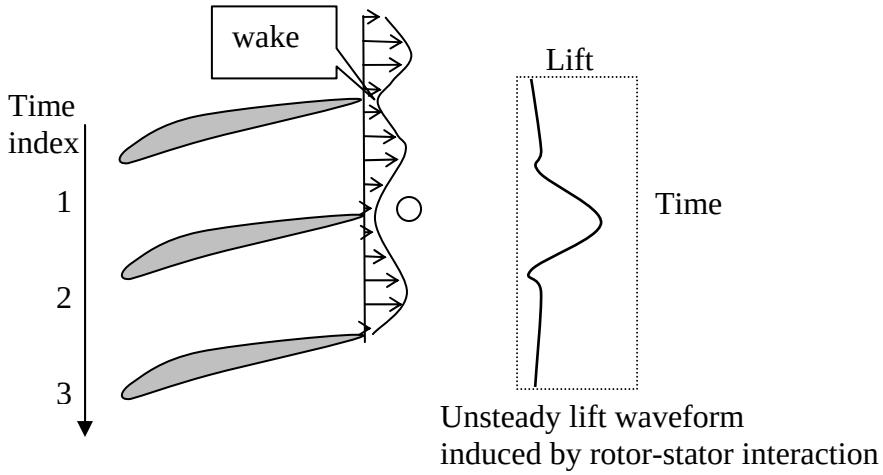

Figure 2.6 Illustration of the potential flow interaction and force fluctuation on the blades.

2.4 Random noise

Random noise here is defined as the difference between the overall noise measured and the rotary average. Notice that some noise mechanisms may be rather periodical in nature but its phase is not locked with the rotation; they would also get filtered out of the averaging process and get accounted in the random noise here. Excessive broadband noise may arise from the operating condition of flow separation (very high or very low loading), stall, or inlet flow turbulence due to obstacles. The general broadband noise mechanisms are described in Sec. 1.2. These mechanisms are

selectively substantiated in relation with the specific fan application with the help of Fig. 2.7.

- Figure 2.7(a) shows that flow separates from the suction surface caused by a large incident angle. It causes unsteady lift which fluctuates randomly. In addition, there might be vortices shed from a distorted inflow, which also causes random lift fluctuation.
- Figure 2.7(b) shows vortex shedding from a strut forming a so-called 'Karman vortex street' in which two rows of vortices are shed alternatively from the cylinder strut. The unsteady lift thus experienced by the strut is not random but its phase is normally unrelated to the fan rotation. Because of this, the sound generated may also be counted as random noise.
- Figure 2.7(c) illustrates the flow leakage across the gap between the blade tip and the shroud/annulus wall, which is the region of the tip clearance. The leakage flow arises due to static pressure difference across the two surfaces of the blade at the tip, which rolls up into vortices due to shear flow instability. The tip clearance vortex interacts with the inner span of a blade or with a neighboring blade and radiates sound.
- Figure 2.7(d) shows that the action of fluid viscosity causes a thin boundary layer to form along the surface of the blade. Due to flow instability, pressure waves develop inside the boundary layer and these waves are convected within the boundary layer at a very low speed. The sudden termination of the convection pattern by the tailing edge causes the scattering of the slow wave energy into sound. The trailing edge acts as a point source for the far field.

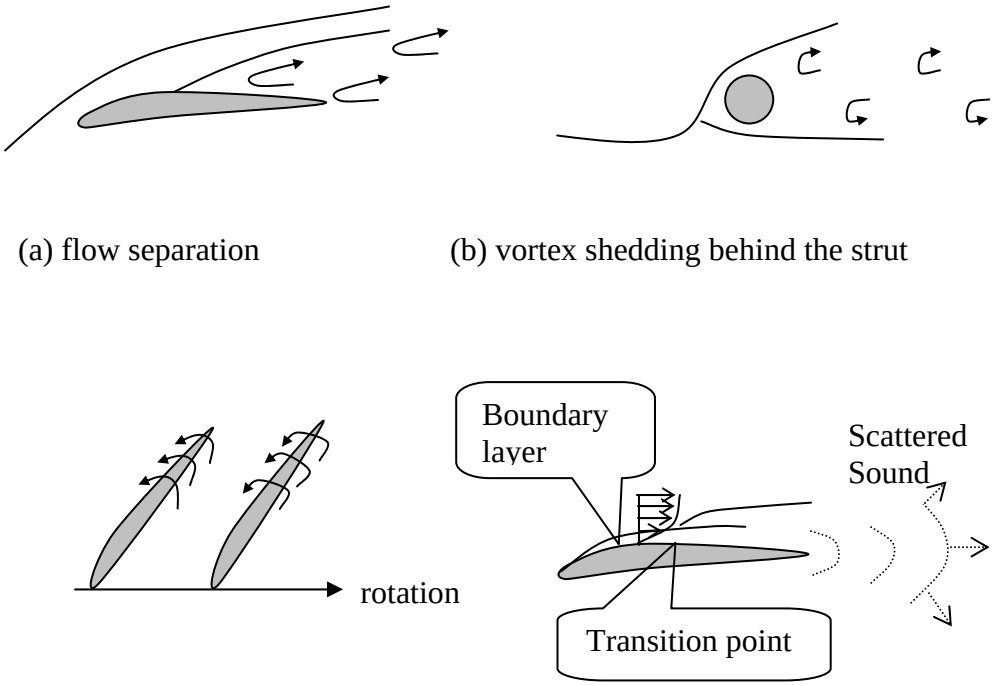

(a) flow separation (b) vortex shedding behind the strut

(c) tip leakage flow (d) scattering of wave at trailing edge

Figure 2.7 Illustration of the random noise mechanisms, (a) flow separation; (b) vortex shedding behind the strut; (c) tip leakage flow, and (d) trailing edge scattering of converted boundary layer wave.

The aerodynamic performance of the sample fan can satisfy the design condition, and the inlet flow distortion represents an unnecessary source for generating the broadband noise. This is demonstrated by measuring the noise generated by a rig in which the square inlet frame is replaced by the bellmouth, and there is no downstream strut in the close proximity of the rotor blades. The results are shown in Fig. 2.5(b), and compared with the noise for the inlet frame shown in Fig. 2.5(a). A reduction of 3.8 dB is achieved for the overall noise when the square inlet is replaced by the bellmouth. The rotary noise is reduced by 12.9 dB when there is no interaction between the four-lobe inlet flow and the rotating blades. For the random noise component, a 2.0 dB reduction is achieved. The ratio of the bellmouth-only random noise to that of the fan with a square inlet frame is $10^{-0.2}$=0.63. Assuming that the

random noise caused by the rotor installed in a bellmouth is not correlated with the noise caused by the inlet flow distortion, it is concluded that the square inlet is responsible for 1-0.63=37% of the random noise, while the rotor blades themselves are responsible for 63% of the random noise.

To further investigate the noise caused by the inlet flow distortion, the aerodynamic pressure is measured right on the inlet surface by a flush-mounted miniature electric microphone, for which details are described in Chapter 5. The locations for the measurement on the bellmouth and the square inlet frame are made equivalent. The signal records the waveform of the fluctuating aerodynamic pressure caused by the passing rotor blades. Figure 2.8(a) compares the two waveforms; the solid line is for the bellmouth, and the dashed line is for the square inlet. The signal from the bellmouth is very periodic and looks like a discrete pure tone. When the observer is placed on the square inlet, the waveform is no longer periodic. In fact, it appears more like a multiple-tone waveform. The spectra of the two signals are shown in Fig. 2.8(b), the BPF component contained in the bellmouth signal accounts for 86% of the total energy, while the content of the distorted inlet is 57%. The reduction in this percentage means the increase in flow turbulence and potential flow unsteadiness. The inlet flow turbulence is expected to hit the blades and cause random lift fluctuation and consequently random noise, while inlet flow unsteadiness is expected to make more tonal noise. This pressure comparison in Fig. 2.8 shows the origin of the broadband noise induced by the inlet flow distortion.

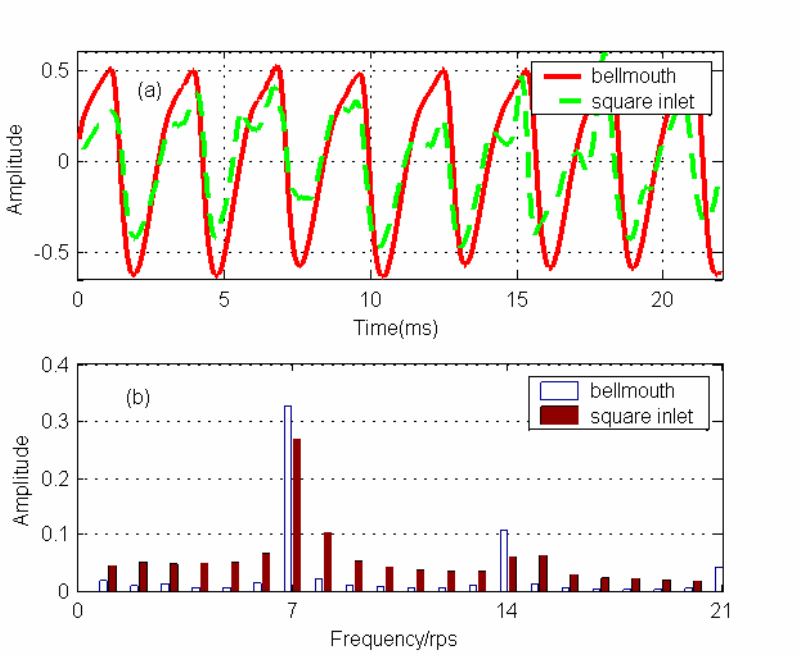

Figure 2.8 The comparison of waveforms with bellmouth and with square inlet. (a) The pressure-time waveform. (b) The spectral comparison.

Chapter 3 Theoretical study of rotor-strut interaction noise

In this chapter, the acoustics of the rotor-strut interaction is studied for the following purposes: (a) to elaborate on the details of the interaction sound radiation, especially the reason why some components of the interaction forces are radiated and some are not; (b) to study the directivity pattern of the sound radiated by various force components; (c) to obtain closed-form formulas for the sound power from the interaction by making use of the small fan characteristics. Gutin noise is also estimated in the process and is proved to be totally negligible. The basic approach of the point-force formulation by Lowson (1965,1970) and the physical interpretations by Huang (2003) followed. Elaboration on details beyond these references are necessary for discussions in the next chapters.

3.1 Point force formulation

The quadrupole term in the integral form of the Ffowcs-Williams and Hawkings (FWH) equation, Eq. (1.2), can be left out for most low speed applications, $M<<1$. At first sight, the monopole source seems to be dominant. However, for a compact solid object, the monopoles distributed over the whole body is an effective dipole since one side pushes the air while the other side pulls. In other words, for every element of positive monopole on one side, there is a negative monopole element on the other side of the rigid body while the volume remains constant. Isom (Farassat 1979) demonstrated that this monopole term can be simply expressed as a dipole term using a constant surface pressure of $\rho_0 c_0^2$. The FWH equation is reduced to

$$4\pi c_0^2 \left(\rho - \rho_0\right)^2 = -\frac{\partial}{\partial x_i}\int_S \left[\frac{\left(p_{ij}^{'} + \rho_0 c_0^2\right) n_j}{r\left(1 - M_r\right)}\right]_{ret} dA \tag{3.1}$$

where subscript ret denotes retarded time, τ, which is related to the reception time t by $t = \tau + r/c_0$. The results can be further simplified in the far field $r = \left|\vec{x} - \vec{y}\right| >> l$, where l is the characteristic length of the source, $\vec{x}, \vec{y}$ are the vectors for the observer and the source, respectively. The space derivative $\frac{\partial}{\partial x_i}$ can be swapped with that for time (Howe 2003),

$$\frac{\partial}{\partial x_i} \leftrightarrow -\frac{1}{c_0}\left(\frac{x_i - y_i}{r}\right)\frac{\partial}{\partial t}, \quad \frac{\partial}{\partial t} = \frac{1}{1 - M_r}\left[\frac{\partial}{\partial \tau}\right]_{ret}. \tag{3.2}$$

With these simplifications, the above equation is found to be equivalent to the one used by Lowson (1965) for a moving point force with components described as F_i,

$$p\left(\vec{x}, t\right) = \frac{x_i - y_i}{\left(1 - M_r\right) c_0 r}\frac{\partial}{\partial \tau}\left(\frac{F_i}{4\pi r(1 - M_r)}\right)_{ret}. \tag{3.3}$$

The coordinate system defined in Fig. 2.3(a) is adopted here. When viewed from the upstream, the fan rotates anti-clockwise from the +y axis towards the +z axis, and the angular position of a rotor blade is shown in Fig. 3.1(a) and described by:

$$\theta = \Theta + \omega\tau, \tag{3.4}$$

where τ is time used for the source motion, Θ is the initial angular position of the point source on the rotor relative to the stationary observer, and ω is the angular speed of the motor rotation. The far-field sound is

$$p\left(\vec{x}, t\right) = \frac{1}{4\pi r\left(1 - M_r\right)^2 c_0}\left[\frac{\partial F_r}{\partial \tau}\right]_{ret}. \tag{3.5}$$

Applying integration by parts, Lowson (1970) wrote the complex amplitude of the far field sound from the point force as

$$c_n = \frac{\omega}{4\pi^2}\int_0^{2\pi/\omega} -\frac{in\omega F_r}{c_0 r} e^{in\omega(\tau + r/c_0)} \left[d\tau\right]_{ret}, \tag{3.6}$$

where F_r is the unsteady force (source) pointing to the observer, and ω is the rotating speed of the motor.

For the purpose of qualitative studies for a small cooling fan, the interaction force on a moving blade can be lumped into a point force circulating on a circle of radius R on the plane of x=0. As shown in Figs 3.1(a) and 3.1(c), the point force can be divided into three components, thrust T, drag D and radial force E. In the far field, $r_0 \gg R$, r can be approximated as:

$$r \approx r_0 - y\left(R/r_0\right)\cos\theta, \tag{3.7}$$

where r_0 is the distance between the observer and the fixed fan centre. The relationship between r and r_0 is shown in Fig. 3.1(b).

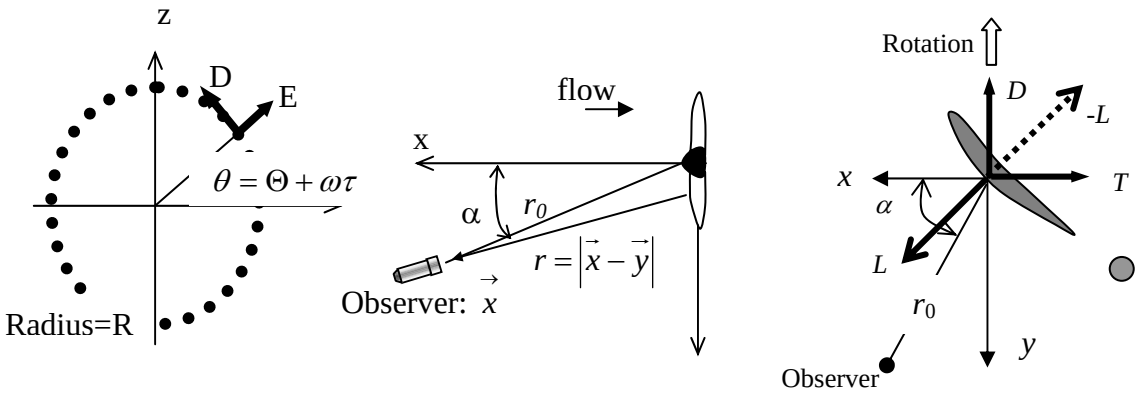

Figure 3.1 Coordinate system and force definitions. (a) Front view of the rotating forces. (b) Top view with observer, and (c) top view of the force

Note that the radial force E is only substantial when a blade leans. Struts are typically leaning in the direction of rotation, e.g. in (Envia and Nallasamy 1999). The noises radiated by T, D, and E are called thrust noise, drag noise and radial noise,

respectively. In fact, the sound radiated by a radial force can also be modelled by that from a drag force with a 90° phase shift, so the terms involving E is dropped in the following discussions. Figure 3.1(c) shows that the drag and thrust are related to the pitch angle β given as:

$$T = -L\cos\beta, D = -L\sin\beta\,, \tag{3.8}$$

where L is the airfoil lift. The projection of the total unsteady force on the source-receiver direction r is:

$$F_r = \left[-\frac{x}{r}T + \frac{y - R\cos\theta}{r}D\sin\theta - \frac{R\sin\theta}{r}D\cos\theta\right] \approx r^{-1}\left[-xT - yD\sin\theta\right]. \tag{3.9}$$

The integration of Eq. (3.6) can be evaluated once all the force components are expanded into Fourier Series,

$$\begin{aligned}
&\begin{pmatrix} T \\ D \end{pmatrix} = \sum_{\lambda=-\infty}^{\infty}\begin{pmatrix} T_\lambda \\ D_\lambda \end{pmatrix}e^{-i\lambda\omega\tau} \xrightarrow{\omega t = \theta - \Theta} \sum_{\lambda=-\infty}^{\infty} e^{i\lambda\Theta}\begin{pmatrix} T_\lambda \\ D_\lambda \end{pmatrix}e^{-i\lambda\theta}, \\
&\begin{pmatrix} T_\lambda \\ D_\lambda \end{pmatrix} = \frac{\omega}{2\pi}\int_{\Theta}^{2\pi+\Theta}\begin{pmatrix} T \\ D \end{pmatrix}e^{i\lambda(\Theta-\theta)}d\theta,
\end{aligned} \tag{3.10}$$

and the phase angle involving r in Eq. (3.6) is approximated by

$$n\omega r/c_0 \approx nk_0r_0 - nM\sin\alpha\cos\theta, M = \omega R/c_0\,. \tag{3.11}$$

Disregarding the mean phase shifting term nk_0r_0, and noting $\omega d\tau = d\theta$, Eq. (3.6) can be rewritten as

$$c_n^{(1)} = \frac{in\omega}{4\pi^2 c_0 r_0}\sum_{\lambda=-\infty}^{\infty} e^{i(\lambda-n)\Theta}\int_{\Theta}^{2\pi+\Theta}\begin{bmatrix}\left(T_\lambda\cos\alpha + D_\lambda\sin\alpha\sin\theta\right)\times \\ \exp\left[i\left(n-\lambda\right)\theta - inM\sin\alpha\cos\theta\right]\end{bmatrix}d\theta\,, \tag{3.12}$$

where a superscript (1) is added to denote sound radiated by the interaction between one rotor blade with one strut. These integrations lead to Bessel functions of the first kind,

$$\int_0^{2\pi} \exp\left[i\left(\nu\theta - z\cos\theta\right)\right] d\theta = 2\pi i^{-\nu} J_\nu\left(z\right),$$

$$\int_0^{2\pi} \exp\left[i\left(\nu\theta - z\cos\theta\right)\right] \sin\theta d\theta = -2\pi i^{-\nu} \frac{\nu}{z} J_\nu\left(z\right),$$

$$J_{\nu-1}\left(z\right) + J_{\nu+1}\left(z\right) = \frac{2n}{z} J_\nu\left(z\right), J_{-\nu}\left(z\right) = \left(-1\right)^\nu J_\nu\left(z\right).$$

Hence

$$c_n^{(R1)} \approx \frac{in\omega}{2\pi c_0 r_0} \sum_{\lambda=-\infty}^{\infty} i^{-\nu} e^{-i\nu\Theta} \left[\left(T_\lambda \cos\alpha - \frac{\nu}{nM} D_\lambda\right) J_\nu(nM\sin\alpha)\right], \nu = n - \lambda. \quad (3.13)$$

Note that Eq. (3.13) is not valid for the strut sound or the stationary rotor since the angular position θ used in the expression of F_r in Eq. (3.10) is not related to the radiation time τ in the time integration of Fourier transform.

The unsteady point force exerted on the stationary struts by the rotation of the upstream wakes can be determined through the time-domain formula of Eq. (3.3), where $M_r = 0$, and r is a constant. The sound generated by the force fluctuation on the struts can be found in a similar process,

$$c_\lambda^{(S1)} = \frac{-i\lambda\omega}{4\pi c_0 r_0}\left[T_\lambda \cos\alpha + D_\lambda \sin\alpha \sin\theta_s\right] e^{i\lambda(\theta_R - \theta_s + M\sin\alpha\cos\theta_s)} \quad (3.14)$$

where the angular positions of the strut of index s and rotor of index j at time $\tau = 0$ are given as

$$\theta_s = \theta_{s0} + 2\pi s/S, \;\; \theta_R = \theta_{R0} + 2\pi\, j/B\,.$$

3.2 Acoustical interference of multiple blades

The sound from a rotor with B blades can be found by linear superposition of sounds from each blade, whose initial blade positions are given below,

$$\theta_R = \Theta + \left(j-1\right)2\pi/B, \;\; j = 0,1,2,B-1,$$

where Θ is the initial angular position of the first blade relative to the stationary observer. The summation over *B* blades gives

$$\sum_{j=0}^{B-1}\exp\left[-i\left(\theta_{R0}+jn2\pi/B\right)\right]=\frac{\sin\left(\pi n\right)}{\sin\left(n\pi/B\right)}\exp\left[-i\theta_{R0}-in\left(B-1\right)\pi/B\right]. \qquad (3.15)$$

For any interger *n*, one has $\sin(n\pi)=0$. The only non-trivial result is given when the denominator also vanishes. This occurs when $n=mB$, and the result is

$$c_{n=mB}=\frac{in\omega B}{2\pi c_0 r_0}\sum_{\lambda=-\infty}^{\infty} i^{mB-\lambda}\left[\left(T_\lambda\cos\alpha-\frac{mB-\lambda}{mBM}D_\lambda\right)J_{mB-\lambda}\left(mBM\sin\alpha\right)\right], \qquad (3.16)$$

which is exactly *B* times the sound radiated by a single blade. This contrasts with the superposition of random noise that might be radiated by *B* blades. Due to their incoherence, there is no coupling between sounds radiated by different blades, and the total sound energy would be *B* times that from a single blade, while the amplitude is only $\sqrt{B}$ times that from a single blade.

Similarly, sounds from the interaction of rotor with *S* struts can be found by the summation of Eq.(3.16),

$$\sum_{s=0}^{S-1} e^{i\lambda\left(\theta_{S0}+2\pi s/S\right)}=\frac{\sin\left(\pi\lambda\right)}{\sin\left(\lambda\pi/S\right)}e^{i\lambda\left[\theta_{s0}+(S-1)\pi/S\right]}.$$

Non-trivial result is found only when the frequency index $\lambda=kS$ when the sound radiated is exactly *S* times that from a single strut. Finally, the acoustical interference of *B* rotor blades interacting with *S* struts is found as

$$c_{n=mB}^{(rotor)}=\frac{in\omega BS}{2\pi c_0 r_0}\sum_{k=-\infty}^{\infty} i^{-\nu}\left[\left(T_{kS}\cos\alpha-\frac{\nu}{nM}D_{kS}\right)J_\nu\left(nM\sin\alpha\right)\right], \qquad (3.17)$$
$$\nu=mB-kS$$

where ν is the difference between the frequency indices of the perceived sound, *mB*, and the source component *kS*, both *m* and *k* are integers. The parameter ν is also

called the mismatching frequency index, and it plays a crucial role in the strength of sound radiation and its distribution pattern. Mathematically, it enters the formula as the order of Bessel functions.

Similarly, sound generated by *S* struts interacting with *B* rotor blades is given by

$$c_{n=mB}^{(strut)} = \frac{inBS}{2\pi c_0 r_0} \sum_{k=-\infty}^{\infty} i^{-\nu} \left[\left(T_n \cos\alpha - \frac{\nu}{nM} D_n \right) J_\nu \left(nM \sin\alpha \right) \right], \qquad (3.18)$$
$$\nu = mB - kS.$$

Comparing this result with Eq. (3.17), the only difference is the frequency index of the unsteady force. Sound waves from both rotor and stator are heard at the BPF and its multiples, $n = mB$. For the strut noise, the source frequency is also *n*, but the source frequency for the rotor sound, *kS*, can be different due to the Doppler effect of the moving source.

For the problem of the computer cooling fan, the Mach number *M* is very small, and typically $BM < 0.2$. The argument of the Bessel function, $z = nM \sin\alpha$, is very small except for very high frequencies. High frequency sound may not be a concern here since the source strength, T_n and D_n, may have decayed quite considerably in the first place. For small *z*, the Bessel function can be approximated as (Huang 2003)

$$J_0(z) \approx 1 - \frac{z^2}{4}, J_\nu(z)\big|_{|z|<<\nu} \approx \frac{1}{\sqrt{2\pi\nu}} \left(\frac{ze}{2\nu} \right)^\nu, \qquad (3.19)$$

and the comparison of the exact and approximate values are compared in Fig. 3.2.

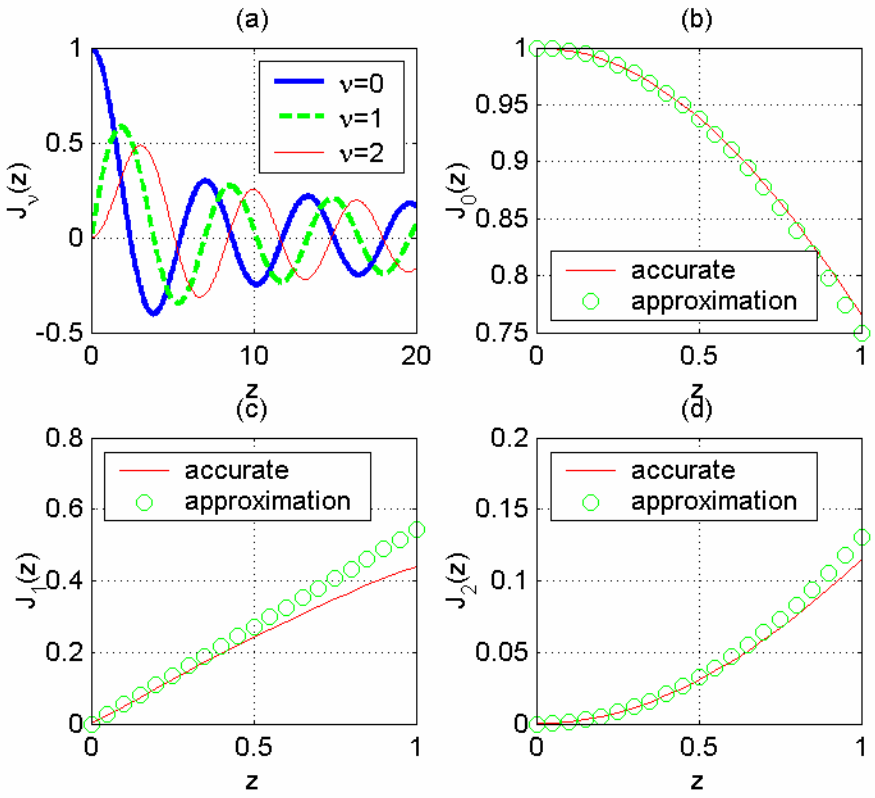

Figure 3.2 Exact Bessel function and its approximations. (a) Behaviors of the first three order; (b) the zero order at z<1; (c)the first order at z<1; (d) the second order at z<1.

The figure shows that, for small argument z, the value decays rapidly with the order ν, which is the index of the pressure spinning mode. The dominant interaction noise should have a small ν, and the following sections focus on |ν|=0,1,2.

For Gutin noise, the source frequency $\lambda = 0$, and the sound is radiated by the rotation of the steady loading only. The linear amplitude of the Gutin noise is:

$$\left|c_m^{(Gutin)}\right| = \frac{m\omega B^2 S}{2\pi c_0 r_0}\left(T_0\cos\alpha - \frac{D_0}{M}\right) J_{mB}\left(mBM\sin\alpha\right) \tag{3.20}$$

The directivity for this noise is illustrated in Fig. 3.3. It is essentially a drag noise since the thrust term T_0 is much smaller than the drag term D_0/M due to the small denominator M. Note that the order of the Bessel function becomes

$\nu = mB - kS = mB$ and is very large, the value of the function is extremely small since, for m=1, $|c_B| \propto J_B(MB) \propto BM^B$. More specifically, the amplitude of the Gutin noise is estimated below for the sample fan used in the experimental study.

If the area of the ventilation flow passage is A, and the mean inlet flow velocity is U. A volume flow rate of UA is created by the rotor at the free-delivery condition, which gives the total thrust and power transfer (P) as

$$T = A\frac{1}{2}\rho U^2, P = TU = D\omega R, \frac{T}{D} = \frac{\omega R}{U}. \tag{3.21}$$

At the free delivery condition, the volume flow rate Q is measured for the sample fan and is found to be 0.022m^3/s. The area A for the sample fan of tip radius R=45 mm is

$$A = \pi\left(R_{tip}^2 - R_{hub}^2\right) \approx \pi\left(0.045^2 - 0.017^2\right) = 0.0055 \text{ m}^2,$$

and the mean velocity is $U = Q/A = 0.022/0.0055 = 4$ m/s. The air density is $\rho = 1.225$ kg/m^3. For the fan operating at 50 rps, the tip rotating velocity is $\omega R = 2\pi 50R = 14.14$ m/s and $M = \omega R/c_0 = 0.0416$. The steady loading induces a thrust of T=0.054 N and drag D=0.0153 N. If the loading is even for all blades, the thrust and drag on each blade needs to be divided by the blade number B, i.e., $T_0 = 7.7mN, D_0 = 2.2mN$. The Gutin noise can be estimated for an observer at a distance of r_0=0.5 m on the rotational plane α=90^o,

$$\left|c_{m=1}^{(Gutin)}\right| = \frac{\omega B^2 S}{2\pi c_0 r_0}\frac{D_0}{M}J_B(BM)$$
$$= \frac{2\pi 50 \times 7^2 \times 4}{2\pi 340 \times 0.5} \times \frac{2.2 \times 10^{-3}}{0.0416} J_7(0.0416 \times 7) = 8.4 \times 10^{-10} \text{ Pa}$$

The sound pressure level for a sound of such peak amplitude is

$$SPL = 20\log_{10}\left[8.4 \times 10^{-10} / \left(\sqrt{2} \times 2 \times 10^{-5}\right)\right] = -90.5 \text{dB}.$$

Comparing with the measured SPL=50 dB from the actual fan, Gutin noise is indeed totally negligible.

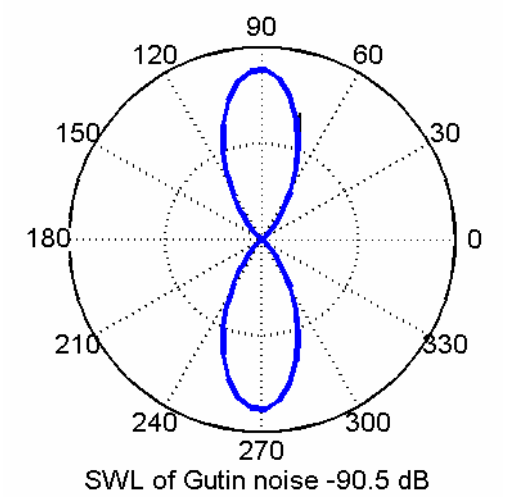

Figure 3.3 Sound intensity directivity of the Gutin noise

3.3 Modal directivity

Returning to Eq. (3.17) for the interaction rotor noise, it is noted that the source frequency index is *kS* because each blade experiences blockage by *S* struts during one cycle of rotation. The observed noise has the frequency index of *mB* because noise of other frequency components is cancelled out among themselves as *B* rotor blades all radiate sound with a certain phase relation. When the two indices coincide, *mB*=*kS*, the noise is rather loud since the noise radiation by all blade-strut interaction events is simultaneous and their sounds simply add up. This radiation is denoted here as the coincident mode. The reason why noise can also be made when the two frequency indices do not match, $\nu = mB - kS \neq 0$, is due to the Doppler effect of the source motion on the rotating blade. The strength of the Doppler effect is governed by the Bessel function $J_\nu(z)$ of order ν and argument $z = mBM \sin\alpha$. For small cooling fan operating at low speeds, normally *BM*<0.2, Eq. (3.19) gives the Bessel functions as

$J_0 \approx 1$, $J_1 \approx 0.54z$, and $J_2 \approx 0.125z^2$ for the orders of v= 0,1,2. Comparing the three values, the second order can be essentially ignored. The acoustic directivity of the drag and thrust noise components can be plotted according to Eq. (3.17) for v= 0,1 for the sound intensity with the phase angle marked by the signs of '+' and '-' on the lobes. Note that the result for $v = -1$ is similar to that of $v = 1$.

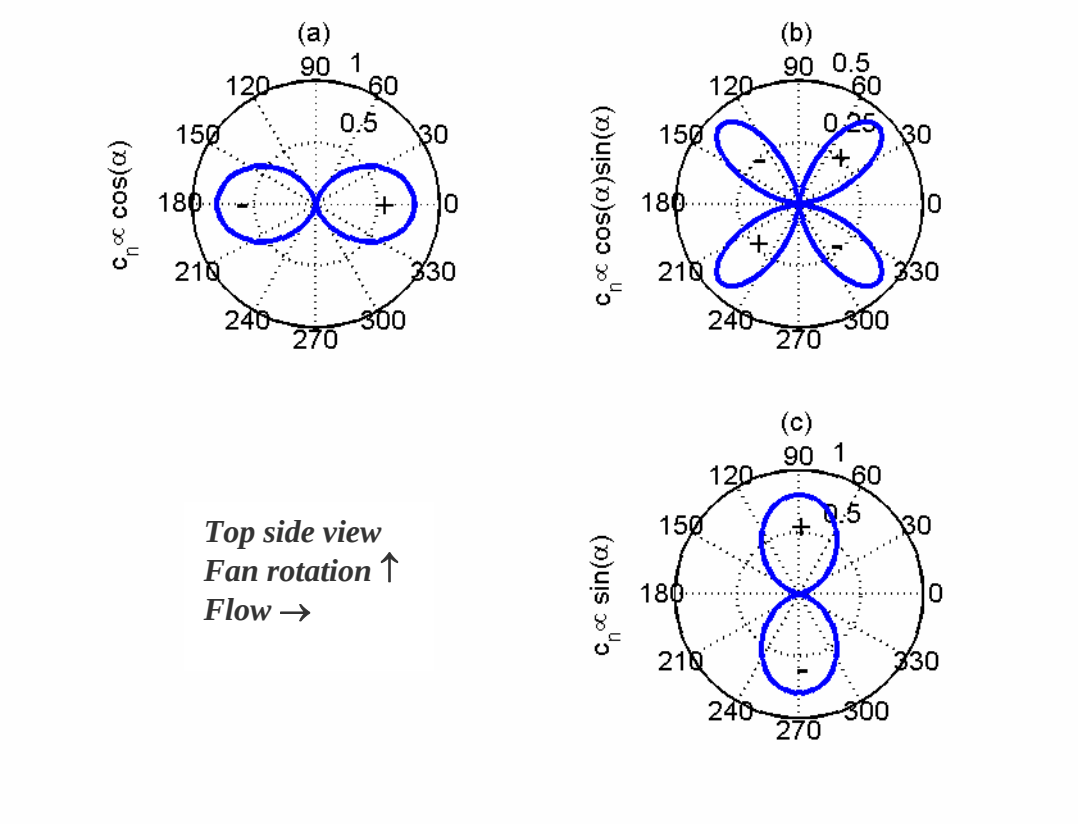

Figure 3.4 The modal directivity of fan sound with the leading modes of v=0 &1: (a) thrust, v=0; (b) thrust, v=1; and (c) drag, v=1,

The sound distribution patterns are determined by two factors. One is the nature of the source force, another is the motion of the source. When a source leaves the observer, the motion has the effect of decreasing the perceived frequency. When the source approaches the observer, the Doppler effect increases the perceived frequency. The

source motion also changes the source-observer distance *r*. More details are discussed below for each mode.

A. Coincident mode (the leading mode for the thrust noise), ν=0

The directivity pattern of the thrust component in the coincident mode of $\nu = n - \lambda = 0$ is plotted in Fig. 3.4 (a). The magnitude of the thrust sound is found from Eq. (3.17) by substituting $J_0(nM\sin\alpha) \approx 1$,

$$\left|c_{n=mB}\right| \approx \frac{m\omega B^2 S}{2\pi c_0 r_0} \sum_{k=-\infty}^{\infty} \left|T_{kS=mB}\cos\alpha\right|. \tag{3.22}$$

As usual, the axial dipole features the directivity factor of $\cos\alpha$. The drag term in Eq. (3.17) vanishes at ν=0. The drag force cannot radiate sound in the coincident mode. This is explained as follows. For the fundamental frequency of BPF, $m = 1$, $D_{\lambda=B}$ changes its direction once in a cycle when viewed from one rotor blade. When the blade rotates, the direction of the drag also changes once relative to the stationary observer. The result is that there is no change of the drag force for this particular frequency component, hence no sound is generated. Figure 3.5 (a) shows that, for the horizontal observer $\theta = 0, \pi;\ \ z = 0$, the drag cannot produce sound when it passes through the horizontal plane since the force is perpendicular to the horizontal plane. The highest sound pressure is expected to occur when it reaches the angular position of $\theta = \pi/2$ when the force almost points to the observer, but it is cancelled out by the sound generated by the drag force at the opposite position of θ=3π/2 as far as the frequency component $n = \lambda$ is concerned. In summary, only the thrust noise is significant noise at the coincident mode. It is generated by the simultaneous sum of

the thrust forces on all blades. The coincident mode is then called the leading mode for the thrust noise. In this mode, there is no drag noise.

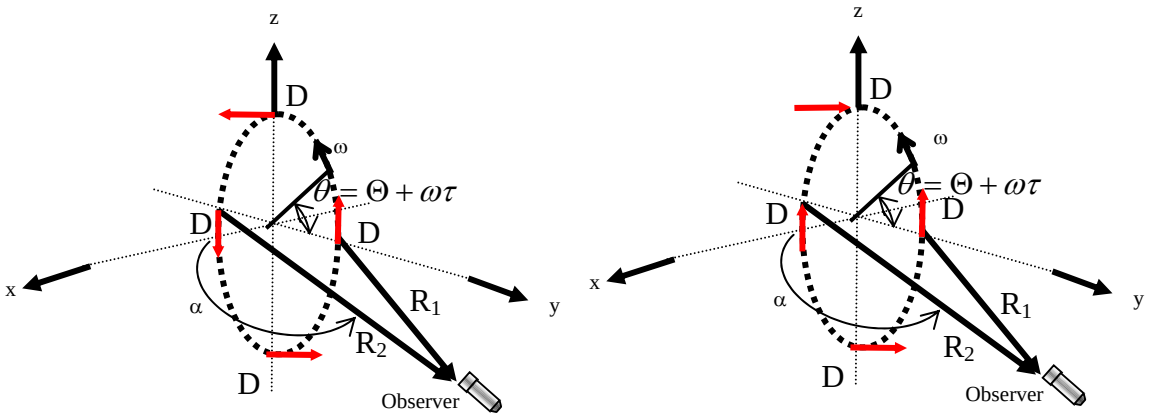

(a) (b)

Figure 3.5 Observed rotating drag by a stationary position at the fundamental frequency BPF: (a) v=0; (b) v=1

B. The first spinning pressure mode (the leading mode for drag noise, ν=1)

The noise distributions of the first spinning pressure mode or the mismatching mode are plotted in Figs 3.4 (b) and 3.4(c), in which $n-\lambda=1$. By substituting $J_1(z)\approx 0.54z$ into Equation (3.16), the linear amplitude of sound is found for the thrust and drag noise components, respectively.

$$\left|c_{n=mB}\right| = \frac{m\omega B^2 S}{2\pi c_0 r_0} \times \begin{cases} 0.54nM\left|T_{kS=mB\pm1}\cos\alpha\sin\alpha\right|, \\ 0.54\left|D_{kS=mB\pm1}\sin\alpha\right|. \end{cases} \tag{3.23}$$

The directivity of the thrust noise features (cosα sinα). Note that cosα is attributed to the thrust force projection and sinα is due to the Doppler effect. The 1st spinning pressure mode for the thrust noise belongs to the higher order noise generation. Figure 3.4(b) shows that it is a lateral quadrupole formed by two coupled dipoles. It differs from the jet noise quadrupole. The latter is the limiting case of two dipoles coupled together and most sounds from the dipoles are cancelled by each other, and the result is a true mathematical quadrupole. In contrast, the higher-order thrust noise is radiated

by tightly coupled dipoles. But the coupling is not that tight, and the sound radiated is not completely negligible. As is shown in later chapters, the higher order thrust noise is typically 10 dB below the leading mode dipoles.

For the mode of ν=1, the drag noise dominates. It becomes the leading mode with a sound amplitude directivity featuring sinα, as shown in Fig. 3.4(c). The mechanism of the leading mode drag noise generation is illustrated in Fig. 3.5(b) for the simplest case of fundamental BPF, m=1. The drag component on a rotor blade $D_{\lambda=B\pm1}$ is a rotating force oscillating once in each blade rotational cycle. For the horizontal observer, the noise is generated by two variations of the force direction and distance r. In terms of the amplitude of the radiated sound, the maximum appears in the rotational plane. This is explained as follows. On the rotational axis, α=0,π, the drag force has no projected component. In addition, r hardly changes when the force rotates. When the observer is in the rotational plane, α=π/2, r changes most dramatically. The maximum drag force projection on the source to the observer is also obtained at $\alpha = \pm\pi/2$, as shown in Fig. 3.5(b), since the projected component of the drag noise to the receiver is $D_\lambda \sin\alpha$.

Mathematically, the loudest drag noise is heard when $\nu = \pm 1$, as can be seen from the presence of $mBM \propto z$ in the denominator in Eq. (3.17). It means that the drag noise in the first pressure spinning mode has the order of $\left(z^0\right)$, which is equivalent to the coincident mode of the thrust noise. The drag noise radiated in the mode of $\nu = \pm 1$ is denoted as the leading-mode radiation, which is, in principle, equally noisy as the coincident mode or the leading mode thrust noise.

3.4 Sound power integrations

Refer to the angular position given by Eq. (3.15), where θ_{R0} in the exponential function, $\exp(-i\theta_{R0})$, is the initial position of the rotor blade relative to the observer assumed to be at θ=0. This exponential term has effect on the amplitude of the radiated sound. Note that, for a certain initial rotor position, θ_{R0} signifies the observer position relative to the initial rotor position. In other words, $\exp(+i\theta_{R0})$ represents the directivity of the observed sound. Since $|\exp(+i\theta_{R0})|$=1, the latitudinal angular position of the observer has no effect on the observed sound. Therefore, the observed sound in terms of intensity $I(\alpha,\theta)$ can be simplified by $I(\alpha)$ to calculate the sound power integration by one horizontal plane measurement on the plane of z=0, as shown by Eq. (2.2). The sound power integration thus becomes

$$W_n = \int_0^{\pi} \frac{|c_n|^2}{2\rho_0 c_0} 2\pi r_0^2 \sin\alpha d\alpha \tag{3.24}$$

where complex $c_{n=mB}$ is given in Eqs (3.17) and (3.18) for the rotor sound and struts sound, respectively. Before carrying out the above integration, there are two possible acoustic interferences that need to be considered. First, sound radiated at one frequency, such as $n=mB$, can be originated from different sources, some from the source with the same frequency, and some from sources at neighbouring frequencies shifted by the Doppler effect. The latter can also be called the Doppler sound. The second interference is between sounds from the thrust and drag forces.

For the first type of interference, the following investigation is conducted. If the sound radiated with the Doppler effect is significantly smaller than the leading mode radiation, it can be neglected, and the formulation would become more tractable. To

examine the significance of the Doppler sound, the following estimations are carried out for the dominant BPF tone of the computer cooling fan. Assuming that $BM<0.2$ for this kind of fan, so the magnitude of the argument $|z|=BM|\sin\alpha|<0.2$. Using the moderately high value of $z=0.2$, the ratio of the Doppler thrust noise to the leading order thrust noise is $J_{\nu+1}(z)/J_{\nu}(z)$ is 0.1,0.05,0.03 for $\nu=0,1,2$, respectively. The highest ratio 0.1 means $-20\log_{10}(0.1)=20$ dB difference. For the drag noise, the ratio of amplitudes is $(\nu+1)J_{\nu+1}(z)/[\nu J_{\nu}(z)]$, which is 0.1,0.05 for $\nu=1,2$, respectively, again at least 20 dB difference. In short, in carrying out sound power integrations, only the sound from the lowest order mode needs to be considered.

For the second type of interference, one has $J_{\nu}(z)\propto z^{\nu}$, and the total sound shown in Eq. (3.17) can be rewritten as follows,

$$c_n=\left(aT_{\lambda}\cos\alpha+bD_{\lambda}\right)\sin^{\nu}\alpha, \tag{3.25}$$

where a and b are constants carried over from terms in Eq. (3.17) when the asymptotic formula of Eq. (3.19) is substituted.

$$\left.\begin{aligned}
&W_n\propto\int_0^{\pi}\left(aT_{\lambda}\cos\alpha+bD_{\lambda}\right)^2\sin^{2\nu+1}\alpha d\alpha\\
&=\int_{\pi}^{0}\left(a^2T_{\lambda}^2\cos^2\alpha+b^2D_{\lambda}^2\right)\left(1-\cos^2\alpha\right)^{\nu}d\cos\alpha\\
&=C_T\left(\nu\right)a^2T_{\lambda}^2+C_D\left(\nu\right)b^2D_{\lambda}^2,\\
&C_T(\nu)=2\int_0^1x^2\left(1-x^2\right)^{\nu}dx,C_D(\nu)=2\int_0^1\left(1-x^2\right)^{\nu}dx.
\end{aligned}\right\} \tag{3.26}$$

The term that involves the thrust-drag coupling, $T_{\lambda}D_{\lambda}$, vanishes in the integration. As a result, the sound powers contributed by T_{λ} and D_{λ} can be integrated individually.

Finally, the total sound power is given below

$$W_n = \frac{(nBS\omega)^2}{4\pi\rho_0 c_0^3}\left[T_\lambda^2 W_{n\lambda}^{(T)} + D_\lambda^2 W_{n\lambda}^{(D)}\right], \tag{3.27}$$

where the power coefficients are

$$W_{n\lambda}^{(T)} = \int_0^\pi \cos^2\alpha J_\nu^2 \sin\alpha d\alpha,\ W_{n\lambda}^{(D)} = \int_0^\pi \left(\tfrac{\nu}{nM}\right) J_\nu^2 \sin\alpha d\alpha \tag{3.28}$$

and the results are given in the following table for the two leading order modes.

Table 3.1 The coefficients of sound power from the two forces

Mode \ Power coefficients	$W_{n\lambda}^{(T)}$	$W_{n\lambda}^{(D)}$
ν=0	2/3	0
ν=1	$1.25(nM/4)^2$	0.39

A few observations are made:

- For the coincident mode of $\nu = mB - kS = 0$, noise is mainly made by the unsteady thrust.
- For the first spinning pressure mode of $\nu = \pm 1$, the drag noise dominates over the thrust noise in terms of the noise generation ability.
- For the higher order modes of $\nu = \pm 2$, the noise generation ability of all force components is reduced. The drag noise is dominant when compared to the thrust noise. It can be understood that the drag noise induced by the rapid change of direction has more strength than the thrust force under the Doppler effect.
- The source radius *R* is involved in the rotation Mach number *M*. When the sound power does not contain *M*, the location of the source does not make any difference; the sound radiation in this situation is said to be in the leading mode. The leading mode for the thrust noise is $\nu = 0$, while that for the drag

noise is $v = \pm 1$. The sound intensity of these particular modes is only a variable of the latitudinal angular position of α.

- For the potential flow, the unsteady force is proportional to the mean flow speed, so that $T_\lambda^2, D_\lambda^2 \propto M^4$ in Eq.(3.27) . The power dependency for a given geometrical shape can be expressed as $W \propto M^6 R^2 W_{n\lambda}^{(T,D)}$. For each leading mode, the dominant component of $W_{n\lambda}^{(T,D)}$ is a constant, so the sound power follows the 6th power law with respect to the Mach number. For the secondary mode radiation, it becomes at least the 8th power law, depending on the circumferential order v and the force component concerned.
- The thrust noise and the drag noise are decoupled in power calculations due to their othorgonal directions. The total sound power is the sum of three component sounds. When the radial force is neglected, the sound power is the summation of the thrust and drag noise.

3.5 Near field effect

Normally, a compact source (dipole) model is appropriate when the source size is small compared to the wavelength of the radiated sound. A simple point dipole source of fluctuating force along the *x* direction located at the origin

$$F_x = Ae^{i\omega t} \tag{3.29}$$

radiates sound with the following pressure and particle velocity (Dowling 1998)

$$\left.\begin{aligned} p\left(\vec{x},t\right) &= \frac{ik\cos\alpha}{4\pi r_0}\left(1+\frac{1}{ikr_0}\right)F_x e^{i\omega t} \\ u_r &= \frac{ik\cos\alpha}{4\pi\rho_0 c_0 r_0}\left(1+\frac{2}{ikr_0}-\frac{2}{k^2 r_0^2}\right)F_x e^{i\omega\left(t-r_0/c_0\right)} \\ u_a &= \frac{\sin\alpha}{4\pi\rho_0 c_0 r_0^2}\left(1+\frac{1}{ikr_0}\right)F_x e^{i\omega\left(t-r_0/c_0\right)},\ u_\theta = 0 \end{aligned}\right\} \tag{3.30}$$

where α and θ are the latitudinal and longitudinal angles using the force direction as the axis of symmetry. The exact sound intensity is $I = \frac{1}{2}\mathrm{Re}\left(pu_r^*\right)$, where u_r^* is the conjugate of the radial component of the acoustic particle velocity. However, the particle velocity can only be measured by intensity probes. With one microphone, what is measured is the local pressure which consists of both far field and new field contributions. If the measured pressure, p_{rms}, is taken as the far field pressure, sound intensity can be approximated by $I = p_{rms}^2/\left(\rho_0 c_0\right)$. Ideally, the measurement microphone is placed as far away as possible from the source, but a close proximity is necessary if the source is weak and a good signal to (electronic) noise ratio is desired. The compromise chosen in the experiment is r_0=0.5 m. The far-field approximation can be assessed by comparing the sound power integration calculated by the far field approximation with the one calculated with the exact intensity formula. This is shown in Fig. 3.6. The frequency used for the assessment is the fundamental BPF of 350Hz, which represents the frequency at which the near effect is the strongest. The

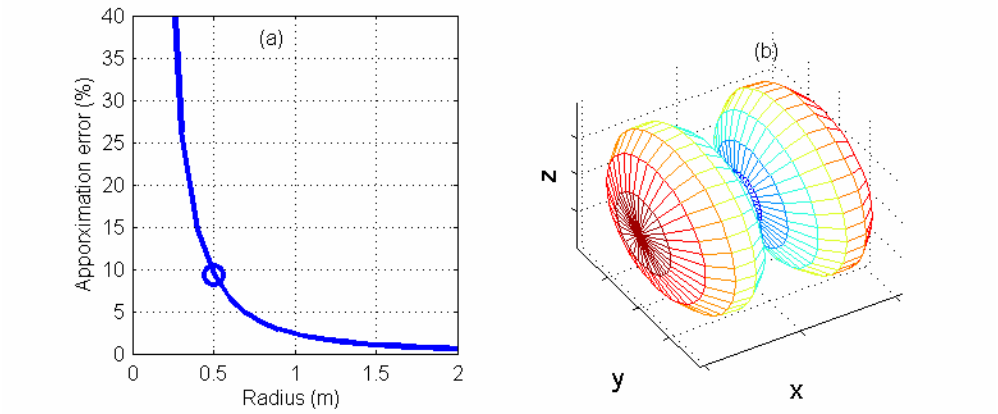

Figure 3.6 The far field approximation. (a) Comparison sound intensity and far field term only. (b) Sound intensity at r_0=0.5m

percentage error is shown in Fig. 3.6(a), and the approximated sound intensity is shown in Fig. 3.6(b). The error caused by the far field approximation for r_0=0.5 m is

about 9%, which is marked as an open circle in Fig 3.6(a). The error translates into a dB value of $10\log_{10}(1+0.09)=0.37$, which is deemed acceptable.

Chapter 4 Source separation and design optimization

In this section, we set out to investigate the source mechanisms responsible for tonal noise radiation in the real cooling fan, and attempt to quantify each source mechanism. The noise emitted by the thrust and drag components are measured by the two configurations for the leading radiation modes of $\nu = 0, \nu = \pm 1$, respectively. The sound radiation of the coincident mode is simply added up by the event on every blade, it can be applied to quantify the force fluctuations on one blade. The quantification of this method is then used to predict the interaction sound of other configurations, and the results are compared with the experimental measurement. Some success is achieved.

Apart from the basic findings in the rotor-strut interaction, the investigation continues to reveal other source meachanisms. One prominent noise source is the inlet flow distortion, and the other is the unequal size of struts. Corrective measures are taken to eliminate the inlet flow distortion and reduce noise caused by unequal struts with significant noise reductions. Together with the shift of the leading mode radiation to a higher order mode radiation by changing the strut number, the total tonal noise reduction from the original sample fan is about 12 dB.

4.1 Sound source separation

In Chapter 3, we find that the radiation of the thrust and drag noise is most effective in their leading modes. The structure of the sample fan is modified to give such leading modes in this section. The experimental investigations of the leading mode configuration serve two purposes: (a) the validation of the modal directivity, and (b)

the separation of the thrust and drag noises by the directivity characteristics of each component.

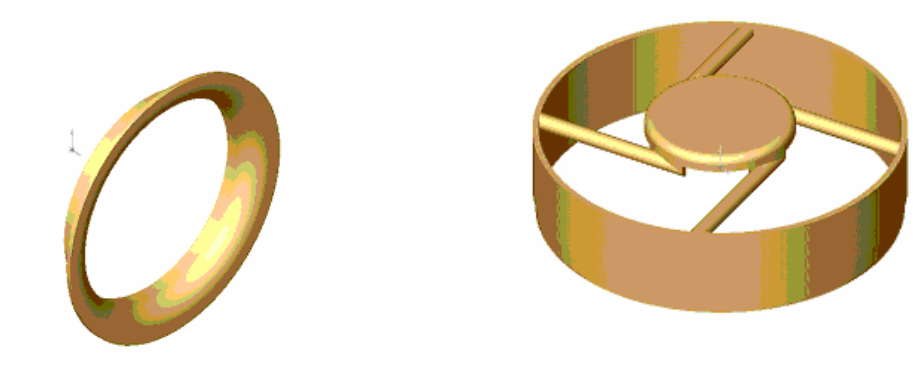

(a) (b)

Figure 4.1 The modifications of the fan by using (a) a bellmouth, and (b) four equal struts with motor base.

As discussion in Chapter 2, the square inlet frame can contribute significantly to the rotary noise from its four sharpe edges. In order to concentrate on the interaction between the rotor blades and downstream struts, the square inlet frame is replaced by a full-circle bellmouth. The modification of the fan features are manufactured by a prototyping machine using a plastic material, as shown in Fig. 4.1(a) for the full-circle bellmouth. Figure 4.1(b) is a configuration of four equal struts attached to the motor base. The struts are 4 mm in diameter. In all the fan configurations for the measurements, the axial distance between the blade trailing edge and the strut leading edge is 3 mm, which is the same as the sample fan.

Before the experimental investigations, the directivity separations of noise components are introduced. For the leading mode, the thrust beams in the rotational axis direction with a sound pressure directivity of $\cos(\alpha)$, while the drag is in the rotational plane with pressure directivity of $\sin(\alpha)$. The separation of the next higher

order modes is determined by the distribution function of $T_1 \propto \cos\alpha \sin\alpha$, $D_2 \propto \sin^2\alpha$. The modal directivities of the two leading orders and the higher order radiation modes are shown in Fig. 3.4.

During the measurement, the fan stands upright in free space, the horizontal cross section of the observer sphere of radius r_0 can be divided into four quadrants according to ϕ, as shown in Fig. 2.3(a). The sound pressure measured in the symmetrical positions of the four quadrants, denoted as p_1, p_2 , p_3, p_4, can be combined in time-domain to separate the thrust noise p_T and drag noise p_D. With reference to flow stream direction, p_1 and p_4 are located in the upstream while p_2 and p_3 in the downstream, the leading mode components can be represented by the pressure measured on the four quadrants:

$$\left.\begin{aligned} p_{T0} &= \frac{p_1 - p_2 - p_3 + p_4}{4}, \quad p_{T1} = \frac{p_1 - p_2 + p_3 - p_4}{4} \\ p_{D1} &= \frac{p_1 + p_2 - p_3 + p_4}{4}, \quad p_{D2} = \frac{p_1 + p_2 + p_3 + p_4}{4} \end{aligned}\right\} \tag{4.1}$$

where the numeric subscripts 0,1,2 indicate ν. The drag D is related to the thrust T through the unsteady force on a representative rotor section (airfoil) of pitch angle β: $T = -L\cos\beta$, $D = -L\sin\beta$, where the unsteady force is the reaction of the aerodynamic lift exerted on the air and denoted as $-L$. For the fan used in the present studies, interaction occurs near the trailing edge of the rotor blade and near the tip region of the rotor span. The local pitch angle $\beta \approx 45^\circ$. For the purpose of the estimation, $T \approx D$ can be assumed. Of course, the assumption is not suitable for the force on the struts. One of the purposes of the experimental studies is to validate an intuitive expectation that noise is mainly radiated by the rotor, for which this approximation would give consistent deductions.

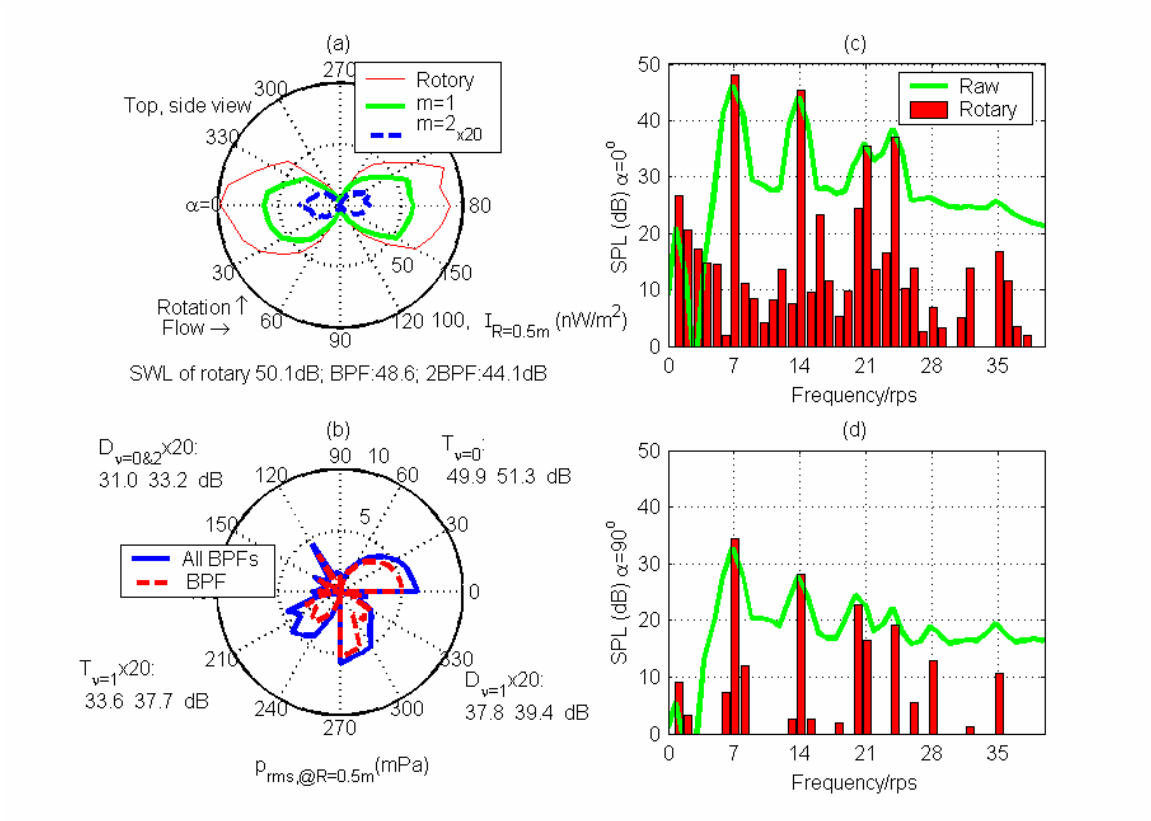

Figure 4.2 Directivity of the fan seven struts and a bellmouth. (a) Experimental rotary noise. (b) Decomposition of modal directivity (T_0,T_1,D_1,D_2). The typical spectral of the leading mode ($v=\pm1$) at (c) $\alpha=0$, and (d) $a=\pi/2$.

When the numbers of the rotor blades and struts are the same, $B=S$, the frequencies of source and its radiation coincide for all the harmonics, $m=1, 2, 3\ldots$. This configuration isolates the thrust noise from the drag noise, in which the drag noise is cancelled out by the phase shifting of the rotating blade. The sample fan has seven blades, so the seven struts with even spacing are designed for the coincident mode with a denotation of S7. The basic experimental procedure given in Chapter 2 is followed. The experimental investigations start from the measurement of the coincident configuration of S7. The results of the coincident mode are plotted in Fig. 4.2.

Figure 4.2(a) shows the sound intensity directivity for the rotary sound (thin solid line), the first BPF tone (solid line), and the second BPF tone (dashed line). The flow is drawn from left to right. The sound power level (SWL ref 10^{-12}Watt) is labeled on the bottom of the polar plots. The rotating axial dipole pattern demonstrated in Fig. 4.2(a) agrees with the expectation of the leading mode thrust noise radiation. As expected, the *S*=*B* configuration radiates sound with ν=0 for all BFP harmonics, for which the first two are shown in Fig. 4.2.

Figure 4.2(b) plots the contributions from the components separated by Eq. (4.1) with the labels to show the sound power levels. The first quadrant shows the distribution of the dominant thrust noise at the coincident mode, T_0, for the BPF component (dashed line) and the sum of all BPF harmonics (solid line, denoted as BPFs). The sound power levels for the two are SWL=49.9 dB and 51.3 dB. Theoretically, the only spinng pressure modes available to radiate sound is $\nu = 0, B, 2B, \cdots$. Since the modes of order 2 and above are numerically insignificant, the only mode available is ν=0. For this mode, there is thrust noise and, according to Huang (2003), radial noise which behaves as a higher order mode and it is indistinguishable from the drag noise. In reality, all modes can be found according to the separation methods of Eq.(4.1) . Bearing these in mind, the drag noise with the even modes, $D_{0\&2}$, is given in the second quadrant and is amplified by 20 times for clarity. The sound power levels for $D_{0\&2}$ are 31.0 dB and 33.2dB for BPF and BPFs, respectively. This is a very low level compared with the SWL for T_0. In this regard, the experiment agrees very well with the theoretical expectation that the noise from the coincident rig is only radiated by the leading order mode T_0. The first order mode components of T_1 and D_1 are plotted in the third and forth quadrants, respectively. Again, the SWL levels of 33.6, 37.7dB

for T_1 noise, and 37.8, 39.4dB for D_1 noise are all well below the dominant T_0 noise. The sound power levels are, however, relatively higher. The occurrence of T_1 and D_1 noise in reality can be explained as follows. Blades on the rotor may differ from one another due to geometry, or aerodynamic loading. The effect of such difference is equivalent to having a strut of S=1, which causes noises of mode ν=1. One factor in the low-cost small cooling fan is that the chord lengths of airfoil of the seven blades are not identical, nor are the distance between the blade trailing edge and the downstream struts. Secondly, there is natural variation of sound radiation from one cycle to the next in every direction. Since the four pressure signals, $p_{1\text{-}4}$, used in Eq. (4.1) are taken at different measurements, they would have such natural variation and the difference of such variation between two positions could be a pseudo source of T_1 and D_1 noises.

Figures 4.2(c) and 4.2(d) show two spectra for the axial point of α=0 and the rotational plane α=90^o, respectively. A rather regular decline of sound pressure level with the harmonics index is observed. This phenomenon is explained below. It is assumed that the lift experienced by a rotor blade passing over S struts is a pluse train of height C_L. A model of aerodynamic interaction lift is given by Huang (2003) for the Fourier components,

$$L_{\lambda=kS} = C_L \Big/ \left(Sk^2\right) \tag{4.2}$$

where C_L depends purely on the kinematics of how a strut interacts with the blade rows. Substituting n=mB and Eq. (4.2) into Eq. (3.17), one has

$$c_{n=mB}^{(rotor)} \propto \frac{m\omega B^2 S}{2\pi c_0 r_0}\left(\frac{C_L}{Sk^2}\right) \tag{4.3}$$

Substituting k by mB/S for the coincident mode of $mB=kS$, the above expression becomes

$$c_{n=mB}^{(rotor)} \propto \frac{\omega S^2 C_L}{2\pi c_0 r_0 m} \tag{4.4}$$

Therefore, the sound power, which is proportional to $\left[c_{mB}^{(rotor)}\right]^2$, decays with the harmonic index as m^{-2}.

The leading mode of the drag noise component is configured by an assembly of the same rotor with 7 blades in a casing with four equal struts, the rig is denoted as S4. Equation (3.23) predicts that the only effective radiation mode for the first BPF is $\nu = mB - kS = -1$ for m=1, k=2. There is a leading mode drag noise, while thrust noise is of higher order mode radiation. For m=2, the leading mode is $\nu = mB - kS = \pm 2$ for k=3,4. Noise from both drag and thrust is of higher order mode. The experimental results are shown in Fig. 4.3 in the same way as in Fig. 4.2. As shown in Fig. 4.3(a), the rotary noise (thin solid line) and the first BPF (thick solid line) display a pattern close to sin(α), confirming the drag dipole on the rotational plane. The second harmonic (m=2, dashed line) is found to be low; its pattern is shown by 20 times amplification and it does not look like a dipole. This is consistent with the above prediction of $\nu = \pm 2$.

The decomposition of the source mode is shown in Fig. 4.3(b). The dominant source is from D_1, which has 39.8 dB for the first BPF, only 0.1 dB lower than the overall contribution from all BPF tones. It means that the contributions from other harmonics are trivial. The contribution from the mode of T_0 is also plotted for the BPF and all

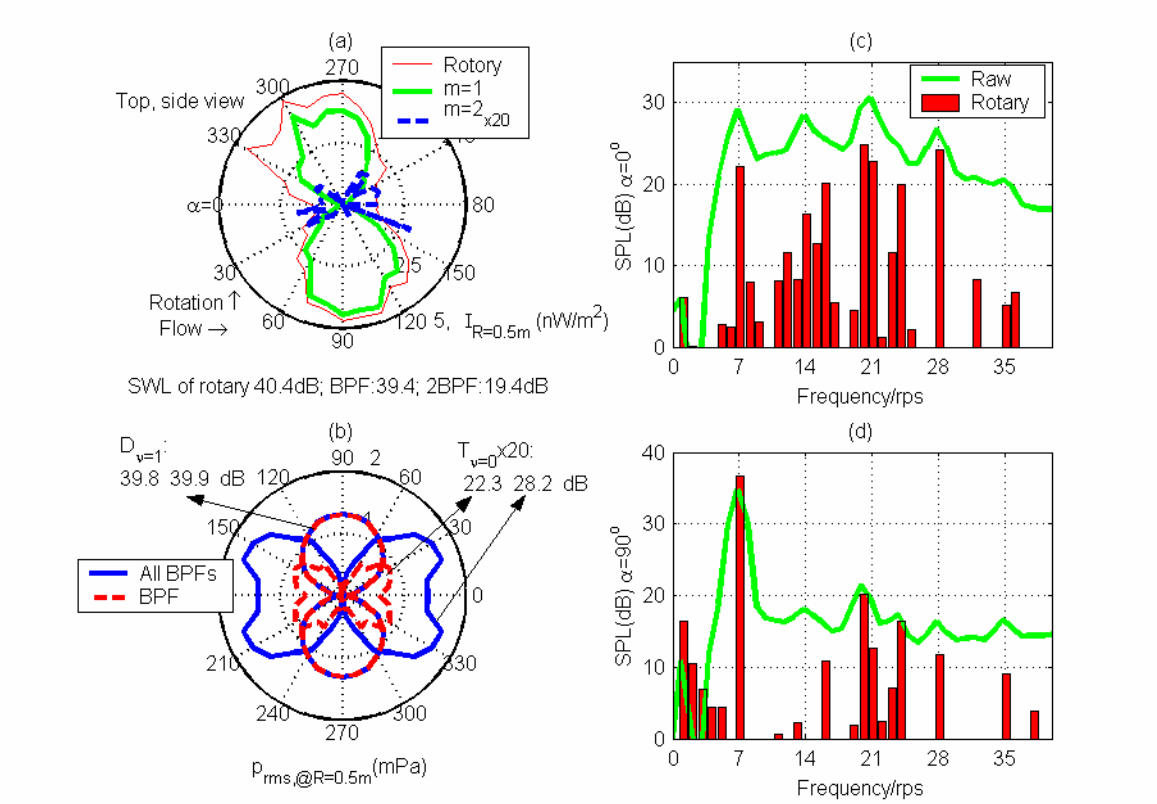

Figure 4.3 Directivity of the fan with four struts and a bellmouth. (a) Rotary noise. (b) Decomposition of modal directivity (T0, D1). The typical spectral of the leading mode ($v=\pm1$) at (c) $\alpha=0$, and (d) $\alpha=\pi/2$.

BPFs. Since their levels are low, the amplitudes are amplified 20 times. The SWL for T_0 is only 23.3 dB for the BPF and 28.2 dB for all BPFs, both considerably lower than the SWL for D_1, validating again the large difference between the leading mode noise and the higher order noise. In fact, the configuration of B=7 with S=4 contains another leading mode radiation for the thrust noise at the harmonic of m=4: $v = mB - kS = 0$ for k=7. The actual level of this harmonic is not as high as the first BPF due to the high harmonic index. But there is still considerable contribution to make for the total T_0 noise and this is reflected by the 5.9 dB difference between the first BPF T_0 noise and the T_0 noise for all BPFs. Due to the combination of the leading mode drag radiation with the leading mode thrust noise radiation, the resulting rotary noise pattern is a little tilted away from the rotational plane, as shown in Fig. 4.3(a).

Fiures 4.3(c) and 4.3(d) show the spectra at the inlet and rotational plane ($\alpha = 0,\ \pi/2$) points, respectively. As shown in Fig. 4.3(d), the noise from D_1 is very high at the rotational plane $\alpha = \pi/2$, while the spectrum becomes more like a white noise at the inlet position of $\alpha = 0$ shown in Fig. 4.3(c). Such difference is expected since the drag force direction changes most dramatically on the rotational plane, while the projection of forces along the rotational axis is small and it hardly changes. The contribution of T_0 noise at the 4th BPF is more significant for the axial direction $\alpha = 0$ shown in Fig. 4.3(c) than the rotational plane $\alpha = \pi/2$ shown in Fig. 4.3(d), which again validates the assertion of the leading mode radiation of thrust noise at m=4.

4-2 Noise from a single strut

The case of a single strut is rather special. Its interpretations can go a long way to validate many aspects of the point source formulation. The interaction noise from the single strut with the rotor blades is a combination of the two leading modes, $\nu = 0$ and $\nu = \pm 1$. The sound amplitude of the rotor interaction with the single blade is:

$$c_{n=mB}^{(rotor)} = \frac{inB\omega S}{2\pi c_0 r_0} e^{i\lambda\Theta_{S0}} (-i)^{\nu} \left(T_{\lambda} \cos\alpha - \frac{\nu}{nM} D_{\lambda} \right) J_{\nu}(nM \sin\alpha) \qquad (4.5)$$

for one particular source mode λ, where S=1, λ=kS=k is an integer, n=mB. Θ_{S0} is the initial angular position of the strut. For the leading mode of the thrust noise, the parameter is $\nu = 0$, $\lambda = n = 7$, the sound is radiated by the force component of T_7. The situation for the leading mode of drag noise is more complex. In the leading mode of $\nu = -1$, the drag component D_6 radiates sound. In another leading mode of $\nu = 1$, the sound is generated by drag component D_8. The interference of the two drag components is determined by the phase difference. The phase of the drag component

is given by the term of $\left[e^{i\lambda\Theta_{S0}} \left(-i\right)^{\nu} \right]$ in Eq. (4.5) . When the strut is perpendicular to the horizontal observing plane, $\Theta_{S0} = \pi / 2$, the phase of the component D_6 is $e^{i6\frac{\pi}{2}}(-i)^{-1} = e^{-i\frac{\pi}{2}}$, that for D_8 is $e^{i8\frac{\pi}{2}}(-i)^{1} = e^{-i\frac{\pi}{2}}$, the radiation of D_6 and D_8 is in phase. When the strut turns 90° , i.e., $\Theta_{S0} = 0$, the radiation of the two components becomes antiphase. The combined leading mode noise is

$$c_{n=B}^{(rotor,S1)} = \frac{iB^2\omega}{2\pi c_0 r_0}\left[T_7 \cos\alpha + i \sin\alpha \left(D_6 e^{-i\Theta_{S0}} - D_8 e^{i\Theta_{S0}} \right) \right]. \tag{4.6}$$

The experimental investigation is designed to demonstrate the combination mode of the single strut. The testing rig denoted as S1 consists the fan rotor installing in a big bellmouth with 10 mm flaring radius. A circular cylindrical strut of 4 mm in width is fixed on the exit of the bellmouth frame to simulate the strut of the sample fan which is 4 mm in diameter. The measured noise radiation is shown in Fig. 4.4. Figures 4.4(a) and 4.4(c) show the results of the vertical strut, while Figs. 4.4 (b) and 4.4(d) are for the horizontal strut orientation. The directivities of the acoustical intensity of both configurations are tilted, which is caused by the combination of the two leading modes associated with the thrust force in the axial direction and that from the drag force in the circumferential direction. Comparing Fig. 4.4(a) with Fig. 4.4(b), it is found that the latter is more tilted towards the axial direction, implying that the drag noise is more in Fig. 4.4(a) than in Fig. 4.4(b). This is consistent with the earlier prediction of in-phase radiation of drag noise from D_6 and D_8 components for a vertical strut. The decompositions of the noise are given in Figs 4.4(c) and 4.4(d) for the two configurations respectively. In both cases, the sound power for the thrust noise is around 38 dB for the BPF, and 39 dB for all BPFs. The thrust noise is the

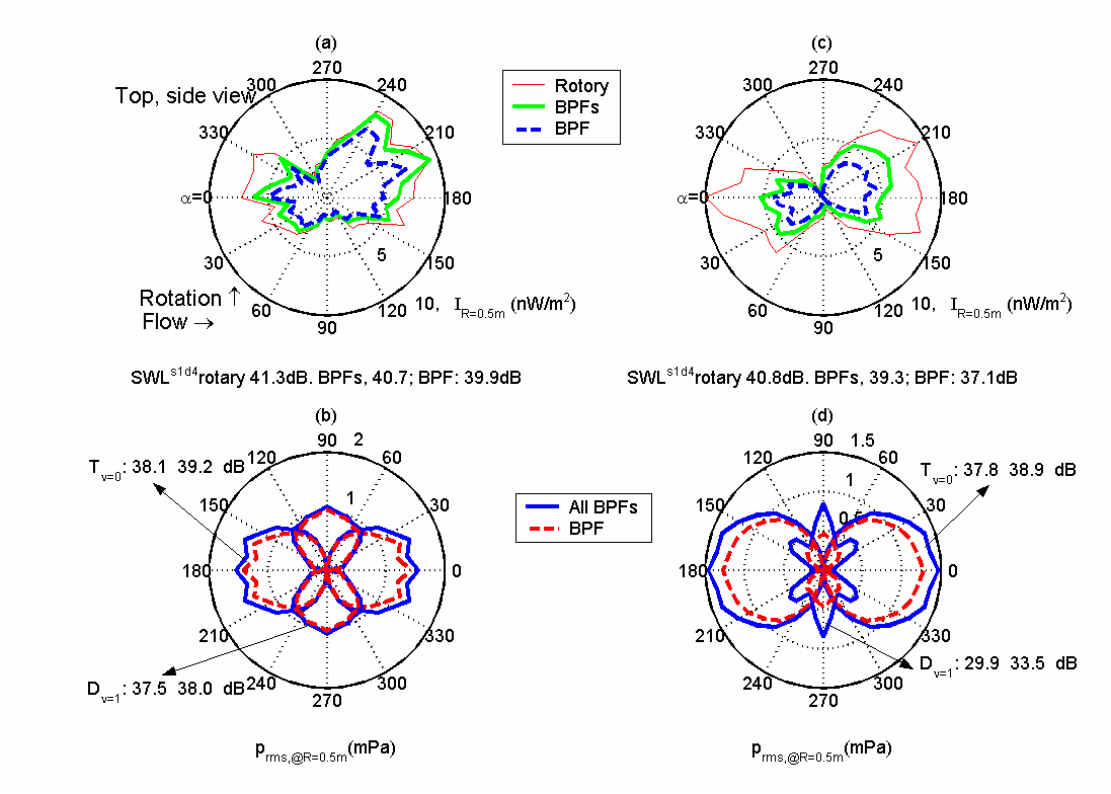

Figure 4.4 Directivity of the fan with a 4mm wide strut and a bellmouth. (a) Rotary noise when the strut is placed vertically. (b) Noise decomposition of (a). (c) Rotary noise when the strut is placed horizontally. (d) Noise decomposition of (c).

same for the two cases because it is generated by T_7 only. The drag noise from the vertical strut is 37.3 dB on the BPF, while it decreases to 29.9 dB for the horizontal strut. The significant difference of 7.4 dB validates the expected acoustic interference between D_6 and D_8 given in Eq.(4.6).

4.3 Noise from a fan with unequal struts

When the square inlet frame of the original fan is replaced by the full-circle bellmouth, as shown in Fig. 4.1(a), the unequal strut size becomes the only extra noise generation feature. The downstream struts include three regular struts with 4 mm diameter and one cable-carrying strut of 6 mm in diameter. The effect of the extra strut size is investigated here by modifying the S4 rig described above. One of the struts is made

to be 6 mm in width. The new rig is denoted as S13, implying one large strut with 3 regular struts. The measured noise is shown in Fig. 4.5.

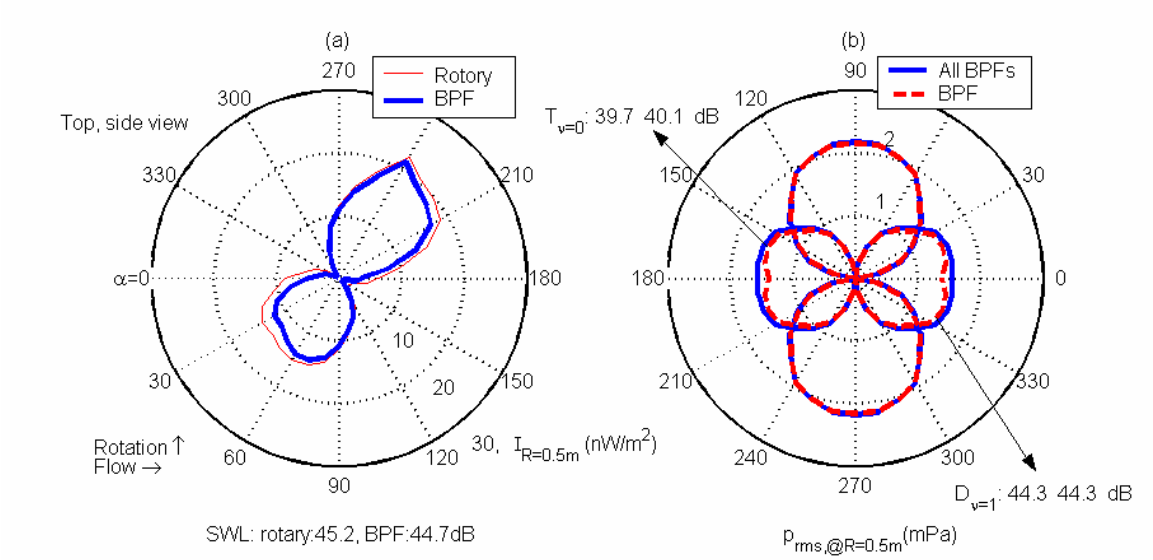

Figure 4.5 Directivity of one large strut with 3 equal struts and a bellmouth. (a) Rotary noise. (b) Decomposition of modal directivity (T_0,D_1).

The rotary noise is shown in Fig. 4.5 (a) as the thin solid line, and the sound power is 45.2 dB. It has a tilted pattern. The BPF noise is shown in thick solid line with a similar pattern and a similar SWL of 44.7dB. The results are now compared with the sound radiation by the S4 rig shown in Fig. 4.3. For the rotary noise, the difference between S13 and S4 represents the extra noise caused by the extra strut size, which is the single strut radiation. The extra drag noise from the extra size of the large strut is proportional to the interference of $|D_6 + D_8|$ as the large strut in S13 is put in the vertical position, while the extra thrust noise is proportional to T_7. The extra thrust makes the rotary noise more titled towards the rotational axis direction. The noise decompositions are shown in Fig. 4.5(b). For BPF noise, the leading mode thrust noise, denoted as T_0, is 39.7 dB, which is much higher than the 22.3 dB found in the S4 rig. In fact, the T_0 noise approaches the similar to the 39.8 dB drag noise from S4. The 44.3 dB drag noise from S13 is also much higher than the drag noise of S4. It

implies that the extra noise from the extra size strut is not a small contribution, and is responsible to the very titled noise pattern of S13.

In order to quantify the contribution of the extra strut size, two sets of S=B, i.e. S7, rigs are designed with different strut size. The small strut is a cylinder of diameter d=4 mm. The large strut is made by attaching a flat piece of 2 mm on the 4 mm rectangular cylinder to make a total width of 6 mm while the gaps between the small cylinder and rectangular cylinder is sealed to form a smooth cross section profile. The coincident configuration of S=B=7 radiates thrust noise only along the rotational axial direction. According to the point force formulation of Eq. (3.5), the thrust sound heard on the rotational axis is related to the thrust force by simple differentiation:

$$p_{\alpha=0}(t) = \frac{-\partial T/\partial \tau}{4\pi r_0 c_0}, \quad t = \tau + \frac{r_0}{c_0} \tag{4.7}$$

For this configuration, the rotor-strut interaction occurs simultaneously for all blades as $T(\tau)$ is the summation of the thrust on all blades. Therefore, p/7 gives the sound caused by one blade-strut interaction. Ideally, the sound pressure found is well localized within the period in which the fan rotates 1/B of a cycle, or one blade passage. When the waveforms from the different interactions are isolated by a specified p=0 as the starting point, then one can assert that the waveform observed is a result of the encounter between one blade with one strut. The thrust waveform found by Eq. (4.7) is then used to predict noise for other configurations of $S \neq B$. It is found that the pressure waveform for one blade passage is relatively localized in time domain (Huang 2003), but the thrust, hence the related lift, has a long tail of lift recovery. It is suspected that the effect of neighboring blades on the interaction dynamics is present, and such effect differs from the coincident configuration to non-

coincident ones. Nevertheless, the assumption is made that this lift force approximates the one occurring in the non-coincident configuration. The measurement results for the two sets are shown in Fig. 4.6. The rotary sound intensity of the small strut (solid curve) and large struts (dashed curve) are presented in Fig. 4.6 (a). The sound power integrations are shown in the labels below the polar plots. The following discussion is focused on the first BPF thrust noise which is caused by T_7, the 7th component of the Fourier transformed thrust amplitude. The corresponding sound power of the force radiation is 47.5 dB for the 4 mm strut, and 55.9 dB for the 6 mm strut. The amplitude of T_7 for the two sets are found by using the thrust term in the right-hand side of the Eq. (4.7),

$$T_7^{(S)} = 0.066mN, \quad T_7^{(L)} = 0.174mN, \quad T_7^{(L)}/T_7^{(S)} = 2.63 \tag{4.8}$$

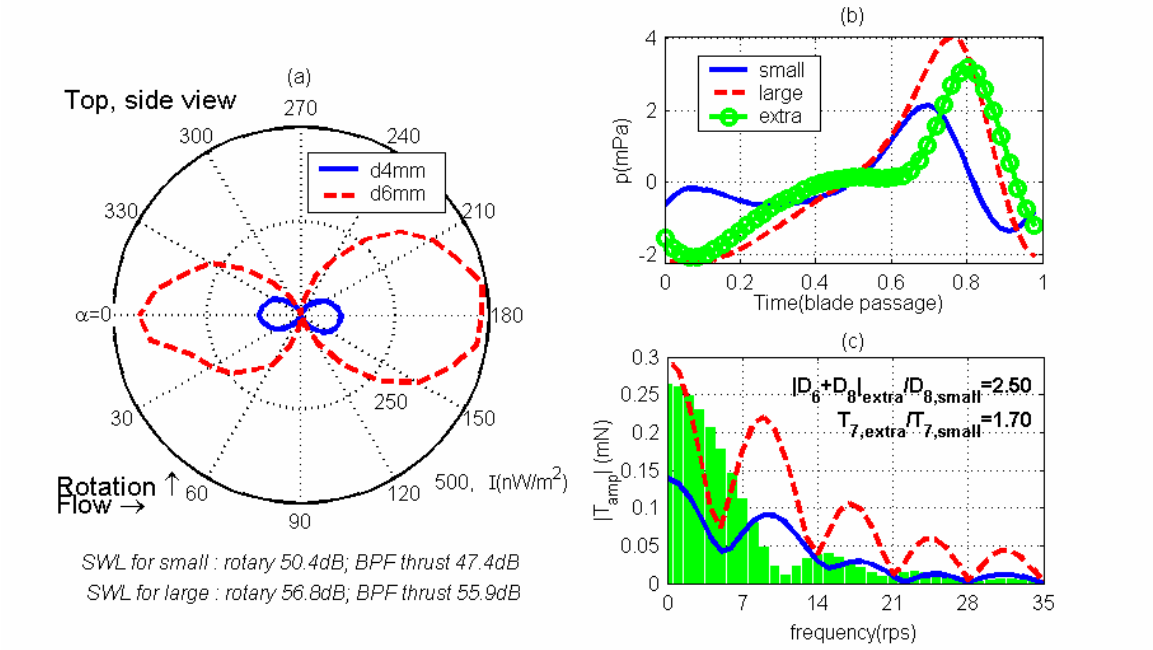

Figure 4.6 Comparison of sound radiated by fans with small (4mm) and large (6mm) seven struts. (a) Directivity of rotary sound, (b) waveform of lift, and (c) the spectral comparison

where the superscripts *L* and *S* represent the small and large struts, respectively. This means that the lift fluctuation is almost proportional to the square of the strut width,

$2.63 \approx (6mm/4mm)^2$, instead of a linear relationship. One blade passing history of lift is shown in Fig. 4.6 (b), in which the solid line is for the small struts and the dashed line for the large struts. The difference between the two is shown with the open-circle line. The spectra are given in Fig. 4.6 (c), where the solid and dashed lines represent the small and large struts, respectively, while the spectrum for the extra thrust component, $T_7^{(extra)} = T_7^{(L)}(\tau) - T_7^{(S)}(\tau)$, is shown as the bar chart. Note that the two peaks of 'pulses' are around the blade passage time index of 0.8. The difference in the two peak times is found to be the time required for the rotor to cover the extra 2mm width near the blade tip. The shift of waveform in that region is thus understood. However, the waveforms between the dimensionless time of 0 and 0.2 show opposite trends for the small and large struts, and the detail fluid dynamics of this phenomenon is yet to be analyzed. As a result of this difference, the extra noise from one blade, as shown in Fig. 4.6 (b) by the open-circle line, features a rather anti-symmetrical pattern like a sine curve. The amplitude of $T_7^{(extra)}$ for the extra strut size is found to be 1.71 times that of the small strut. This differs a little from the value of 2.63-1 found in Eq. (4.8) due to the fact that the intensity directivity in Fig. 4.6(a) is not entirely confirming to the theoretical pattern of cos(α). This ratio of extra thrust force is labeled in Fig. 4.6 (c). Also labelled is the extra drag noise source, which will be used to analyze the combination radiation of S13.

The sound radiated by a combination of three small struts and one large strut with bellmouth inlet, or 'S=1+3,bell' in Fig. 4.5(a), can be decomposed into the sound caused by four equal struts of d=4 mm, plus the sound radiated by the extra lift force on the large strut. The result of the four equal struts is shown in Fig. 4.3, and it features mainly the drag noise. The noise made by the extra strut size, for which S=1,

has both drag noise and thrust noise components with the following source frequency indices,

$$\text{drag}: \lambda = 6,8,\ \nu = mB - \lambda = -1,+1; \quad \text{thrust}: \lambda = 7, \nu = 0.$$

When the large strut is in the vertical orientation, the extra drag noise is radiated by $\left|D_6 + D_8\right|^{(extra)}$ in which both D_6 and D_8 should be complex amplitudes with correct phase angles. The ratio of $\left|D_6 + D_8\right|^{(extra)}$ and $\left|D_8^{(S)}\right|$ display the sound pressure ratio of the extra strut to that of the four equal struts, which is found in the bar chart of Fig. 4.6 (c) to be 2.5. Therefore, the ratio of the sound powers radiated by the large strut and the four equal struts is estimated as follows:

$$\frac{W_{n=B}^{(D,extra)}}{W_{n=B}^{(D,S4)}} = \left[\frac{\left|D_6 - D_8\right|^{(extra)}}{4D_8^{(S4)}}\right]^2 = \left(\frac{2.50}{4}\right)^2 = 0.625^2 = 0.391 \tag{4.9}$$

Since the extra drag noise and the noise from the four regular struts are positively coupled, the resultant total drag noise power is found as $(1+0.625)^2$ times the four strut noise, or $20\log_{10} 1.625 = 4.22$ dB higher. The difference between $SWL^{(D)}$ values shown in Fig. 4. 3(b) and Fig. 4.5(b) is 43.8-39.4=4.4dB, it shows a good agreement with the measurement. In terms of the extra drag noise alone,

$$SWL^{(D,extra)} = 39.4 + 20\lg(0.625) = 35.3dB$$

The extra thrust noise is compared with the S=7 small struts shown as the solid curve in Fig. 4.5 (a),

$$\frac{W_{n=B}^{(T,extra)}}{W_{n=B}^{(T,S7)}} = \left[\frac{T_7^{(extra)}}{7T_7^{(S7)}}\right]^2 = \left(\frac{1.71}{7}\right)^2 = 0.06. \tag{4.10}$$

This means that the extra thrust noise should be $-10\log_{10} 0.06 = 12.2$ dB below the 47.5 dB SWL of $S7^{(S)}$ given in Fig. 4.6(a). The result is $SWL^{(T,extra)}$=35.3dB, while the actual thrust noise shown in Fig. 4.5(b) is 38.2dB. The extra thrust noise would couple

with the thrust noise from S=4 small struts, which is shown in Fig 4.3(b) to be 22.4dB, to give the total measured thrust noise. However, the 22.4dB is too small to have any practical effect. The discrepancy of 38.2-35.3=2.9 dB is, however, not too large.

In terms of acoustic directivity patterns shown in Fig. 4.5 (a), all have some degree of tilting in terms of the major dipole axis. The tilting towards the rotational axis implies contribution from thrust noise, which is small for Fig. 4.3(b) as the thrust noise for S=4 is expected to come from either non-symmetric inlet flow distortions, for which the effective S is unity, or from S=4 itself, which means less efficient radiation of thrust noise at ν=-1. The tilting for both original fan and the S13 is more serious due to the radiation of thrust noise at the most efficient mode of ν=0. However, there is also contribution from $|\nu|$=-1, which feature a quadruple-like directivity of $\cos(\alpha)\sin(\alpha)$. In fact, the directivity pattern of Fig. 4.5 (a) can be mapped very closely by

$$p \propto \left[\cos\alpha + \sin\alpha + 0.22\cos\alpha\sin\alpha\right] \tag{4.11}$$

The rotary sound of Fig. 4.5 (a) is represented together with the approximation of the Eq. (4.7) to show the similar pattern in Fig. 4.7, where the solid thin line represents the measured sound, and the thick solid line is for the approximation.

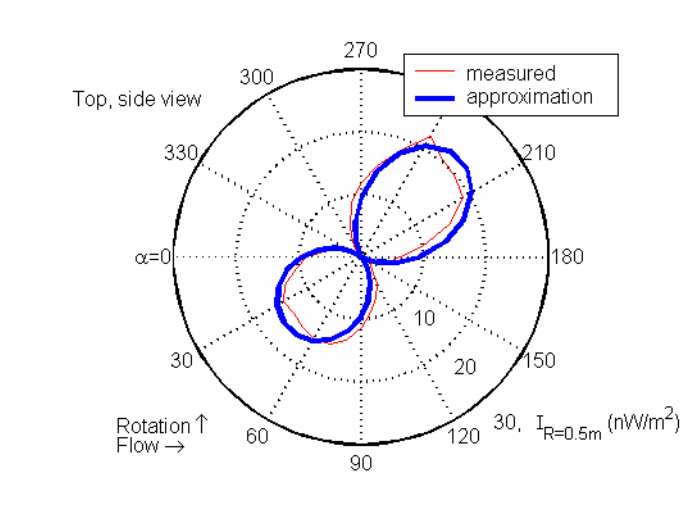

Figure 4.7 Mode combinations for simulating the measured directivity of the S13 configuration

4.4 Noise abatement by structural corrections

According to the studies conducted so far, it has already been identified that the square inlet frame and the large strut are the major sources of the fan noise. The various contributors of the original fan noise are summarized in Fig. 4.8 in the form of sound intensity directivity. Figure 4.8(a) shows the overall noise (thin solid line), rotary noise (thick solid line) and random noise (dashed line). Since the pattern of random noise does not change much in most fan modifications, only the directivity of the rotary noise is shown for the other three sub-figures. The contribution of the inlet frame to the total noise radiation is determined by removing all the struts from the fan assembly. The rotor is held by a cylinder extending downstream from the motor. The original inlet frame of the casing is kept in the same relative position to the rotor as in the original fan. The acoustical directivity measured for this square inlet configuration is denoted as Sqinlet, which is plotted in Fig. 4.8(b). When the square inlet is replaced by a bellmoth, the sound radiation from three regular struts with one larger strut, S13,

and the results are shown in Fig. 4.8(c). The configuration of S13 is then changed to four regular struts, S4, and the results are given in Fig. 4.8(d). All tests are carried out for the rotational speed of 3000 rpm. The axial distance between the blade trailing edge and the strut leading edge is 3 mm in all tests.

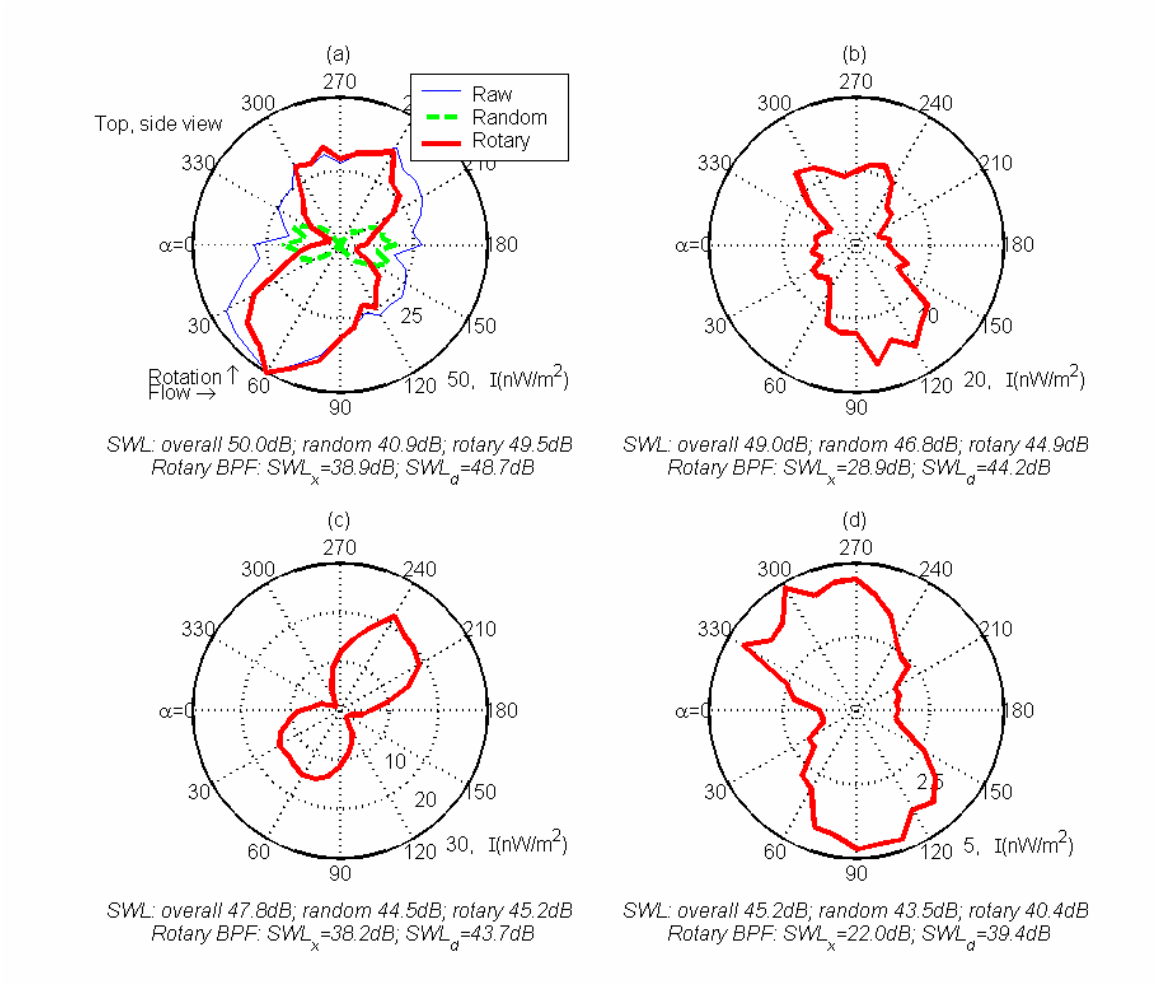

Figure 4.8 Sound intensity distribution of the four configurations. (a) Original sample fan, (b) Square inlet frame only, (c) Three regular struts with one large strut. (d) Four equal struts.

The major difference between the rotary sound of the original fan in Fig. 4.8(a) and that in Fig. 4.8(b) for the square inlet frame is that the latter has a clear major axis along the second and fourth quadrants of α, while the original fan has a more complex pattern of tilting towards α=60^o in the first quadrant together with a collective bending towards the upstream of the fan. This is caused by the acoustic interference

between Sqinlet and S13. Focusing on the sound power in the rotary part of the total intensity, Sqinlet has 44.9 dB while the original fan has 49.5 dB. In both cases, the drag noise dominates. They are 48.8 dB for the original and 44.1 dB for Sqinlet, which are 0.7 dB and 0.8 dB less than the overall sound power, respectively. It means that the drag sound power accounts for an average of about $10^{-0.75/10} = 85\%$ of the total rotary sound power. Rotary noise shown in Fig. 4.8(d) has the similar pattern as in Fig. 4.8(b), in other words, the noise caused by the square inlet frame is similar to that of the four equal struts. This is expected since the four sharp edges lead to a spatial spinning pattern like that from four struts. The rotary sound power from Sqinlet is 44.9 dB and for the four equal struts, S4, is 40.1 dB; it means that the former mechanism dominates. When the large strut effect is preserved, the results is shown in Fig. 4.8(c) with a rotary sound power of 45.2 dB, which is midway between 49.5 dB for the original fan and 40.1dB for the final modified fan with bellmouth inlet and four equal struts. The estimation of the noise generation from the extra strut shows that it radiates 35.3 dB from both thrust and drag components, the total noise power of the extra strut is 38.3dB. In terms of the total rotary sound, the reductions achieved by correcting the inlet frame structure and by trimming the large strut are similar, both being around 5 dB. The total rotary noise reduction is 9.1 dB.

The sound powers from the random noise are given in the labels of all sub-figures in Fig. 4.8, although the directivity is only shown in Fig. 4.8 (a). The fact that the random noise in Sqinlet, 46.8 dB, is much higher than that of the original fan, 40.9 dB, implies that the former interferes destructively with the random noise from the rotor and struts. The so-called random noise may not be truly random in time sequence

after all. The exact mechanism for the random noise defined here is beyond the scope of the project.

4.5 Noise abatement by structural re-design

Based on the investigations carried out on the leading mode studies, it can be found that further noise reduction can be achieved by an optimization of the pressure spinning mode. Ideally, a quiet fan should be designed in such a way that the index of spinning mode $|\nu|$ is at least 2 or above for all integers *k*. The sound pressure on the fundamental BPF has the most strength comparing with the other harmonics. As far as the fundamental BPF is concerned, the rotor has 7 blade with 5 struts should be a good configuration and denoted here as S5. Theoretically, thrust noise for the first two harmonics from S5 is expected to be radiated by the spinning pressure mode with $|\nu| = 1:\ 2B - 3S = -1,\ 3B - 4S = +1$. It belongs to a higher order or lower efficiency mode of the thrust radiation, similar to the drag noise at $|\nu| = mB - kS = 1 \times 7 - 1 \times 5 = 2$ for the fundamental BPF. A five-strut casing is made and the same rotor is installed in this. The measurement results are plotted in Fig. 4.9, in which the main results of S4 is also presented for easy comparison. In both cases the thrust sound is expected to be small, the measured thrust noise for S5 in 33 dB, higher than 22.4 dB from S4, but is still secondary compared with the dominant drag noise. Thrust noise arises mainly due to the mode of $|\nu| = 0$, and it can be induced by many factors, such as the inlet flow distortion caused by the structural imperfection, flow turbulence, vortex shedding from the strut which get interrupted periodically by the passing rotor, etc. Comparing Figs 4.9 (a) for S4 and 4.9 (b) for

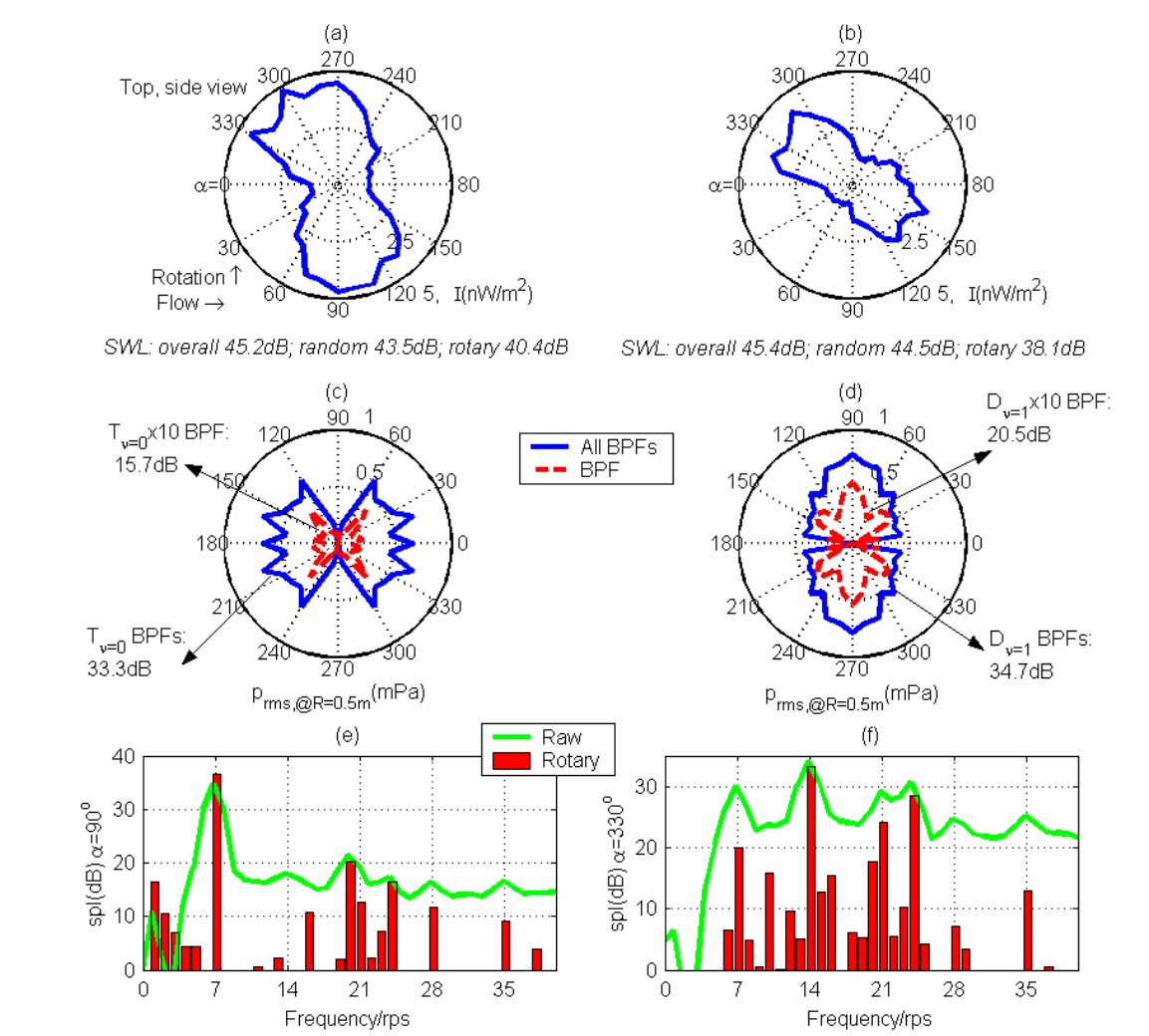

Figure 4.9 Directivity of the fan with four struts and five struts and a bellmouth. (a) Four struts (S4). (b) Five struts (S5). (c) Decomposed T_0 of (a). (d) Decomposed D_1 of (b). The typical spectral of (e) S4 at α=150^o, and (f) S5 at α=330^o.

S5, it is found that the 2.3 dB reduction is achieved for the rotary noise by S5. It is not a significant reduction. This is so because S5 generates the leading mode drag noise at the higher harmonics of m=2,3, for which obvious peaks are found in Fig. 4.9 (f). In order to compare the contribution of the BPF tone in all BPF harmonics, Fig. 4.9 (c) and 4.9 (d) show the comparisons for the thrust and drag components of S5, respectively. In the Fig. 4.9 (c), the BPF tone is amplified 10 times comparing with BPFs. A large difference between the values of BPF and all the BPFs shown in Fig.

4.9 (c) and 4.9 (d) illustrates that the S5 rig is an effective design to reduce the BPF noise, but it may have shifted the sound power to higher harmonics.

In conclusion, the work reported here has focused on the detailed analysis of the noise source separation, particularly the noise radiated by the struts of unequal size, and the acoustic directivity. The extra fluctuation force on the blades is found by the test of coincident configuration of $S=B$. The extra noise is induced both by thrust noise and drag noise, and they are similar in magnitude. The removal of the extra strut size reduces the rotary noise by 5dB. However, such reduction would be undetectable if the step is not taken to correct the inlet bellmouth. The correction of the inlet bellmouth gives a crucial 5dB reduction. Finally, it is also pointed out that the total tonal noise reduction is nearly 12 dB from the original fan to the five-strut fan.

Chapter 5 Active control of thrust noise component

The force on a blade can be divided into a thrust component along the rotating axis, and a drag component in the circumferential direction of a rotor. The radiated noise is a result of complex acoustic interference among noises from these two force components on one blade, and noises from forces on all blades. Typical noise abatement measures are taken for the typical computer fan in Chapter 4. The minimal noise level existing in the improved fan is still a leading mode drag noise. In this and the next chapters, the concept of active noise control is applied to achieve global elimination of the BPF tone radiated by the leading modes of the thrust dipole and rotating drag dipole, respectively. The understanding of the fan noise distribution is a prerequisite to the construction of the leading mode antisound.

This chapter demonstrates the feasibility of globally eliminating the rotation-locked tones by applying a very simple destructive interference to a modified cooling fan with the number of struts equal to the number of rotor blades, $S=B=7$. The rig consists of a miniature electret microphone used as a rotation sensor, an ordinary loudspeaker, and a bandpass filter with adjustable amplitude and phase delay. The microphone is located at the inlet bellmouth of the fan to pick up the fluctuating aerodynamic pressure caused by the passing rotor blades. The pressure spectrum is rich in the blade passing frequency (BPF) and its low-order harmonics, and is shown to provide much better performance than a pulse-generating tachometer. Analysis of the original fan noise shows that about 90% of the radiated tonal sound is phase locked with rotation, and this portion is almost completely eliminated in all directions. The reductions of

the sound radiation power in the first two BPFs are 18.5 dB and 13.0 dB, respectively, and the overall power reduction is 11.0 dB.

5.1 Introduction

Reviewing the area of active noise control (ANC), it is found that the technique has been tried for ducted fan with some success. Tyler and Sofrin's (1962) model for the ducted fan noise requires the use of multiple detection microphones and secondary source to cancel the noise of the higher order modes propagating in a duct. Gerhold (1997) used a delicate ring of 48 microphones and many control sources in a duct. Thomas *et al*. (1993,1994) controlled the plane wave mode in a duct by 12 electromagnetic compression sound drivers, and used 3-channel feedforward method to create a 30deg quiet zone for an operational turbofan engine. For unducted fan noise, ANC has not been practiced as extensively. The main reason could be as follows. Noise from an unducted fan has complex modal composition in space, and it is rather hard to match such distribution with a limited number of secondary sources. Lauchle *et al* (1997) and Quinlan (1992) have both had some success in suppressing the BPF tones of a fan in isolation except that a baffle was used on the rotational plane and that might have changed the acoustic directivity of the fan. The work of Lauchle *et al* (1997) is also remarkable in that the fan itself is shaken in the axial direction to serve as a control source. Apparently it was hoped that the vibrating fan would produce a good directivity match with the original noise pattern. The acoustic radiation from an oscillating fan can be thought of as follows. First, a vibrating fan assembly radiates noise much like a loudspeaker in the absence of flow. Second, the fact that the fan also shakes the flow means that it would induce additional fluid loading hence dipole radiation from the fan. Details of such flow modification by the

fan oscillation are apparently beyond the scope of studies in (Lauchle *et al* 1997). Generally speaking, it can be said that the modification could reduce or eliminate the unsteady loading on the fan structure caused by the wake interactions. It may also generate an anti-sound which matches with the original noise without directly interfering with the source of the original noise. Gee and Sommerfeldt (2004) are among the latest to develop the technique of active fan noise control using a near field error sensor. One common feature in the reported work is that the rotational plane of the fan is placed in a baffle in order to simply the acoustic field before the global control is attempted. The effect of such a baffle on the acoustic directivity has not been quantified, but it can be speculated that the effects on the thrust and drag components of the source would differ. A brief estimation aided with dipole point source formulas (Dowling 1998) is that the baffle effect on the thrust noise is cancellation and that for drag is enhancement. As a result, the acoustic interference between the two fields would also change, as reported by (Lauchle *et al* 1997). Nauhaus *et al* (2003) placed small flow obstructions around the blade tips, and blew air jets into the tip clearance to fill up the deficit in the wake. An active aerodynamic control algorithm was used to counter the rotating instability and suppress the BPF noise originating from the wake interactions. Similar aerodynamic control was also demonstrated by Rao *et al* (2001) and Simonich *et al* (1993). The work reported here shares the acoustic feature of the active noise control described above, but the use of formal control algorithms are de-emphasized in favour of simplicity and the use of knowledge of specific source mechanisms.

Instead of following the strategy of complex aerodynamic control, using complex secondary loudspeaker arrays, or modifying the fan noise directivity by a baffle, this study aims to explore the feasibility of a very simple destructive acoustic interference technique for typical computer cooling fans which consist of a rotor and downstream struts. The technique involves a re-design of the fan strut so that the primary noise becomes a simple dipole in the axial direction. A miniature microphone is used to pick up the information of blade rotation, much like a traditional tachometer, and the signal is filtered, phase shifted, and amplified to drive a single loudspeaker placed just under the fan casing. There is no error microphone and the set-up can be regarded as a simple feedforward, open-loop control. The secondary noise is also a simple dipole with its axis aligned with that of fan rotation. The key question asked are: (a) how effective is the manipulation of the fan noise directivity? (b) can the simplified noise be cancelled by the simple open-loop arrangement? The rationale for using such a simple scheme is based on practical considerations. One cannot afford to have sophisticated control algorithm and complex detection and error microphones for applications like computer cooling. The same limitations apply to many other situations.

Comparing the small cooling fan in the electronic devices to the large-scale turbo-machine in the aerospace and many industrial applications, there are important differences. The studies of the previous chapters showed that noise from the steady loading, tip leakage, and vortex shedding of the trailing edge is not important for the small low-speed cooling fan. For the large-scale turbomachines, however, the loading is high and the Gutin noise and many kinds of noise induced by the viscous flow become significant. More important difference is found in the nature of rotor-stator

interaction noise. In large turbomachines, which are mostly multiple stage, the interaction noise is mainly radiated by the downstream part of the two sets of interacting blades. For the small computer cooling fan, the noise is mainly radiated by the upstream rotor blades since the downstream stator is normally a circular cylinder. Having said these, the noise from the small fan still shares many features with that of the large turbomachines, both have obvious tonal noise induced by the rotor/stator interaction.

In what follows in Section 2, the noise made by the sample fan is analyzed thoroughly. The analysis shows the directivity, the components of noise that can be controlled and those lying beyond the scope of the current scheme. It would also assess whether such a specially designed configuration with a dipole sound radiation is worth the while of practical use. In Section 3, details of the experimental configuration will be presented before the results of noise reduction are given. Such details include the sensor signal, loudspeaker performance, and characteristics of the filters. At the end of this chapter, results of noise reduction and limitations of the method are presented.

5.2 Analysis of the original fan noise

A. Noise mechanisms of the sample cooking fan

The same fan investigated in the previous studies is followed. This is shown again in Fig. 5.1(a), the fan has a diameter of 92 mm, consists of 7 blades and 4 struts at the back for holding the motor. At the design point, the rotational speed is 3200 rpm. With such low blade tip speed, noise generated by the Gutin mechanisms is totally negligible. The acoustic spectrum consists of broadband noise and discrete tones at multiples of the blade passing frequency (BPF). As described in Chapter 2, the

dominant noise source for such a fan is the aerodynamic interactions induced by two noticeable features. One is the interaction between the rotor blades and the downstream struts, another is the interaction between the distorted inlet flow pattern and the rotor, the inlet flow being a four-lobe distortion caused by the four sharp edges of the incomplete bellmouth cut short by the square outer frame. The dominant noise source is the fluctuating force induced by the two interaction processes on the rotor blades. If one compares the noises made by these two interactions, it is possible that the inlet flow distortion is louder. However, this feature can be avoided by using a complete and smooth bellmouth. As a result, the active noise control study focuses on the noise radiated by the interaction between rotor and its downstream struts, which are essential structure that cannot be removed or drastically modified.

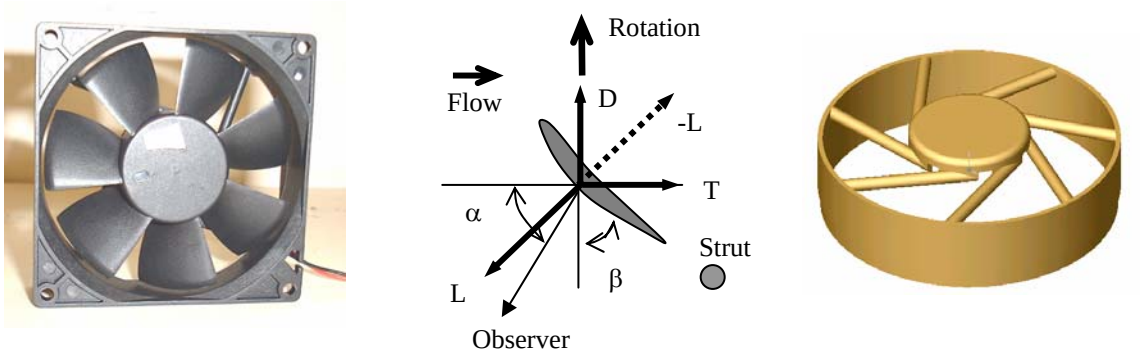

Figure 5.1 Computer cooling fan and its noise sources. (a) is the front view of a typical fan, (b) is the cross sectional view of a blade with forces acting on the surrounding air (L) decomposed into thrust (T) and drag (D) components, (c) is the strut design for the coincident configuration of B=S=7.

It has to be said that noise emanates from both blade surfaces and all other stationary surfaces experiencing unsteady pressure. However, the lift-generating nature of the rotor blade makes it the largest source of noise. Fig. 5.1(b) is the cross sectional view

of a blade, and the unsteady force exerted on the surrounding air, which is the reaction of the lift, -*L*, is divided into two components: drag *D* and thrust *T*. The component of drag should be better named a driving force in this case but the term is kept here in step with literature. If the blade has a significant lean, a radial force component may also exist (not shown). The reason why the force is divided this way is that noise radiated by each of these components has its distinct characters which can be used for source characterization purpose. If the unsteady force on blades is represented by a point force of thrust component *T* and drag component *D*, the rotary noise at the frequency of *m*th harmonic of the fundamental BPF is given below in terms of its complex amplitude c_{mB} (Lowson 1965, 1970):

$$c_{mB} = \frac{imB^2 S\omega}{2\pi c_0 r_0} \sum_{k=-\infty}^{\infty} i^{-\nu} \left(T_{kS} \cos\alpha - \frac{\nu}{mBM} D_{kS} \right) J_\nu \left(mBM \sin\alpha \right), \quad \nu = mB - kS. \quad (5.1)$$

It is exactly the same as Eq. (3.16), where more detailed interpretations are given. Here, *B* and *S* denote the numbers of the rotor blades and struts, respectively, ω is the angular rotating speed, *mB* is the frequency index of the observed sound, *kS* is the frequency index in the spectrum of the unsteady force, the dimensional frequency being the product of these indices and the rotational frequency, rps=rpm/60, r_0 is the distance between the fan centre and the observer, α is the angle between the rotational axis and the observer direction, as shown in Fig. 5.1(b), c_0 is the speed of sound, *M* is the Mach number of the source point motion, T_{kS}, D_{kS} are, respectively the *k*S component of the spectrum of the source forces *T* and *D*. Note that both *m* and *k* here can be any integer. The frequency index differential, $\nu = mB\text{-}kS$, or the index of spinning pressure mode (Tyler & Sofrin 1962), is the most important parameter. The source frequency index is *kS* because each blade experiences blockage by *S* struts during one cycle of rotation. The observed noise has frequency indices of *mB* because

noise of other frequency components is cancelled among themselves since *B* rotor blades all radiate sound with a fixed phase relation determined by the rotation. In fact, the phase relation is an important assumption which is not satisfied completely in reality. For example, there might be unsteady forces arising from vortex shedding from the cylinder and its timing could be very different from the fan rotation. Noise from such dynamic process cannot be modelled easily but can be measured and analyzed to some extent. The acoustic interference designed in this study deals solely with the rotary noise.

When the two frequency indices coincide, $mB = kS$, the thrust forces exerted by all blades occur simultaneously and simply add up, and the noise radiated is a simple dipole whose axis is along the rotational axis. However, the situation for the drag force is different. Drag force changes direction once per cycle, so the frequency perceived by a stationary observer is $kS\pm1$ and no noise is radiated at $mB=kS$, as can be seen by the numerator $\nu=0$ in the drag noise term in Eq. (5.1). For this reason the leading drag noise radiation mode has $\nu = \pm 1$. With such a mismatching mode, some noise is also radiated by the thrust force, and this is caused by the Doppler effect for a moving source. The strength of the Doppler effect is governed by the Bessel function $J_\nu(z)$ of order ν and the argument $z=mBM\sin\alpha$, which is proportional to z^ν for small z. More specifically, the Doppler effect is small for $|\nu| \geq 2$ since a typical computer cooling fan operates at a Mach number around 0.03. For the leading radiation modes of $\nu = 0, \pm 1$, one has

$$J_0(z) \approx 1, \quad J_{\pm 1} \approx 0.54z,$$

and Eq. (5.1) is simplified to give

$$|c_{mB}| = \frac{m\omega B^2 S}{2\pi c_0 r_0} \times \begin{cases} |T_{mB} \cos\alpha| \\ 0.54 |D_{mB\pm1} \sin\alpha| \end{cases} \text{ for leading mode } \begin{matrix} \text{thrust} \\ \text{drag} \end{matrix} \text{ noise.} \qquad (5.2)$$

The drag noise radiated by the leading mode has its peaks on the rotational plane, as indicated by the directivity factor of $\sin\alpha$ in Eq. (5.2). In a three-dimensional view, the drag noise is actually a rotating dipole. On contrast, a thrust noise is a dipole with a fixed axis for which the sound directivity features cosα. If two microphones are placed as mirror images of the rotational plane *y*-*z*, the results, denoted as p_1 at the longitudinal angle α, and p_2 at angle π-α on the same horizontal plane of constant *z*, can be combined to give the thrust noise $(p_1 - p_2)/2$ and drag noise $(p_1 + p_2)/2$ (Wong and Huang, 2003).

B. Acoustics of the coincident configuration

It has to be acknowledged that the increased number of struts increases the time-mean blockage of the flow, and the aerodynamic performance of the fan may suffer. In fact, the actual amount of noise radiated by this coincident design of *B*=*S*=7 would also be higher than the leading order drag noise radiation of the original design, *B*=7, *S*=4, due to more force fluctuations induced by unsteady flow from the increased discharging blockage. A specific estimate of the sound powers from the two configurations was made in (Wong & Huang 2003) and a general analysis is given for the effect of *S* by Huang (2003), both concluding that *S* is a very dominant factor when the size of each strut is fixed. However, the conclusion changes if the size of each strut is allowed to decrease. For *S*=7, the strut size could be cut down to 4/7 of the original. In such case, one strut may not be able to contain all the electrical wires, and two struts might be involved for wiring. This issue of practical design complication is put aside for the moment. Wong and Huang (2003) also found that the

lift fluctuation T_{kS} is almost proportional to d^x where d is the strut diameter and $x>2$. So the reduction in strut size by a factor of 4/7 would give a noise reduction of at least $20\log_{10}\left(7/4\right)^2 = 9.7$ dB. This would, to a large extent, compensate for the difference between the coincident thrust noise and the leading-order drag noise radiation from $S=4$. In addition to this justification, there are cooling fans which feature fewer rotor blades, such as $B=3$ or 4. In such applications, the coincident design of $S=B$ may well be the best choice for structural reasons. In short, the design of $B=S$ is not unrealistic for a fan with few rotor blades, and the original strut size is used for demonstration purpose.

The directivity measured in the full anechoic chamber for the coincident configuration is shown in Fig. 5.2 in the form of sound intensity distribution when the fan operates at 3200 rpm. Comparing with sound pressure level, the use of intensity I in the directivity plot amplifies any non-uniformity existing in the actual acoustic field. The thin outer curve in Fig. 5.2 is the intensity of the overall noise, the thicker inner line is the rotary component found by synchronous averaging with the help of a tachometer. The sound power level (SWL) is the result of integration of the sound intensity I, and details are given in Eq. (2.2). The total sound power levels (SWL ref 10^{-12}W) for the two intensity distributions are indicated in the lower label. Note that, when the inlet flow condition is smoothed out, the original fan with four struts shown in Fig. 4.9(c) has a sound power of around 47.8 dB, while the current coincident configuration has 53.4 dB, which is not too noisy considering the use of $S=7$ struts with its original size.

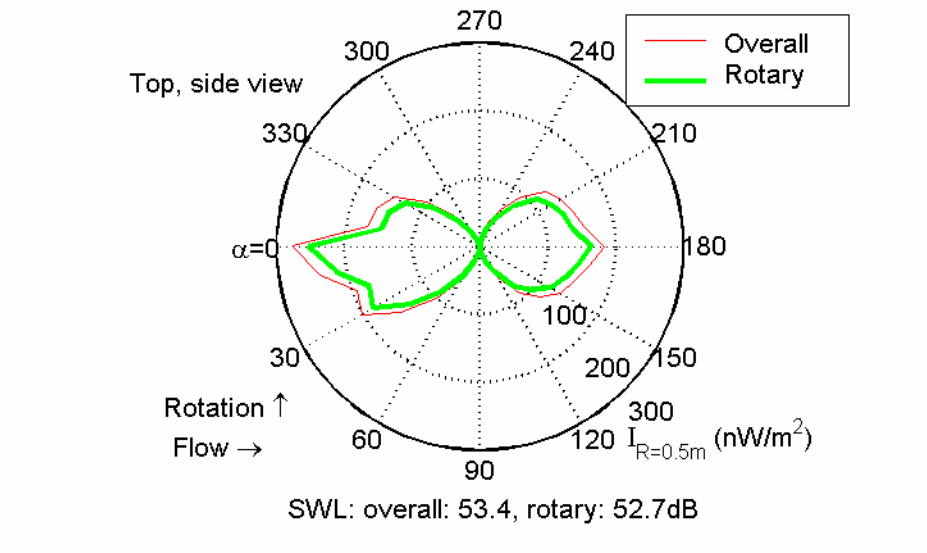

Figure 5.2 Directivity of sound intensity measured at r_0=0.5m when the sample fan operates at 3200rpm.

C. Analysis of the noise components

Ideally, the sound radiated by the fan is a perfect thrust dipole with an intensity directivity of $I(\alpha) \propto \cos^2 \alpha$, and the radiation is perfectly stable with a constant rpm. A single loudspeaker is then able to radiate a perfect anti-sound to cancel the fan noise. The reality deviates from this ideal situation in many ways, and the part of noise that does conform to the ideal assumption is here called controllable noise. Major deviations are analyzed below.

First, the actual sound radiation does not feature *T* and *D* with equal strength on every blades with a perfect time difference locked with the rotation. Unsteady forces can hardly be deterministic given the high Reynolds number flow, which is inevitably turbulent. If the force on one blade is different from the average of the seven blades, the difference can be seen as the effect of having an additional single blade, *S*=1, for which noise of all sorts of spinning pressure mode index ν exists including the drag

noise. Second, the rotational speed varies from one cycle to the next slightly. Since the active control technique can only use the information from one cycle to construct anti-sound to cancel the noise of the next cycle, the imperfection of noise radiation caused by rotational speed variation is another source of uncontrollable noise. Since the directivity shown in Fig. 5.2 is taken by using a single microphone traversing the whole horizontal plane of 360°, its deviation from a perfect $\cos^2(\alpha)$ distribution is also partly attributed to the temporal variation of rotational speed and rotor-strut interaction. The extent to which the measured directivity $I(\alpha)$ conforms to the ideal distribution of, say, $I^{(T)}\cos^2\alpha$, may be measured by the following correlation calculation,

$$I^{(T)} = \int_0^{\pi} I(\alpha)\cos^2\alpha d\alpha \Big/ \int_0^{\pi} \cos^4\alpha d\alpha \tag{5.3}$$

and the sound power from the ideal component with amplitude $I^{(T)}$ is given as

$$P^{(T)} = \int_0^{\pi} \left(I^{(T)}\cos^2\alpha\right) 2\pi r_0^2 \sin\alpha d\alpha = \left(I^{(T)}/3\right)\left(4\pi r_0^2\right) \tag{5.4}$$

The estimated intensity amplitude $I^{(T)}$ for Fig. 5.2 is 1.7×10^{-7} W/m^2 for the observer radius of r_0=0.5 m, and the thrust sound power $P^{(T)}$ is found to be 1.78×10^{-7} W, or

$$SWL = 10\lg\left(P^{(T)}/10^{-12}\,\mathrm{W}\right) = 52.5\mathrm{dB}.$$

The difference between this sound power level and the actual rotary sound power level of 52.7 dB is 0.2dB. The difference must be caused by an additional noise for which the sound power level is estimated as

$$10\lg\left(10^{5.27} - 10^{5.25}\right) = 39.2\ \mathrm{dB}.$$

This additional noise is deemed to be uncontrollable. The difference between the overall noise and the synchronously averaged noise also represents uncontrollable noise by the current method, but this part of noise is mainly broadband and is not the focus of the present study.

The variation of sound radiation from one cycle to the next is studied by taking Fourier transform for each cycle of the measured sound, which contains B=7 pressure oscillations for the BPF component. The temporal borders of each cycle is indicated by the tachometer signal taking into account the time required for sound propagation over a distance of r_0=0.5 m. The rms value of the BPF sound pressure varies with the cycle index n and is denoted as $p_{rms}(n)$, which is shown in Fig. 5.3 for the front, α=0°, and the back of the fan, α=180°. One possible reason for such variation is the change of local rpm with n. Assuming that the radiated sound power follows the usual 6th power law for dipoles, p_{rms} is proportional to (rpm)^3. The value of p_{rms} shown in Fig. 5.3 has already taken this into account by multiplying a factor of (rpm$_0$/rpm)^3, where rpm$_0$ is the mean rpm and rpm is the actual rotational speed for cycle n. Thus corrected, the variation shown in Fig. 5.3 is believed to derive solely from random aerodynamic events. The amplitude of noise from such random events is estimated as follows. If the random event contributes to the BPF noise with an rms amplitude A_r and the deterministic noise has an amplitude A_d, the range of amplitude of the actual noise is, statistically, $[A_d - A_r, A_d + A_r]$. Here, A_d is found easily as the mean of the $p_{rms}(n)$ pattern shown in Fig. 5.3, i.e. $A_d = \overline{p_{rms}(n)}$, while A_r is found as $std(p_{rms})\sqrt{2}$. A_r is found to be roughly uniform over the whole measurement plane, so the sound power associated with the random events is calculated as $P_r = A_r^2 4\pi r_0^2 / (\rho_0 c_0)$, which is found to be 38.4 dB, very close to the result of directivity pattern analysis shown in Eq. (5.3). To summarize, the amount of uncontrollable rotary noise is about 39 dB and the maximum expected rotary sound

power reduction is 52.7-39.0=13.7 dB. In terms of sound power percentage, the uncontrollable part represents some $10^{-13.7/10}$=0.043 or 4.3%.

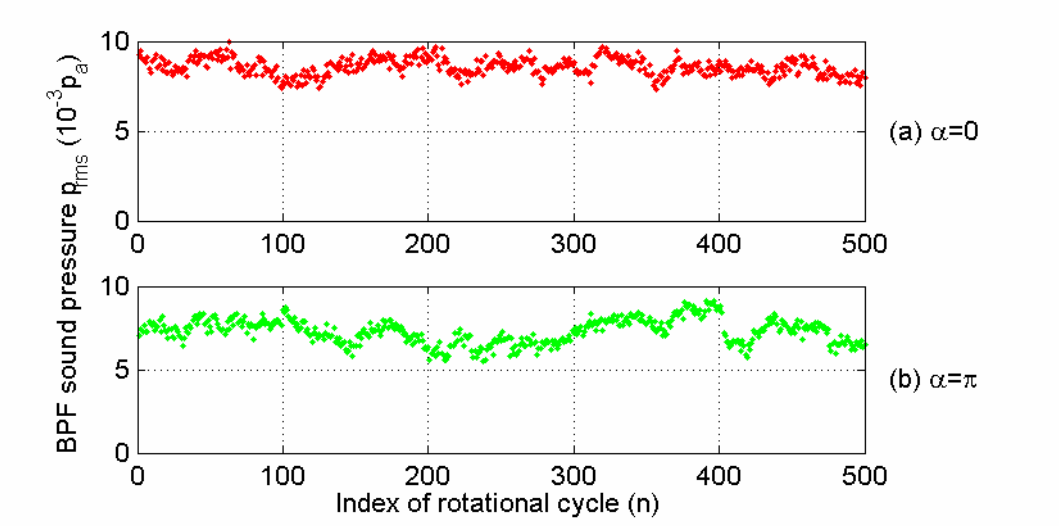

Figure 5.3 The cycle-to-cycle variation of the BPF sound pressure amplitude in the front (upper sub-figure) and the back (lower sub-figure) of the fan.

5.3 Experimental studies

An open-loop, feed-forward control is used for the sample fan being investigated here. The system simply consists of three components. First, a non-acoustic reference from a tachometer-like instrument provides the clock information for the rotating fan blades. To some extent, the amplitude of the signal is also weakly related to the rotational speed. Second, the signal is bandpass filtered to keep the components of BPF and a few chosen harmonics, and further conditioned in terms of amplitude and phase delay. Third, the conditioned signal drives the loudspeaker attached just beneath the fan to produce the anti-sound to cancel the noise made by the fan at the earliest possible blade passage cycle, which is 1/*B* of a rotational cycle. Note that for deterministic sound from the fan, the acoustic signal repeats *B* times during one rotational cycle. The total time delay of the system is found to be such that the signal

from one moment is actually used to cancel noise at the next blade passage. Such a short time delay means that the limitation of the system performance is mainly rooted in the randomness of the aeroacoustic source. In what follows, the three elements of the control rig is discussed before the results are presented.

A. Experimental set-up

The schematic diagram of the experiment is shown in Fig. 5.4. Illustrated at the upper-right corner are a 0.5" survey microphone (B&K type 4187) and a tachometer (B&K type M004) connected to a PC equipped with MATLAB® analysis software and an A/D card. The survey microphone is not used as error sensor here but merely for the purpose of evaluating the results. Note that this part of the experimental set-up can be easily absorbed into the controller block shown in Fig. 5.4, but is kept as a separate part purely for operational convenience. The rig is built around a dSPACE (DS1103 PPC) controller equipped with A/D and D/A boards. The input is derived from a separate rotation sensor and the output goes to the secondary sound source. The digital controller is connected to a personal computer through an ISA bus. The control algorithm is simply based on infinite impulse response (IIR) filters constructed by the Simulink function of MATLAB® assembled in the host personal computer. A real-time interface (RTI) is used to build the code downloaded to and executed on the dSPACE hardware. The rotation sensor signal is sampled at 10 kHz, and the output analogue signal is also constructed with an update rate of 10 kHz; both deemed sufficient for the range of frequencies encountered in the current study. The control is concentrated on the most outstanding peaks on the BPF and 2BPF harmonic, m=1,2, at which the noise level exceeds the broadband by 17 dB and 14 dB, respectively. Two filters are constructed, one for each peak, to extract the rotational

information at the two frequencies, and are put together as parallel channels. Each channel has its own phase delay and amplification variables which can be adjusted manually in computer to optimize the results. The output from the channels are added together before the D/A conversion.

The experiment is conducted in a full anechoic chamber with a cut-off frequency of 80 Hz, and the acoustic directivity is measured by the survey microphone fixed at one position 0.5m away from the fan centre, while the fan and loudspeaker rotate on a tripod to traverse all directions on the horizontal plane at an angular interval of 10^{o}. The pulse signal from the tachometer is sampled together with that of the microphone by a 24 bit A/D card using a sampling rate of 16 kHz. Details of the sensor microphone and other elements in the rig are discussed below.

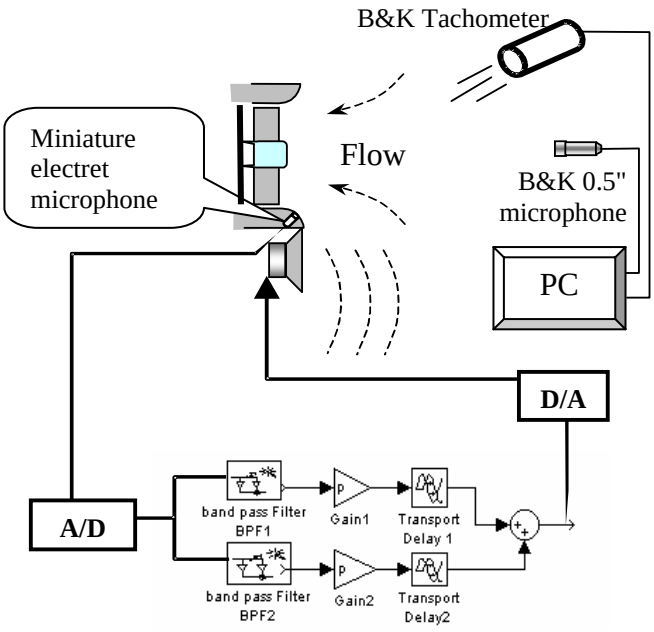

Figure 5.4 Experimental set-up in the anechoic chamber. The fan is isolated and unbaffled, and the secondary loudspeaker is put beneath the fan.

B. Description of rig components

The rotation sensor provides information of instantaneous position of the rotor. This is normally achieved by photoelectric tachometer that generates a pulse at the passing of a marked blade. Since the spectral energy of an ideal pulse (delta function) spreads out over a very wide frequency range, the amount of signal energy in one narrow band of frequency, such as that around the BPF, would be necessarily low in proportion. This makes it less than ideal for the current purpose. In addition to this drawback, the height of the pulse is independent of the rotational speed, and it requires some kind of frequency to amplitude conversion if a higher amplitude of anti-sound needs to be constructed to cancel the noise of the fan running at momentarily higher speed. In this study, a miniature electret microphone is used as the alternative rotation sensor. The microphone used is a 151 series from Tibbetts industries. It has a cylindrical head of 0.1" in diameter and 3 mm in height, with a flat frequency response of 0.018 V/Pa from 300 Hz to 5 kHz. The photoelectric tachometer is located at some 30 cm upstream of the fan, while the electret microphone is flush mounted on the inlet bellmouth of the fan just upstream of the blades. Signals from the photoelectric tachometer (B&K type MM0024) and the electret microphone are compared in Fig. 5.5. The photoelectric tachometer signal is shown in Fig. 5.5(a) and its spectrum in Fig. 5.5(b). Here, the ripples around the edges of the pulses are caused by the high-pass filter installed in the data acquisition system to avoid excessive electronic noise that exist at low frequencies. When the optical reflex paper is attached to all 7 blades of the fan, the main peaks are found at the BPF and its harmonics. The appearance of the peaks at the rotational frequency (rps) and its non-BPF harmonics is caused by the difference among the pulses due to either the variation of tachometer or the changing

fan rotational speed. The difference between the 1st BPF and its two neighbouring non-BPF peaks is 16 dB.

Figure 5.5(c) shows the saw-tooth-like waveform from the electret microphone, and its spectrum is shown in Fig. 5.5(d). The BPF peak is 35 dB higher than its nearest non-BPF peaks. What is measured here is the aerodynamic pressure variation on the bellmouth surface caused by the constant sweeping of the blades, which is a source of far field sound but not all sound by itself. The effect of the blade rotation on the upstream flow is mainly a potential flow blockage, and its magnitude should be of the scale of the dynamic pressure head associated with the velocity change during the sweeping. A brief test shows that the measured peak-to-peak pressure variation is 0.140Pa, 0.154Pa and 0.162Pa for the rotating speed of 3000, 3100 and 3200 rpm, respectively. One suspected drawback of using the miniature microphone is that, in principle, the fan noise and anti-sound can also be sensed leading to a feedback loop in the system. But this worry is unfounded since the near-field amplitude of the loudspeaker sound is found to be around 5×10^{-3} Pa only.

When the two signals in Figs 5.5(a) and 5.5(c) are compared in terms of BPF energy contents, the tachometer has 23% while the electret microphone has 83%. The large spectral clearance between the BPF and its non-BPF neighbours for the electret microphone means that no narrow bandpass filter is necessary to extract the BPF signal. In fact, a very wide band of 200-500 Hz is used in the current study to extract the BPF signal around 373 Hz. This way, the time delay caused by the filtering is minimal, and the effect of noise cancellation is expected to be much better than that based on the photoelectric tachometer.

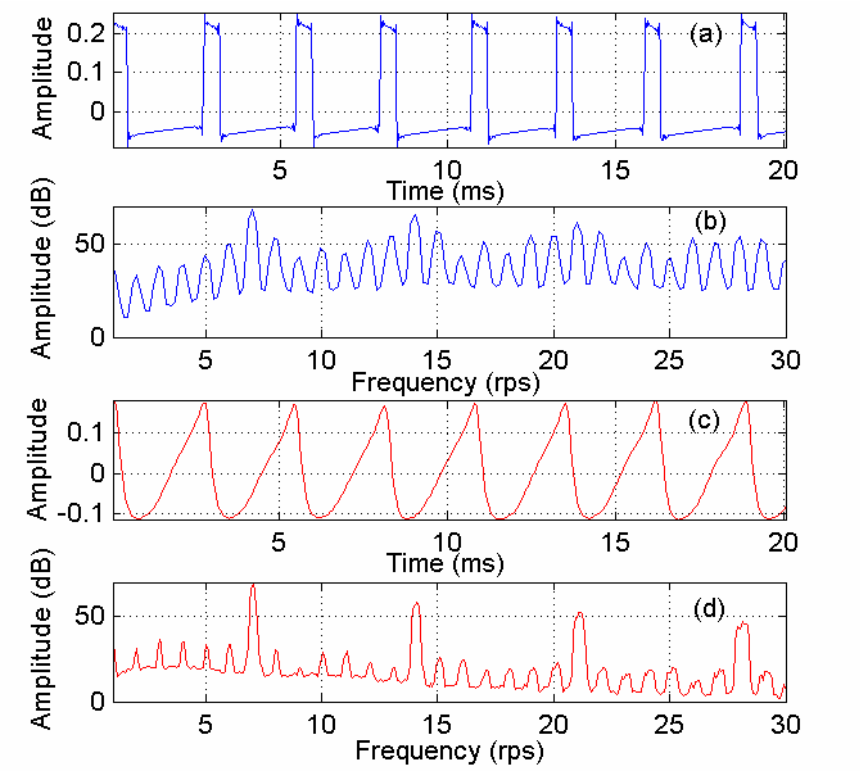

Figure 5.5 Signals from two rotation sensors. (a) is for the photoelectric tachometer and (b) is the spectrum of signal in (a). (c) is the signal from the miniature microphone and (d) its spectrum.

In addition to this crucial time-delay factor, the use of miniature microphone is also more economical and convenient. A much broad bandpass filter also allows simpler analogue construction in future applications.

The overriding consideration for the filter design is the time delay caused by the filter. A time delay here means that the signal of the rotation sensor at one time is used to construct anti-sound for the future. The random variation of the BPF amplitude with respect to the rotational cycle shown in Fig. 5.3 means that such delay should be minimized in order to achieve the best result. Since an Infinite-Impulse-Response (IIR) filter has much smaller time delay than a Finite-Impulse-Response (FIR) filter, the former is chosen. In making this choice, the factor of signal distortion by the IIR filter is not much a factor for the following reason. There is no reason to assume that the

time delay between the component of BPF in the rotation signal shown in Fig. 5.5(c) and the radiated sound is the same as that for the 2nd BPF component. In other words, the required time delays for the fundamental BPF (m=1) and is second harmonic (m=2) may well be different. In fact, due to the variation of rotational speed of the fan, the ideal anti-sound should maintain a fixed phase angle of 180^o with respect to the original noise at its varying BPF and higher harmonics. The varying phase relation between the sensor signal and the final anti-sound for various frequencies means a non-linear phase response might well be ideal. In this study, such non-linear phase response is not studied, nor is the non-constant amplitude response that might be beneficial.

In terms of the secondary source, a 4 in. loudspeaker is used, and its dipole directivity is confirmed by the measurement without fan. Normally, the cone of the loudspeaker is made by a low mass material for small inertia to produce a fast vibration response. Nevertheless, its response time was measured and compared with the 2.7 ms period for the BPF tone. The loudspeaker is driven by a sweep signal with frequency range 100Hz-1kHz over a 10 sec period. The time delay of the loudspeaker is found by the correlation between the driving signal and the measured sound. The correlation between the two data channels is shown in Fig. 5.6 as a function of the time delay (data samples with sampling frequency Fs=16 kHz). It is found that the correlation peaks at the delay of 28 to 29 samples depending on the frequency range of the sweeping signals used. When the time required for sound to travel from the loudspeaker to the microphone at 0.5 m away is deducted, the loudspeaker response time is found as 28.5/Fs-0.5/340=1.8ms-1.4ms=0.4ms. The delay is equivalent to about 0.4/2.7=0.148 times the BPF cycle.

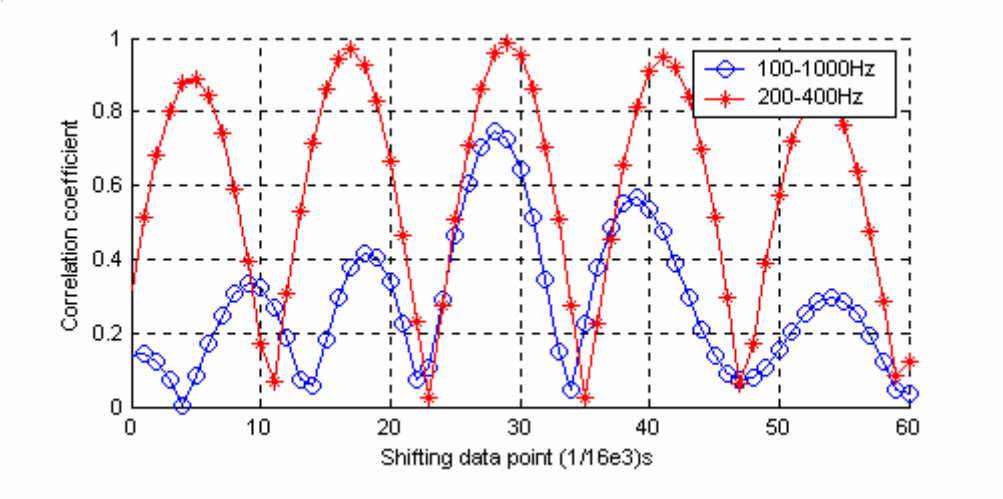

Figure 5.6 Normalized correlation as a function of time space index shifting of the signal between the sound and the microphone response.

As shown in Fig. 5.5(d), the sharp peak on BPF allows a wide passband to be used together with a wide transitional band. This allows a low-order filter to be constructed to achieve a flat response. For the fan operating at 3200 rpm, 373 Hz is the fundamental BPF, and 200Hz-550Hz is chosen as the passband with its centre at 375 Hz. The band of 600 Hz to 900 Hz is chosen for the 2BPF with its centre at 750 Hz. A six-order Chebyshev IIR filter is constructed by using the least p-norm optimal IIR filter design in Simulink of Matlab®, and the responses of the two filters are shown in Fig. 5.7. Based on these filters, a further gain and phase delay are required to construct the anti-sound, as shown in the lower part of Fig. 5.4. These are achieved by manual tuning for the two channels independently, although there is no reason why a formal procedure of system identification cannot be followed to achieve the goal of noise minimization.

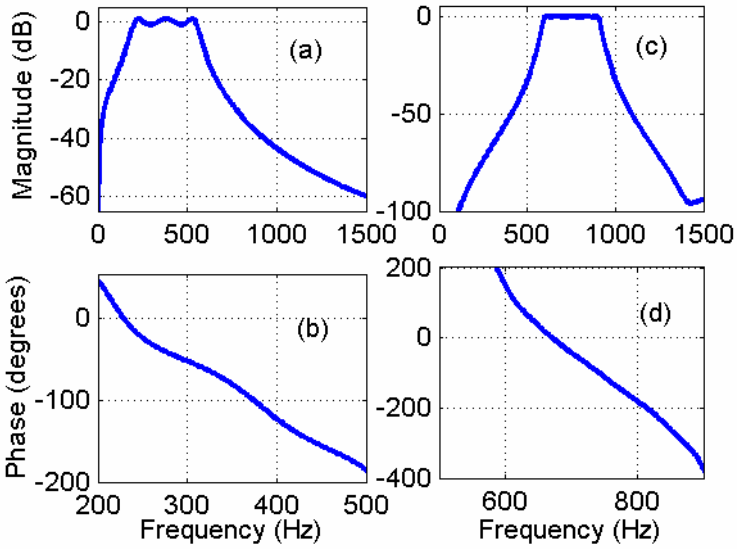

Figure 5.7 The responses of the two filter channels. (a) and (b) are the magnitude and phase response for the first BPF, respectively, (c) and (d) are for the second.

The phase delay of fundamental BPF shown by Fig. 5.7(b) is 99°. Together with the time delay of the loudspeaker of 0.4 ms, which means a phase angle of $0.4\times10^{-3}\times375\times360=54°$ at 375 Hz, a further phase delay of about 180-99-54=27^o is needed to construct the anti-sound. If the two input wires for the loudspeaker is swapped, a phase delay of about 180+27=207^o is needed. In fine tuning the time delay, the noise measured on the axis of α=0^o is used. A sampling period of 10 sec is used with synchronous averaging. First, a quick scan of phase shift within 0-360^o is used to locate the correct phase. This scan is followed by gain scan. Further scan around the initial finding is conducted and the results are shown in Fig. 5.8. Figure 5.8(a) shows the variation of the rms sound pressure at the survey microphone when the phase delay for two frequencies are tuned while the gain is fixed at 2 (open circles) and 3 (open squares), respectively. A clear trough is found at the phase delay of 200^o. When a phase delay of 200^o is chosen, the variation of controlled sound with respect to the gain is shown in Fig. 5.8(b). The finalized gain is 3 and the time delay of 1.5 ms equivalent to the phase delay of 200^o are chosen.

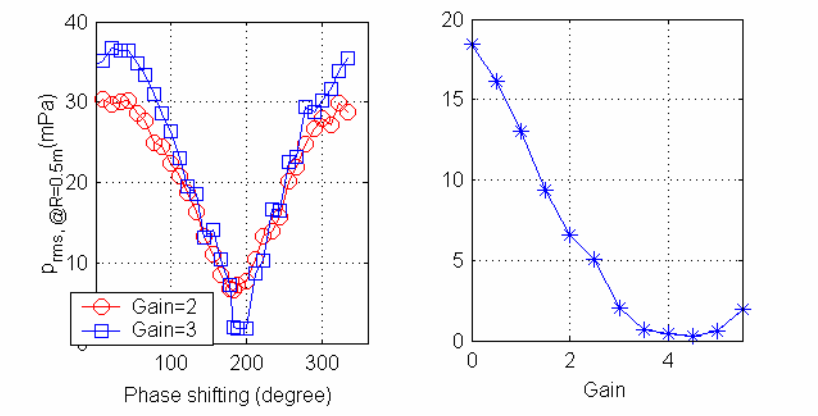

Figure 5.8 Performances of the IIR filters and parametric tuning

C. Results and error analysis

The loudspeaker is put underneath the fan to minimize its influence on the incoming flow stream. The dipole sound from the fan and that from the loudspeaker are coupled as an effective lateral quadrupole with a perpendicular separation distance of d=10 cm between the two parallel dipole axes. The ratio of the quadrupole sound power to the dipole sound power can be shown to be $(kd)^2/5$ (Dowling 1998), where $k=2\pi f/c_0$ is the wavenumber. For frequency f=373 Hz, the ratio turns out to be 0.096, which means a maximum reduction of sound power of -10lg(0.096)=10.2 dB. This is a serious limiting factor. Ideally, a ring of small loudspeakers should be placed around the fan circumference in order to create a better coincidence of the centres of the two noise sources. In practice, two or four loudspeakers might be adequate. Using simple numerical simulation of linear superposition of sounds from two anti-sound speakers placed at the top and bottom of the fan, which is itself modelled by seven point dipoles on a ring of radius 4.5 cm, it is found that the best cancellation is improved to become 24.1 dB, which is quite satisfactory. So, the issue of the relatively large fan-loudspeaker separation distance is temporarily set aside by the following heuristic

method. The parameters of the anti-sound is tuned only on the horizontal plane level with the fan centre, and the finalized result is also measured on the same plane. Incidentally, the idea of shaking the fan itself as a secondary source (Lauchle *et al* 1997) could also be effective in this case since the original sound is a simple axial dipole.

The spectra of synchronous sound measured with and without loudspeaker for α=0 are presented in Fig. 5.9. It is found that 18.5 dB noise reduction is achieved for the first BPF, and 13.0 dB for the second BPF. There is also a peak at approximately 3.5 BPF, for which there is virtually no change in sound pressure level. This peak might be radiated by motor vibration, and is beyond the scope of the current investigation. Acoustic directivity is also measured on the horizontal plane level with the centre of the fan, and the control on-off comparison of sound intensity is made in Fig. 5.10. Figure 5.10(a) compares the total synchronous sound pressure levels in decibels unit, with the total sound powers labelled on the horizontal axis. Figure 5.10(b) gives the

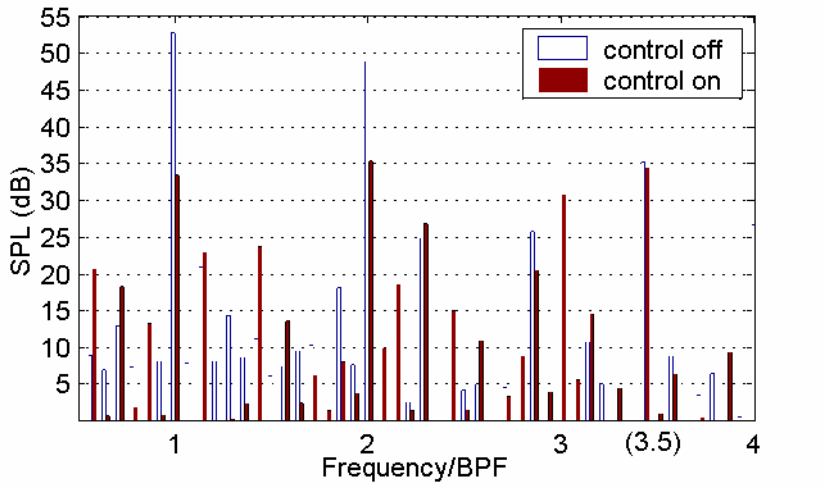

Figure 5.9 Sound pressure spectral at on-axis peak of dipole without (open bar) and with (filled bar) control. The frequencies for the two spectra are deliberately shifted apart a little for visual clarity.

details of the control-on directivity, which includes the overall noise, rotary noise and the random noise derived from, respectively, the original signal measured from the survey microphone, the synchronous average of the measured signal, and the power difference between the original and synchronous signals. Note that the rotary noise includes sound at frequencies other than the harmonics of BPF, such as 3.5 BPF shown in Fig. 5.9. The total reduction in the rotary noise power is 52.7-41.9=10.8 dB. The overall noise reduction is 53.4-46.3=7.1 dB while the random noise, about 50.0 dB, is essentially unchanged. Figures 5.10(c) and 5.10(d) show the sound intensity directivity of BPF and 2BPF noise for control-off and control-on, respectively. While the control-off pattern is clearly an axial dipole with some limited distortions, the control-on pattern is quite irregular and the scale for this figure is amplified for about 20 times when compared with Fig. 5.10(c). The irregular shape indicates that most harmonic noise that can be controlled by the simple scheme have already been suppressed successfully. The sound power reductions for the two frequencies are 14.8 dB and 9.8 dB, respectively.

The result of this simple control scheme is determined by many factors, and the main one has been recognized earlier as the random variation of sound radiation by the rotating fan, see Fig. 5.3.

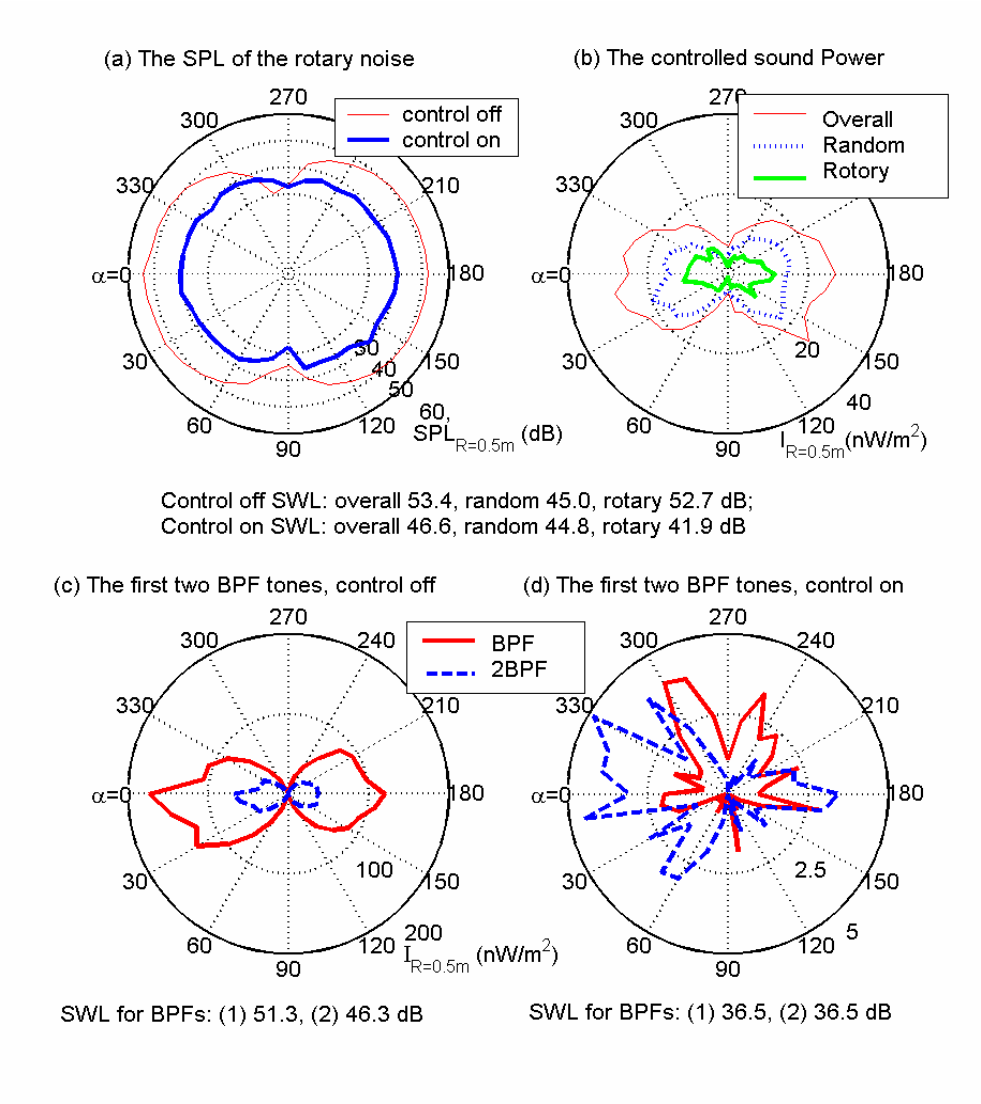

Figure 5.10 Sound power level ($P_{ref}=10^{-12}$ Watt) comparisons for with and without control. (a) Sound pressure comparisons with control of and on, (b) Sound Intensity directivity with control on, (c) the first two BPF tone without control on, and (d) the first two controlled BPF directivities.

The standard deviation of sound pressure amplitude is 15.9% while that for the rpm is 0.4%. If the radiated sound pressure grows with rpm by the 3rd power law, the variation in the sound pressure amplitude would have been only 3x0.4=1.2%. The difference between this prediction and the actual 5.6% change in the radiated sound amplitude means that the variation is rather independent of the rotational speed change. In fact, the correlation study between one-cycle p_{rms} and rpm^3 shows a peak correlation of only 20%. The deterministic error of using rotation signal from one

blade passage to control the noise radiated by the next blade passage is also analyzed in terms of the phase error due to the response characteristics of the filter shown in Fig. 5.7(b). The error of 0.4% BPF period means a frequency error of $0.4\times10^{-2}\times373=1.5$ Hz, or a phase response difference of $\delta\theta=1.5^{o}$ based on the phase response curve in Fig. 5.7(b). This phase angle error can only lead to an error of $\delta\theta$ in radian, which is 0.026 or a limit of noise reduction of -20lg(0.026)=31.7 dB, which is also unlikely to be a bottleneck of performance.

5.4 Conclusions

The reported scheme of destructive acoustic interference demonstrates that the sound locked with rotation from the typical computer cooling fan can be significantly attenuated by a simple design. More specifically, the following conclusions are drawn.

(1) The noise of the sample computer cooling fan is sufficiently deterministic to allow a meaningful implementation of the proposed scheme. For the dominant BPF sound, it is shown that the noise associated with the seemingly random variation of sound radiation with respect to the fan rotation is about 13.7 dB below that of the deterministic part. In other words, 95.7% of sound energy is deterministic, and the maximum expected noise reduction is 13.7 dB. The experimental rig deals with the first and second BPF frequencies, and the reduction in the total sound power for these frequencies are 14.8 dB and 9.8 dB, respectively, while the total synchronous sound is reduced by 10.8 dB. The reduction of sound power in the experiment for the BPF, 10.8 dB, is close enough to the limit of 13.7 dB forecasted for the deterministic acoustic interference.

(2) The cause of the random variation could have a complex origin in turbulent fluid dynamics, and the limitation imposed by this factor is much more stringent than those imposed by the known phase delay and amplitude mismatch problems associated with the inevitable variation of fan rpm from one cycle to the next. In fact, this variation is rather small since the total time delay involved in the current study is only about half of the blade passage, or 1/14 of the rotational cycle. A more stringent limitation appears to be the separation distance between the fan centre and the single loudspeaker, but this problem would be alleviated if two loudspeakers are used.

(3) If the rotation signal is provided by a traditional photoelectric tachometer, the pulse signal does not carry sufficient BPF content and it would limit the performance of the method. In this study, a miniature electret microphone is used to provide the unsteady pressure arising from the blade rotation just upstream of the rotor. The signal is found to be very rich in BPF content and is rather smooth. Spectral analysis shows that the peak at the BPF is well above the neighbouring rps harmonics. As a result, a broad passband can be used to extract the BPF signals to drive the loudspeaker. The time delay for the filter is thus minimized. Apart from this technical advantage, the miniature microphone is also relatively cheap and small to allow implementation of the technique in practice.

(4) The sample fan used in this study is a modified version of a typical computer cooling fan. In a typical fan, the number of struts differs from the number of rotor blades, $S \neq B$. It is pointed out in this study that this seemingly correct design avoids the worst coincident mode sound radiation by the unsteady flow thrust, but it's almost

impossible to avoid the equally efficient radiation of drag noise. Since drag noise originates from a rotating dipole with a changing dipole axis, the modification from the usual design with drag noise domination to the coincident design of $S=B$ with thrust noise domination carries the following important technical advantage: a simple loudspeaker can be used as the secondary source for the thrust noise but the same cannot be done easily for the drag noise. This advantage over-rides the disadvantage of having a higher base-line noise to deal with in $S=B$ design than $S\neq B$.

Chapter 6 Active control of drag noise component

In Chapter 5, a special design of a computer cooling fan eliminates all noises associated with the drag force component, and the resulting thrust noise pattern is a simple axial dipole. The antisound is constructed by one loudspeaker to achieve global noise abatement. A more usual design of a cooling fan, however, features more drag noise than thrust noise. Drag noise is essentially a rotating dipole and is more complex acoustically. This is the topic of active fan noise control in this chapter. The primary motivation is the pursuit of simplicity and global effectiveness of the technique so that it might be economical and realistic enough to be applied in practice.

The previous open-loop, feed-forward active control scheme is basically followed in this chapter, which is briefly summarized here. A miniature electret microphone flush mounted on the fan bellmouth picks up the unsteady aerodynamic pressure. The signal is filtered to keep the spectral content around the blade passing frequency, phase shifted, and amplified to drive a loudspeaker. A second signal path with time derivative operation drives another loudspeaker which radiates sound with a 90^{o} phase difference. The two loudspeakers are perpendicular to each other and form a rotating dipole, an antisound for the drag noise. In this study, two pairs are installed on the frame of a 120 mm computer cooling fan to achieve the source collocation with the fan centre. The result shows a 13.0 dB sound power reduction, and the limiting factor for the performance is found to be the random variation in sound radiation with a possible origin in the flow turbulence.

6.1 Introduction

As explained below, the sample fan used in the current study is one for which known structural improvements have already been made, and the dominant noise source is the drag component of the rotor-stator interaction. The timing of the interaction is determined by the relative position between a rotor blade and the stationary struts. In this sense, the unsteady lift force occurs mainly when a rotor blade passes by a strut. As a result, the location is fixed relative to the stationary struts. However, as one blade comes to interact with a set of struts in a fixed sequence, the unsteady lift repeats from the position of one strut to the next with a fixed time delay, forming a pattern which can also be considered to be an oscillating force rotating continuously in space. Whether the source is better described by such a rotating force or fixed force with a rotating phase relation is purely a mathematical choice. Physically, the latter description is easier to model. For a fan erected vertically with airflow drawn from the left to the right (x axis) of an observer, the drag component of each interaction site, usually near the tip of a blade span, can be further decomposed into two parts, one in the horizontal direction, F_y, and another in the vertical direction, F_z. A normal fan has a set of evenly spaced rotor blades and struts, the summation of F_y from all interaction sites can be simulated by a concentrated horizontal force located at the fan centre. Since one oscillating force radiates an acoustic dipole, the difference between the distributed interaction forces and the total force located at the fan centre represents two tightly coupled dipoles, or a quadrupole, which has a much smaller sound power and can be ignored in the current study. Likewise, the summation of F_z can be represented by a concentrated vertical force on the fan centre, and the result of all drag forces in all interaction sites can be represented by a pair of two forces at the fan

centre, which can also be represented by a radial force rotating around the centre. Using the same methodology of point source representation and correlation studies, Abom and Berglund (2003) measured and modelled the acoustic field from a small fan as a dipole source with three force components driven by the same action of the fan rotation. In the current context, they are the thrust (axial) and rotating drag (circumferential) forces.

The objective of this study is therefore to (a) examine experimentally how well the fan noise can be modelled by such a point source, and (b) explore how much global tonal noise suppression can be achieved through the superposition of the fan noise with an antisound mathematically equivalent to a rotating dipole. In Sec. 6.2, the acoustic characteristics of the sample fan is measured and analyzed thoroughly. The knowledge leads to a quiet design in which a rather pure drag noise represents the minimal noise from such fans. Section 6.3 describes the active control scheme, which consists of numerical simulations of what can be expected of such a simple control device, experimental configuration, experimental results and analysis.

6.2 Acoustic characters of the sample fan

The drag noise radiated by the leading mode $\nu = \pm 1$ is formulated by Eq. (5.2). The directivity of the drag noise is a distinct pattern of $\sin\alpha$. In a three-dimensional view, the drag noise is actually a rotating dipole. The leading mode of drag noise is the dominant source of the fan for which known structural improvements have already been made. The 10 dB noise reduction was found by these improvements and reported in Chapter 4. With such 10 dB noise reduction, the primary source is somewhat too

low for the purpose of demonstrating the active control technique, so a bigger fan with 120 mm in diameter, as shown in Figs 6.1(a) and 6.1(b), is used instead for the drag noise study.

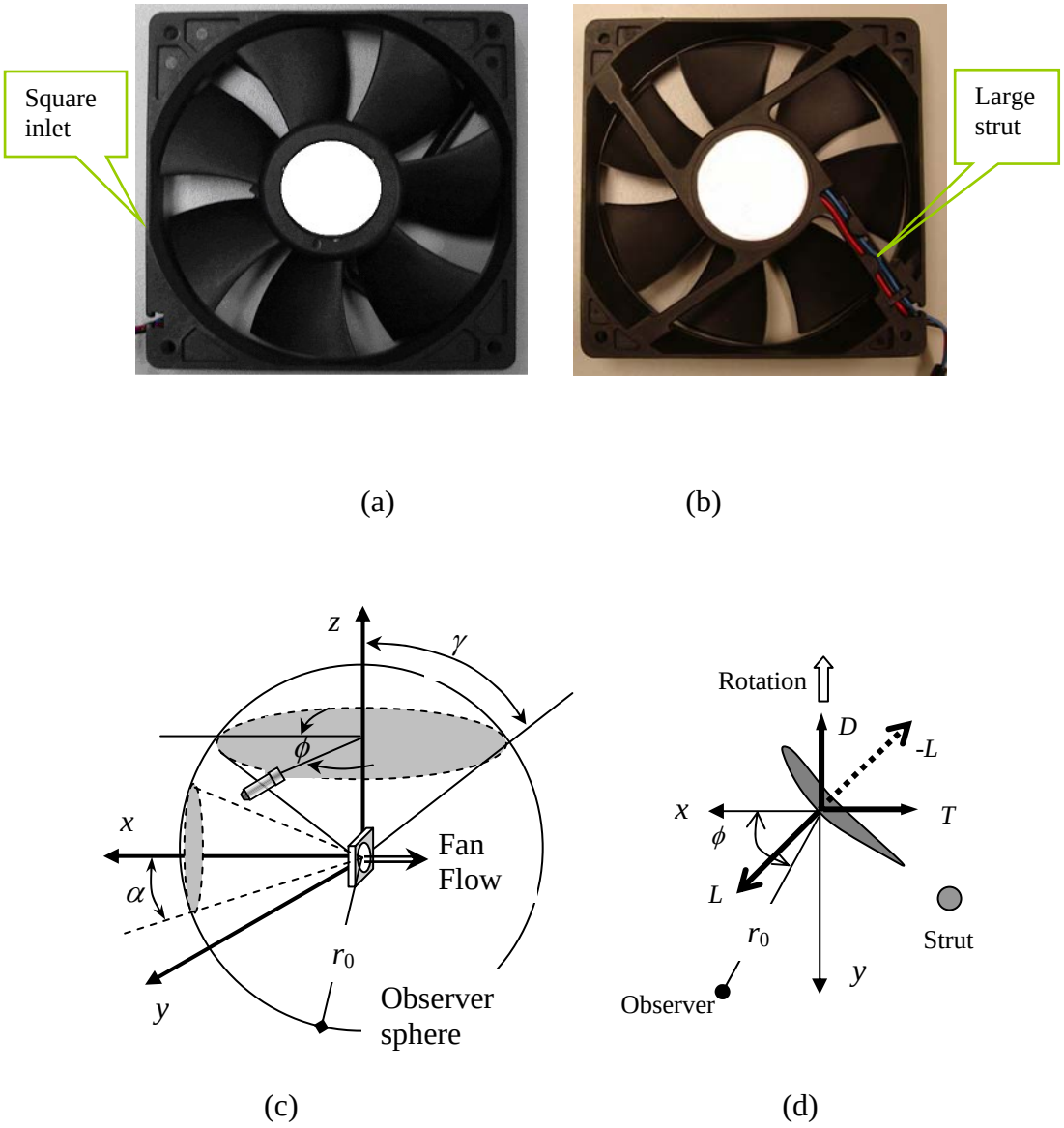

Figure 6.1 The sample cooling fan and geometrical definitions. (a) and (b) are the front and back views of a typical fan, respectively, (c) shows the definitions of two latitudinal angles, $\alpha,\gamma\in[0,\pi]$ and one longitudinal angle, $\phi\in[0,\pi]$, over a horizontal measurement plane in a 3D sphere of the observer, (d) is the cross sectional view of a blade and a strut, with the reaction of the unsteady lift force, -L, partitioned into thrust (T) and drag (D) components.

The design rotational speed is 3000 rpm. The noise radiated by the movement of the steady flow loading, i.e. Gutin noise, for such a small fan at such a low rotational speed is negligible. A typical noise spectrum, such as the one shown in Fig. 6.2(c), consists of a broadband superimposed by discrete tonal peaks at the multiples of the blade passing frequency, $f=m\times BPF$, $BPF=B\times rps$, where m is an integer, and rps is the fan rotational speed in revolutions per second or Hz. For this fan, the peak of the first BPF is more than 20 dB above the broadband floor, while the other harmonics are less distinctive. Two undesirable features are eliminated. The inlet flow distortion is smoothed by using a bellmouth. The effect of the extra size of the large strut shown in the Fig. 6.1(b) can be considered to be that of a single strut. The large strut is trimmed down to size, so that a set of four equal strut is formed.

The comparison of the noises from the original fan and the improved fan is shown in Fig. 6.2 by the sound intensity (I) directivities and sound pressure level spectra. Figure 6.2(a) shows the overall noise (outer dashed line), random noise (dash-dot line with a pattern almost parallel with the horizontal axis), rotary noise (thin solid line) and the BPF component of the rotary noise (thick solid line). The sound power levels (SWL ref 10^{-12}Watt) for the overall noise and the random noise are labeled at the lower margin of the plot while the values of SWL for other components are described below. The SWL is a result of integration of the sound intensity I according to Eq. (2.2).

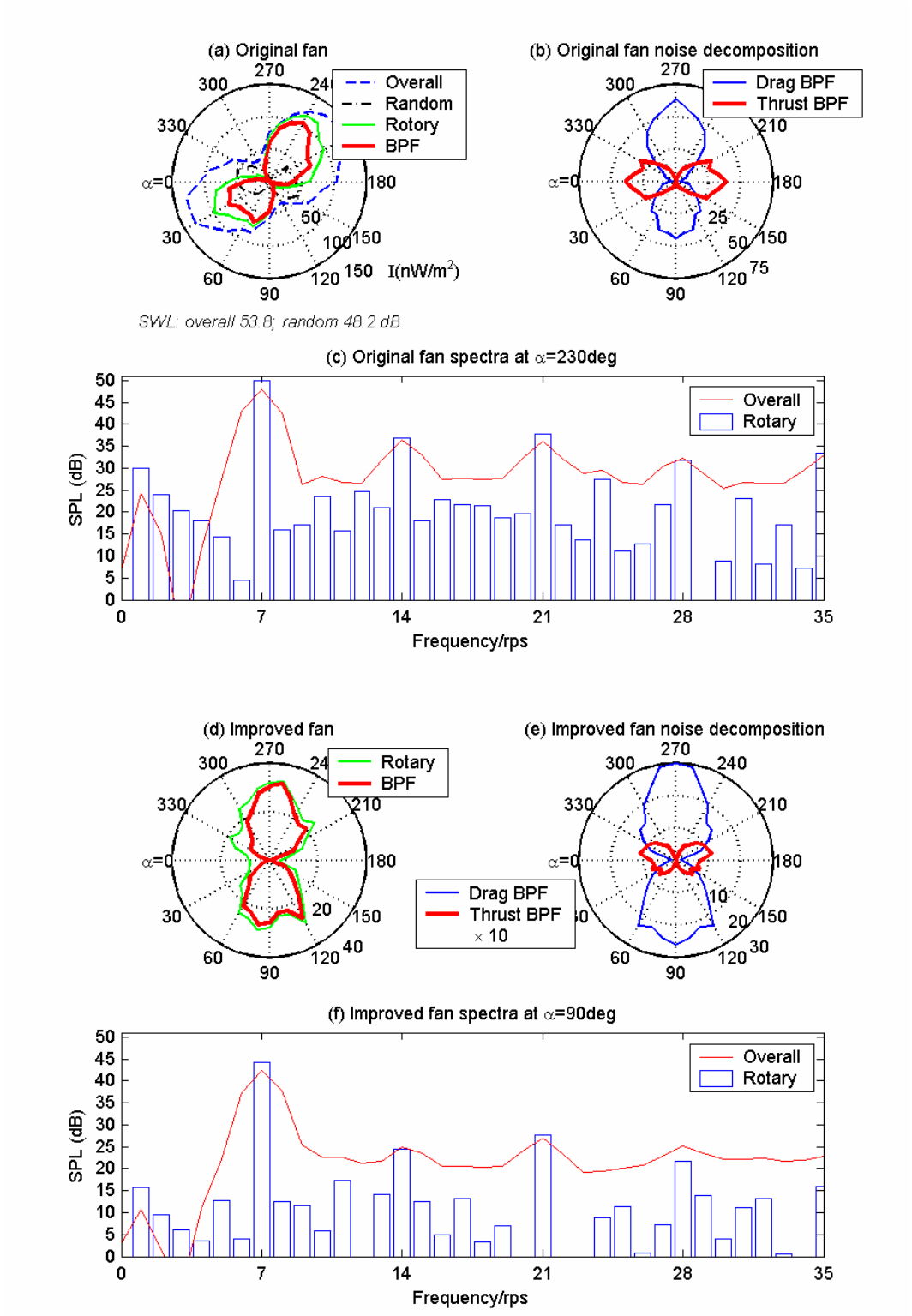

Figure 6.2 Comparison of the sound intensity directivity and spectra from the original and the improved fans. (a) Directivity of the original fan. (b) Separation of the rotary noise into drag and thrust components. (c) Typical spectra at α=230^o. (d), (e) and (f) are, respectively, the directivity, noise component separation and spectra for the improved fan.

As shown in Fig. 6.2(a), the major axis of the overall noise pattern is tilted along the direction of α=30^o, 210^o. This oblique distribution is a result of the interference between the drag noise, which spans out on the rotational plane, and the thrust noise, which beams along the rotational axis. The two components are separated in Fig. 6.2(b). The integrated power of the BPF component of the drag noise (thin line) is SWL=50.4 dB, only 4.8 dB higher than the thrust noise (thick line). As explained above, such a prominent contribution from the thrust noise is caused by the extra size of the strut carrying the wires, which acts like a single strut, S=1. For the spectral component of k=B, it gives the leading mode thrust noise radiation with ν=mB-kS=0. Meanwhile, the modes of k=B-1, B+1 also give the leading mode drag noise radiation with $\nu = \pm 1$. The typical sound pressure level (SPL ref 20 μPa) spectrum measured at the angle of α=230^o is shown in Fig. 6.2(c), which shows high peaks for the first few BPF harmonics.

When the square inlet frame is replaced by the full-circle bellmouth and the large strut is trimmed down to form a set of four equal struts, the only leading mode noise radiation comes from the drag component. The results for the BPF are shown in Figs 6.2(d) and 6.2(e). Since the random noise does not change much after the modifications, only the rotary noise is shown. Compared with the original fan, the total rotary noise is reduced from 52.44 dB to 48.52 dB, or by 3.92 dB. Notice that the reduction was about 10.0 dB for the 92 mm fan, for which the interaction of the rotor with the four struts was more dominant (Wong and Huang, 2003). For the current 120 mm fan, the thrust noise power at the BPF is reduced from 45.6 dB for the original fan to 32.2 dB for the improved fan, which is a more significant reduction than that of the overall rotary noise. As shown in Fig. 6.2(e), the improved fan has a drag noise of

SWL=47.76 dB at the BPF while that of the thrust noise is 15.56 dB below this level. As a result, the thrust noise can only be shown in the same plot after being amplified by 10 times. A typical SPL spectrum for α=90^o is shown in Fig. 6.2(f) for the improved fan. The first BPF peak is still about 20 dB above the broadband floor but, compared with the original fan, the improved fan is very quiet and is chosen to be the starting point for the proposed active noise control scheme.

6.3 Active control studies

As shown in (Huang, 2003), the configuration of B=7 blades with S=4 struts feature rotating dipoles for the fundamental BPF tone and the third harmonic, while the second harmonic (m=2) is in the higher spinning pressure mode with $v = 2$. The latter can be seen as a set of tightly coupled dipoles or an approximate quadrupole. The sound power levels for the three harmonics are experimentally found to be 47.83 dB, 30.33 dB and 33.75 dB, respectively. The 3BPF harmonic is indeed low and is not much of a concern here, while the third harmonic is higher than the second due to the leading mode radiation. However, its absolute level is also not very high and is left out of the control scheme. The control rig focuses on the BPF only. In what follows, numerical simulations for the effect of the destructive acoustic interference are described before details of the experimental rig are introduced.

A. Simulation of the destructive interference

Drag noise is radiated by an unsteady force rotating on the rotational plane, as shown in Fig. 6.1(c) with the Cartesian coordinates of y (horizontal) and z (vertical).

Theoretically, the so-called rotating force can be represented by two oscillating force components,

$$F_y = Ae^{i(\omega t+\pi/2)},\ F_z = Ae^{i\omega t}, \tag{6.1}$$

in which the *y*-component leads the *z*-component by 90^o as the fan rotates from the +*y* axis towards the +*z* axis. The sound radiated by each point force, say $F_z e^{i\omega t}$, can be simulated by the following formulas (Dowling, 1998),

$$\left.\begin{aligned} p &= \frac{ik\cos\gamma}{4\pi r_0}\left(1+\frac{1}{ikr_0}\right)F_z e^{i\omega(t-r_0/c_0)}, \\ u_r &= \frac{ik\cos\gamma}{4\pi\rho c_0 r_0}\left(1+\frac{2}{ikr_0}-\frac{2}{k^2r_0^2}\right)F_z e^{i\omega(t-r_0/c_0)}, \\ u_\gamma &= \frac{\sin\gamma}{4\pi\rho c_0 r_0^2}\left(1+\frac{1}{ikr_0}\right)F_z e^{i\omega(t-r_0/c_0)},\ u_\phi = 0. \end{aligned}\right\} \tag{6.2}$$

Here, the source is placed at the origin along the +*z* direction, the source-observer distance is r_0, and $k = \omega/c_0$ is the wave number. By changing the relative directions of the source and the observer, the sound radiated by the two coordinated forces given in Eq. (6.1) can be derived. The directivity of such a coupled dipole features a ring shape with the null axis in the third direction *x*, as shown in Fig. 6.3(a).

In the current control scheme, there is no feedback or error microphone. However, the phase relations between the fan rotation and the four loudspeakers have to be fixed prior to the operation of the control. Experimentally, this is achieved by using a survey microphone placed at a strategic point. A correct amplitude and phase is determined by driving the sound at this point down towards zero. In this sense, the location is analogous to that of an error microphone in a closed-loop control. The choice of such 'error microphone' position affects the final control results, and this can be simulated numerically prior to the actual experiment. The result is shown in

Fig. 6.3(b). The abscissa is the angular location for the 'error microphone' on the rotational plane ($\alpha=\pi/2$). Negative γ here means the positions in the $-y$ half of the rotational plane. Maximum sound power reduction, ΔSWL, is expected when the 'error microphone' is placed near the central plane, $\gamma = \pm\pi/2$, although there is another peak around γ=-30^o. The asymmetry of the ΔSWL curve with respect to γ=0 is caused by the near field effect since r_0=0.5 m is also used in this simulation. In the experiment, the point of x=0, y=r_0, z=0 is chosen as the error sensor position.

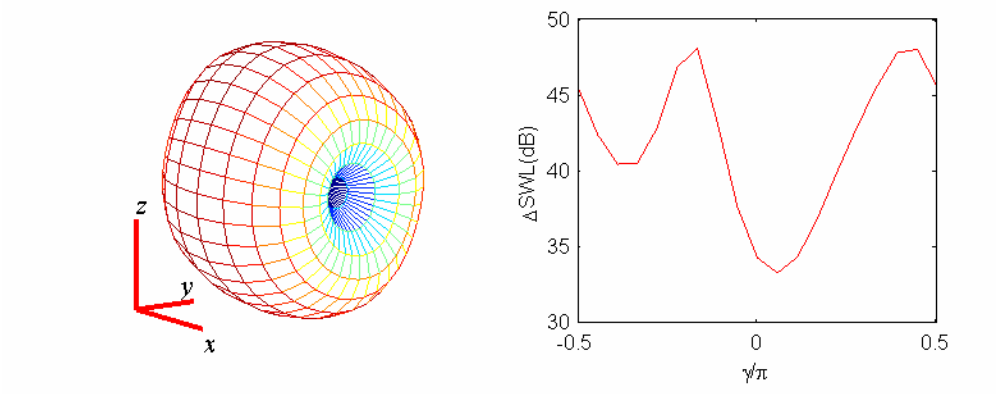

(a) (b)

Figure 6.3 Simulation of the rotating dipole and its destructive interference. (a) The sound field induced by four point dipoles on a fan. (b) The effect of the error microphone location on the control performance measured by the reduction of the sound power level.

B. Experimental set-up

A schematic of the experimental set-up is shown in Fig. 6.4(a). The schematic is divided into two blocks. The left-lower part is the control rig, while the upper-right shows the instrumentation for the purpose of measuring the sound power before and after the control is applied. In fact, the measurement instrumentation is somewhat redundant since the control rig has, in theory, most of the capacity to deal with the measurement. The extra instrumentation only serves to speed up the measurement process, and no signal from this part has any involvement in the control action.

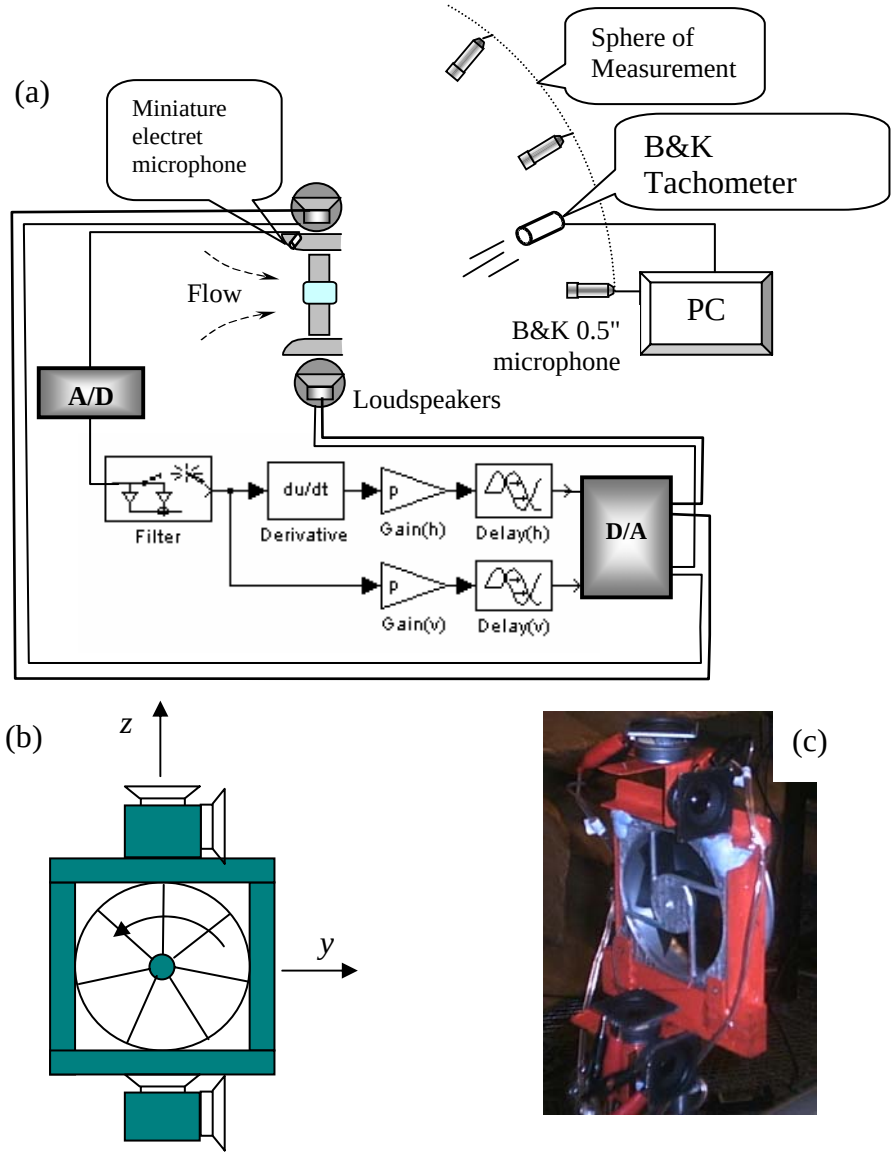

Figure 6.4 Experimental set-up. (a) Overall view of the control circuit and the measurement system. (b) The schematic of the arrangement for the two pairs of loudspeakers. (c) The photo of the fan back view with four loudspeakers installed.

In the measurement block, three ½" condenser microphones (B&K type 4187) provide simultaneous measurements for three horizontal cross sections of γ=30^o, 60^o, 90^o on the observer sphere of radius r_0=0.5 m. A photo-optic tachometer (B&K type M004) is used to provide a clock signal for synchronous averaging. A PC equipped with MATLAB® signal analysis software and an A/D card is also used. A sampling

frequency of 16 kHz is used, and the test is conducted in an anechoic chamber with a cut-off frequency of 80 Hz. The fan is installed on a tripod together with the tachometer, which are rotated at an angular interval of $\Delta\alpha = 10^{\circ}$.

The control part of the rig is an open-loop, feed-forward scheme consisting of three components. First, a non-acoustic reference from a miniature electret microphone located on the bellmouth of the fan provides the clock information of the rotating fan blades. Second, the signal is bandpass filtered to keep the components of the BPF tone. Third, the filtered signal is magnified and phase adjusted to drive the loudspeakers to generate the antisound for the drag noise. This study differs from the previous one (Chapter 5) in that the signal from the electret microphone is divided into two paths, one direct path, which drives the two horizontally oriented loudspeakers, and another with time derivative, which gives a $\pi/2$ phase delay to drive the two vertically oriented loudspeakers. Together they form a dipole rotating anti-clockwise, simulating the drag noise from the fan rotating in the same direction.

The control algorithm is built on a dSPACE (DS1103 PPC) controller, which is a real-time system with multiple A/D and D/A channels, and a Motorola PowerPC 604e microprocessor running at 333 MHz, which is connected to a personal computer through an ISA bus. The IIR filter and the differentiation block are constructed by the SIMULINK function in MATLAB® assembled in the host personal computer. A real time interface (RTI) is used to build the code downloaded to and executed on the dSPACE hardware. The rotation sensor signal is sampled at 10 kHz, and the output analogue signal is also constructed at an update rate of 10 kHz; both are deemed sufficient for the range of the frequencies encountered in the study for the

fundamental BPF tone. The two output channels have independent amplification and phase variables. These are found manually by driving the 'error microphone' signal shown in the measurement block to a minimum. Once the coefficients are found, they are not changed and no feedback signal is used.

Details of the miniature electret microphone (151 series supplied by Tibbet industry) and the IIR filter are described in Chapter 5. It senses the near field aerodynamic pressure on the bellmouth surface, and the signal is a saw-tooth-like waveform, whose spectrum is much richer in the BPF content than narrow pulses provided by a photoelectric tachometer, the difference being around 20 dB. The microphone has a flat frequency response of 0.018V/Pa from 300 Hz to 5 kHz. This sensitivity is very low compared with that used in the measurement microphones. In other words, the aerodynamic pressure oscillation sensed is much higher than the radiated sound, eliminating a possible feedback path in the control rig. For the filter design, the overriding consideration is the time delay caused by the filter calculation since the signal of the rotational sensor at one cycle is used to construct the antisound for the next cycle. Since the input signal is already very much concentrated around the BPF, the transition bands in the filter do not have to be very narrow, and a low-order filter can be used. A six-order Chebyshev infinite-impulse-response (IIR) filter is constructed by using the least p-norm optimal IIR filter design in MATLAB®'s SIMULINK package. The IIR filter is chosen since it has much smaller time delay than a finite-impulse-response (FIR) filter with equivalent bandpass performance.

In order to construct the antisound for the rotating drag noise, a pair of two loudspeakers are needed, one for F_y and one for F_z, as given in Eq. (6.1). Physically,

these two loudspeakers cannot be located at the centre of the cooling fan. They can only be located outside the casing of the fan, and the result would be two not-so-tightly-coupled dipoles with their centres away from the fan centre. In order to align the antisound with the fan noise source, two pairs are used, one above and one below the centre of the fan. The exact arrangement is sketched in Fig. 6.4(b), while a photo is given in Fig. 6.4(c) showing the back of the fan with the four loudspeakers each with two inches in diameter.

C. Results and analysis

The synchronously averaged sound is used to calculate the far-field approximation of the sound intensity, $I \approx p_{rms}^2/\rho_0 c_0$, where p_{rms} is the rms value of the BPF component of the synchronously averaged pressure oscillation. A total of 36 points are measured for each horizontal plane with an angular interval of $\Delta\phi = \Delta\alpha = 10^\circ$, and the data of three planes, $\gamma = 30^\circ, 60^\circ, 90^\circ$, are used to calculate the total sound power radiation by the fan by assuming a perfect symmetry of the upper (+z) and lower (-z) hemisphere,

$$W = 2\int_0^{\pi/2} r_0^2 \sin\gamma \left[\int_0^{2\pi} I(\gamma,\phi)\, d\phi \right] d\gamma \approx 2(\Delta\phi\Delta\gamma) r_0^2 \sum_{n=1}^{3} T_n \sin\gamma_n \sum_{m=1}^{36} I(\gamma_n, \phi_m), \quad (6.3)$$

where $T_n = 1, 1, 0.5$ for $\gamma_n = 30^\circ, 60^\circ, 90^\circ$ are the weighting coefficients for the numerical integration following the trapezoidal rule. Note that the plane of $\gamma = 0$ is reduced to one point on the top of the sphere with $\sin\gamma = 0$; it makes no contribution to the numerical summation and is left out. In order to plot the results in three dimensional view smoothly, the sound intensity is further interpolated from 3 to 9 horizontal mesh sections of $\gamma = 10^\circ, 20^\circ, \cdots, 90^\circ$, where γ=0 also provides one data point for interpolation. The comparison of the BPF drag noise for the conditions of

control-on and control-off is made in Fig. 6.5, where only one quadrant of the 3D directivity for sound pressure level is given. This figure confirms that the noise suppression for the rotating dipole is global in nature. However, it is noted that the noise is not reduced along the rotational axis where thrust noise peaks and the applied control has, theoretically, no effect.

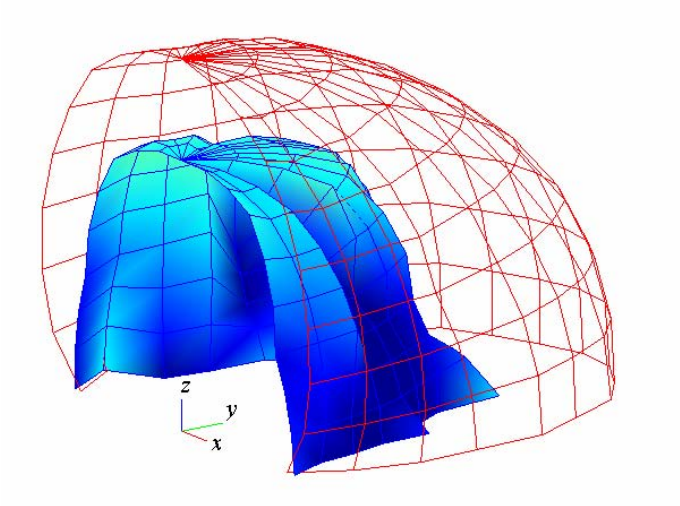

Figure 6.5 Comparison of the experimental data of the sound pressure level for the control off (outer wire-mesh) and control on (inner surface) configurations for one quarter of the observation sphere.

The numerical comparisons for the sound power levels for various components are given in Table 6.1. As shown in the first row of Table 6.1, the random noise hardly changes; in fact it increases by 0.23 dB. The focus is on the tonal noise, namely the rotary noise in the current context. Looking down the first column for the control-off state, it is found that the rotary noise is mainly dominated by the BPF component, which is in turn dominated by the drag noise. In fact, two decimal points are used here just to differentiate between the rotary noise and the drag noise. For the control-on state, the second column shows less dominance by the drag noise in the total rotary noise since drag noise is suppressed by the active control scheme. The direct objective

of the control is the BPF component of the drag noise, which is reduced by 12.99 dB, as shown in the last row of the table. The total rotary noise is decreased by 7.08 dB, which is much less impressive than the drag noise reduction since it contains all frequencies and all noise mechanisms. In terms of the rotary noise for the first BPF, it is reduced by 12.34 dB, which is very close to the 12.99 dB reduction for the drag noise.

Table 6.1. Changes in sound power levels (all in dB ref 10^{-12}W)

Sound Power Level	*Control off*	*Control on*	*Reduction*
Random noise	49.60	49.83	-0.23
Rotary total	48.52	41.44	7.08
Rotary BPF	47.83	35.48	12.34
Drag noise BPF	47.76	34.77	12.99

Figure 6.6 gives the spectral comparison between the configurations of control-on and control-off. The three sub-figures are for three rotational plane points ($\alpha = 90^\circ$) on the three measurement planes of $\gamma = 30^\circ, 60^\circ, 90^\circ$. The sound pressure level reductions for the BPF are, 10.7, 18.6, and 20.6 dB for the three positions, respectively. The amount of control-on sound power represents the level of uncontrollability for the fan noise with drag component dominating the source mechanisms. In what follows, three possible reasons are analyzed as to why not all BPF sound is cancelled.

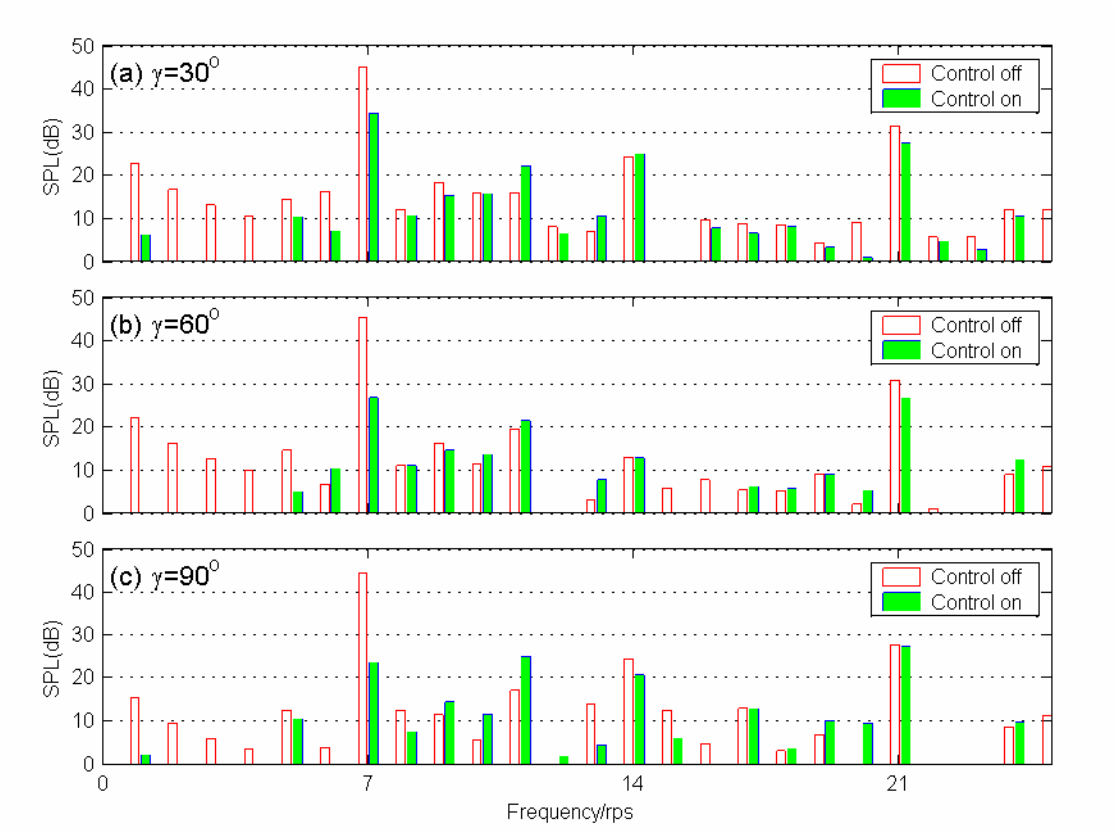

Figure 6.6 Spectral comparison for the control off (open bars) and control on (filled bars) for three points on the rotational plane ($\alpha=\pi/2$).

(1) Placement error for the secondary sources. Each loudspeaker has a certain size (2 inches in diameter in the current rig), and it is not possible to collocate two of them at one point to create an ideal rotating dipole. In addition, the installation of the four loudspeakers in the frame containing the fan is the source of axial asymmetry. When the actual positions are used by the simulation code, the optimal sound power reduction decreases from the 47.0 dB shown in Fig. 6.3(d) down to 27.0 dB. The comparison of these figures with the actual reduction of 12.99 dB means that this factor is important but not the limiting factor.

(2) Deterministic variation of sound radiation caused by the fan rotational speed. The standard deviation for the rpm is found to be 0.4%. If the radiated sound pressure

amplitude grows with rpm by the third power law based on the sixth power law for sound power for a typical dipole radiation, the variation in the sound pressure amplitude would have been only 3×0.4=1.2%. This difference is far less than the actual variation of sound radiation from one cycle to the next from the control-off fan, which is analyzed below. Similarly, the change in the phase angle mismatch between the fan noise and the anti-sound caused by the varying rpm is also found to be trivial, which is in agreement with the results of Chapter 5 on thrust noise control.

(3) Random variation of the fan noise radiation under constant rotational speed. Due to the turbulent nature of the aerodynamic source mechanisms, the radiation of sound from the fan can change from one cycle to the next even if the rotational speed of the fan is fixed. Since the antisound radiated for the present cycle is always based on the input from the previous cycle, the inevitable time delay in the control scheme causes incomplete cancellation of sound. In the present rig, the input signal is the aerodynamic pressure on the bellmouth surface, and this signal may also have incoherent variation with regard to the sound radiated to the far field. It is difficult to pinpoint exactly how much random variation there is in the whole system, but a rough estimate of the variation of the control-off sound radiation can serve as an indication as to whether this is a limiting factor for the active control performance. When the BPF component of the sound pressure amplitude is calculated for each cycle of index *j*, denoted as $p_{rms}(j)$, and the series is examined, a standard deviation is found. This local variation is then regarded as the amount of uncontrollable noise according to the method of Chapter 5. When the sound intensity due to this uncontrollable source is

integrated over the sphere using Eq. (6.3), a sound power of 36.4 dB is found. Comparing this value with the BPF sound powers for the control-on state shown in Table 6.1, it is found that the uncontrollable noise is close to both the drag noise (34.77 dB) and the total rotary noise (35.48 dB) at the BPF. The comparison with the rotary noise may make more sense since the local random variation contains both drag and thrust noise components.

6.4 Conclusions

The findings of this work are summarized before comparison is made with the thrust noise control in Chapter 5.

(1) A typical computer cooling fan available in the market is very noisy due to two gross features of the structural design. One is the square frame which distorts the inlet flow to form a four-lobe pattern. The other is the wire-carrying strut which is a powerful noise source for both drag and thrust components. When these two features are corrected, the rotary sound power is reduced by about 3.9 dB. The measurement of the noise radiated by the improved fan shows a very ideal rotating dipole pattern, with the BPF peak still standing about 20 dB above the broadband of the spectrum.

(2) A pair of two loudspeakers can be used to construct the rotating dipole when the two are perpendicular to each other with a 90^{o} phase difference. In the current study, two such pairs are used in order to collocate the secondary sources with the fan centre. The anti-sound approximates the primary fan noise very well, and a

power reduction of 12.99 dB for the drag noise is achieved at the blade passing frequency.

(3) Performance analysis shows that the variation of the fan rotational speed is not responsible for limiting the noise reduction to 12.99 dB. Nor is the imperfection involved in placing the loudspeakers around the fan. Since the antisound is constructed from the signal input from the previous cycle of the rotation, any random variation of sound radiation from a fan operating at a constant speed would cause such incomplete noise cancellation. Analysis of the randomness of sound radiation shows that the residual rotary noise is very close to the uncontrollable noise, for which the mechanism might be rooted in the turbulent nature of the aerodynamic process.

The present work adopts many common techniques used in the previous work on the thrust noise in Chapter 5, but there are also differences. The present work focuses on the rotating drag noise, while the previous one is on the thrust noise. In both cases, the global suppression of the dominant noise is achieved. The original fan is also modified in both cases before the active control is applied. In the case of the thrust noise control, a special coincident design of B=S=7 is used. That modification actually represents an increase of the noise radiation from the dominant source although the increase can be minimized if smaller strut size is adopted. In the present study, however, the modifications of the inlet bellmouth and the strut size equalization serve as a significant noise reduction from the original fan with the same number of struts. In other words, the current work begins with an already quiet design version of the most popular design configuration of B=7, S=4. In this sense, this study goes

much beyond the previous. However, a rotating antisound is more difficult to construct, and more loudspeakers are used in the current study than in the previous. For a general case where both drag and thrust noises are present at the leading radiation modes, perhaps at different frequencies for each component, a minimum of three loudspeakers would be needed to construct the antisound for the three force components.

Chapter 7 Conclusions

A range of theoretical and experimental studies are conducted for the acoustics of a typical computer cooling fan. During the studies, many interesting phenomena are found and understandings derived. The results are essential for the design of quite fans. The unsteady force induced by the aerodynamic interaction is identified as the dominant source of noise. Part of the interaction is phase locked with the fan rotation, and is the focus of this study. The interaction force can be decomposed into orthogonal components, and distinctive acoustic directivity exists for each component. The measurement of the directivity is used as the major tool to characterize the noise sources. The work carried out is a combination of theoretical modelling and experimental investigations. Following the identification and the separation of the source mechanisms, noise abatement is achieved by both passive control and active control means. The main conclusions and findings are summarized in three categories. They are (a) the studies of noise mechanisms with source separation, (b) noise abatements by structural re-design, and (c) active noise control.

7.1 Noise mechanisms

The computer cooling fan has small numbers of rotor blades, e.g. B=7, and downstream struts, e.g. S=4. For a typical fan taken from the market, two noticeable features are identified. One is the inlet bellmouth is distorted by four sharp intersections of the circular flow passage by the square outer frame. Another is the extra size of one strut carrying the electrical wires. Generally, the noise mechanism of can be categorized by the broadband noise and discrete noise. The later is phase

locked with the rotating blades, and can be picked out by the synchronous averaging with the rotational signal. The noise is thus denoted as the rotary noise. The difference between the overall noise and the rotary noise is defined as the broadband noise or random noise. Several conclusions are drawn for the study of source mechanisms.

(1) For the slow speed applications, the broadband noise of the small axial-flow fan is believed to be generated by three regions. (a) The random or organized but broadband pressure fluctuations on the blade and other surfaces caused by incident vortices. The inlet vortices are not entirely coordinated with the rotation, and the incoherent part tends to generate random noise. When the inlet distortion is corrected by a full circular bellmouth, the broadband noise is reduced together with the tone noise associated with the non-uniform inlet flow pattern. (b) The sharp trailing edge scattering of the convected waves within a turbulent boundary layer. No specific study is conducted for this particular component of noise source. (c) Vortex shedding from the downstream strut, as well as from the blades, depending on the flow conditions. This mechanism is not studied exclusively but differences of random noise from rigs with and without struts do provide the evidence of its contribution. In this study, the three broadband noise mechanisms are not separated, and preliminary data imply that they do have some interference despite the gross definition of random noise. Overall, the random noise does not change much in all modifications as the focus of our study is on the more annoying deterministic tones.

(2) The discrete tones are induced by the unsteady loading on blades and struts arising from two deterministic interactions: (a) between the rotor blades and struts, and (b)

between certain distorted inlet flow pattern and the rotor blades. For mechanism (a), interaction forces exerted on rotor blades are believed to be dominant over that on the struts as the rotor blades are so profiled to generate lift. This is contrary to the situation in multi-stage turbomachines where the downstream set of blades definitely experiences more interaction force. In the case of rotor-stator interaction in multi-stage turbomachines, the origin of the interaction can be categorized as being viscous, while in the present rotor-strut interaction, the force exerted on the upstream blades is derived from potential flow blockage. For mechanism (b), experiments reveal that it is more powerful than (a) in terms of the noise generated. However, this mechanism is not the focus of study since it can be avoided easily by using a full-circle bellmouth.

(3) Interaction noise is a result of many self-cancellations and the acoustic radiation efficiency is mainly determined by the kinematics determined by the number of rotor blades and the number of struts. The result of such interaction is characterized by the so-called index of spinning pressure modes ν. A configuration with $|\nu|=1$ leads to loud drag noise spreading over the whole rotational plane, while $\nu=0$ is a coincident condition which gives thrust noise beaming in the direction of the rotational axis. Both conditions are acoustically effective, and their overall effect can be described as a fixed dipole for the thrust force and a rotating dipole for the drag force. The higher mode number $|\nu|$ should be much quieter and its acoustic radiation is equivalent to a quadrupole. The traditional designs often create $|\nu|=1$ for the fundamental BPF, and it can be categorized as a noisy design. Due to the small numbers of blades, however, it is

not always possible to create a design with $|v|\geq 2$ for the BPF and many of its harmonics.

7.2 Passive noise abatement

Passive noise abatement for the sample fan is achieved through structural improvements which include the optimization of the strut number. Finally, a 12 dB noise reduction is obtained. Before this is achieved, two designs for the leading mode sound radiation are constructed to study the details of the interaction forces on blades. The two designs are (a) B=S=7 for the pure thrust noise, and (b) B=7, S=4 for the drag noise. In addition, a special case of S=1 is also studied as it contains the leading mode radiation of both thrust and drag noise. The understandings gained from these studies underpin the structural improvements for the sample fan, which are described as follows.

(1) The directivity measurements show that the original fan noise has an oblique axis. It is found to be the result of interference of the drag noise and thrust noise. The drag noise is induced by the interaction between 7 rotor blades with the 4 struts, which gives a mode of $v=mB-kS=-1$ for m=1 and k=2. The other source of the drag noise is the interaction between the rotor and the four-lobe pattern of the distorted inlet flow, which is equivalent to that of the four equal struts. For the original fan, the rotary sound power level induced by the inlet flow distortion is 4.9 dB higher than that of the four downstream struts. It is concluded that, for the sample fan, the inlet flow distortion is more powerful in generating tones than the

downstream struts. When the bellmouth is installed, the rotary noise reduction is about 5dB.

(2) The thrust noise for the fan with B=7 and S=4 is mainly from the extra size of a strut carrying electrical wires. Extra noise is radiated and it has features similar to the noise radiated by the rotor interacting with a single strut, S=1. The Fourier transform of the interaction force contains all frequency indices kS=k=1,2,3,… For k=mB, it gives the coincident configuration of ν=mB-kS=0, and it is the leading mode thrust noise beaming along the rotational axis. For k=mB±1, leading mode drag noise is formed as one of the two possible combinations of $D_{mB-1} \pm D_{mB+1}$, depending on the orientation of the large strut. When the large strut is in the vertical position, the two components are in phase for noise measured on the horizontal plane. When the large strut is in the horizontal position, the two components are anti-phase. The trimming of the large strut down to the size of other struts gives a noise reduction of 5 dB. Together with use of the bellmouth, the improved fan shows a total of 10 dB reduction in tonal noise.

(3) For the fundamental BPF tone (m=1), the design of four struts can be changed to five struts (S=5). This gives a mode of ν=mB-kS=2 for m=1,k=1, which is a higher-order radiation for both drag and thrust forces. Measurement shows that the BPF tone is reduced by 15.1 dB. However, the radiation mode for the second and third BPF feature ν=-1 for m=2,k=3, and ν=1 for m=3,k=4. Both have the leading mode drag noise. As a result, the total tonal noise reduction is only 2 dB when compared with design of S=4. This result highlights the difficulty of passive noise control for small axial flow fans with few blades and struts.

7.3 Active noise control

The noise abatement from the optimization of the structure shows a reduction of tonal noise by up to 12 dB. The leading mode radiation still exists in the improved fan. Active control is introduced as additional tool to deal with the residual leading mode noise radiation. To demonstrate how and whether this can be done, two rigs are constructed, one for the control of thrust noise and another drag noise. A simple open-loop feed-forward control scheme is used. The motivation of the study is to maximize the simplicity and global effectiveness of the technique so that it might become economic enough to be applied in practice. The results are summarized as follows.

(1) The active control rig consists of a miniature electret microphone used as a rotation sensor, ordinary loudspeakers, and a bandpass filter with the adjustable amplitude and phase delay. The use of the miniature electret microphone is novel in active control studies. If the rotation signal is provided by a traditional photoelectric tachometer, the signal is a train of pulses whose spectrum spreads over all harmonics of the rotational speed. The energy at the BPF is insufficient, and it requires a high-order filter to extra this energy from the neighbouring rps peaks. This would limit the performance of the method. A miniature electret microphone measures the unsteady pressure arising from the blade rotation just upstream of the rotor. The signal is found to be very rich in BPF content and is rather smooth. Spectral analysis shows that the peak at the BPF is well above the neighbouring rps harmonics. As a result, a broad passband can be used to extract the BPF signals to drive the secondary source. The time delay for the filter is thus minimized. Apart from this technical advantage, the miniature microphone is also relatively cheap and small to allow implementation of the technique in practice.

(2) For the thrust noise control rig, the sample fan used is a drastic modification of a typical computer cooling fan. In a typical fan, the number of struts differs from the number of rotor blades, $S \neq B$. The modification from the usual design with drag noise domination to the coincident design of $S=B$ with thrust noise domination carries the following important technical advantage: a simple loudspeaker can be used as the secondary source for the thrust noise. This simplified interference can be effectively suppressed by the proposed scheme, and the dominant first two BPF tones are reduced by 14.8 and 9.8 dB in the coincident design, respectively.

(3) The drag noise control is implemented on a larger fan with acoustic improvements already carried out to eliminate the inlet flow distortion and the unequal struts. The measurement shows a very distinct rotating dipole pattern with the BPF peak standing 20 dB above the broadband floor. A pair of two loudspeakers is used to construct the rotating dipole sound with a 90^{o} phase difference with each other. In the current study, two such pairs are used in order to collocate the secondary sources with the fan center. The anti-sound approximates the primary fan noise very well, and a reduction of 12.4 dB drag noise is achieved for the fundamental BPF. The second BPF is low for the rig of $B=7$, $S=4$ and there is no need to control this. The third BPF features the leading mode drag noise, but its absolute level is also found to be low.

(4) Analysis of the residual sounds for the two active control exercises shows that the limiting factor for the simple control scheme is likely to be the mismatch between the antisound constructed from the signal input from the past rotational cycle and

the actual sound radiated at the present cycle. Sound radiation from the fan varies from one cycle to the next even when it operates at a constant speed. The cause for the random variation could have a complex origin in turbulent fluid dynamics, and the limitation imposed by this factor is much more stringent than those imposed by the known phase delays and amplitude mismatch problems associated with the inevitable variation of fan rpm from one cycle to the next. In fact, the latter is rather small since the total time delay involved in the current study is only about half of the blade passage, or 1/14 of the rotational cycle. For the thrust noise control, one more stringent limitation appears to be the separation distance between the fan centre and the single loudspeaker, but this problem would be alleviated if two loudspeakers are used.

(5) For a general case where both drag and thrust noise are present at the leading modes, perhaps at different frequencies for each component, a minimum of three loudspeakers would be needed to construct the antisound for the three point dipoles.

References

Abom, M., and Berglund, P-O. (2003). “Dipole source data for small axial type fans,” Symposium on Fan Noise 2003, Senlis, France, 23-25 September.

Blake, W. K. (1986) ‘‘Mechanics of flow-induced sound and vibration,’’ Academic Press, Orlando.

Boltezar, M., Mesaric, M., and Kuhelj, A. (1998) ‘‘The influence of uneven blade spacing on the SPL and noise spectra radiated from radial fans,’’ J. Sound Vib. 216, 697-711.

Brookfield, J. M., and Waitz, I, A. (2000). “Trailing-edge blowing for reduction of turbomachinery fan noise,” J. Propulsion and Power. 16(1), 57-64.

Curle, N. (1955) ‘‘The influences of solid boundaries upon aerodynamic sound,’’ Proc. Roy. Soc. Lond. A231, 505-514.

Dowling, A. P. (1998). ‘‘Steady-state radiation from sources,’’ in Handbook of Acoustics, edited by Malcolm J. Crocker, (John Wiley & Sons), Chapt 8.

Envia, E. and Nallasamy, M. (1999) ‘‘Design selection and analysis of a swept and leaned stator concept,’’ J. Sound Vib. 228, 793-836.

Farassat, F. (1979) ‘‘The extension of Isom's formula to the acoustic near field,’’ J. Sound Vib. 67, 280-281.

Ffowcs Williams, J. E. and Hall, L. H. (1970) ‘‘Aerodynamic sound generation by turbulent flow in the vicinity of a scattering half-plane,’’ J. Fluid Mech. 40, 657-670.

Ffowcs Williams, J. E. & Hawkings, D. L. (1969) ‘‘Sound generation by turbulence and surfaces in arbitrary motion,’’ Phil. Trans. Roy. Soc. A264, 321-342.

Fitzgerald, J. M. and Lauchle, G. C. (1984) ‘‘Reduction of discrete frequency noise in small, subsonic axial-flow fans,’’ J. Acoust. Soc. Am. 76, 158-166.

Fukano, T., Takamatsu, Y., and Kodama, Y. (1986) ‘‘The effects of tip clearance on the noise of low pressure axial and mixed flow fans,’’ J. Sound Vib. 105, 291-308.

Gee, K. L., and Sommerfeldt, S. D. (2004). “Application of theoretical modeling to multichannel active control of cooling fan noise,” J. Acoust. Soc. Am. 115(1), 228-236.

Gerhold, C. H. (1997) ‘‘Active control of fan-generated tone noise,’’ AIAA J. 35, 17-22.

Gutin, L. (1936) ‘‘On the sound field of a rotating propeller,’’ NACA TM 1195 (Translated in 1948 from Zhurnal tekhnicheskoĭ fiziki 6, 899-909.

Howe, M. S. (1998) ‘‘Acoustics of Fluid-Structure Interactions,’’ Cambridge University Press.

Howe, M. S. (2003) ‘‘Theory of vortex sound,’’ Cambridge University Press.

Huang, L. (2003) ‘‘Rotor-strut interaction force in an axial flow fan,’’ Proc. Fan Noise Symp. CETIM Senlis.

Huang, L., (2003) ‘‘Characterizing computer cooling fan noise,’’ J. Acoust. Soc. Am 114(6), 3189-3199.

Kemp, N. H. and Sears, W. R. (1953) ‘‘Aerodynamic interference between moving blade rows,’’ J. Aeron. Sci. 20, 583-598.

Kemp, N. H. and Sears, W. R. (1955) ‘‘Unsteady forces due to viscous wakes in turbomachines,’’ J. Aeron. Sci. 22, 478-483.

Lauchle, G. C., MacGillivray, J. R., and Swanson, D. C. (1997) ‘‘Active control of axial-flow fan noise,’’ J. Acoust. Soc. Am. 101, 341-349.

Lewy, S. (1992) ‘‘Theoretical study of the acoustic benefit of an open rotor with uneven blade spacings,’’ J. Acoust. Soc. Am. 92, 2181-2185.

Lighthill, M. J. (1952) ‘‘On sound generated aerodynamically: I. General theory,’’ Proc. Roy. Soc. Lond. A211, 564-587.

Longhouse, R. E. (1978). “Vortex shedding noise of low tip speed, axial flow fan,” J. Sound Vib. 53, 25-46.

Longhouse, R. E. (1976) ‘‘Noise mechanism separation and design considerations for low tip-speed, axial-flow fans,’’ J. Sound Vib. 48, 461-474.

Lowson, M. V. (1965) ‘‘The sound field for singularities in motion,’’ Proc. Roy. Soc. Lond. A286, 559-572.

Lowson, M. V. (1970) ‘‘Theoretical analysis of compressor noise,’’ J. Acoust. Soc. Am. 47, 371-385.

Majumdar, S. J. and Peake, N. (1998) ‘‘Noise generation by the interaction between ingested turbulence and a rotating fan,’’ J. Fluid Mech. 359, 181-216.

Morfey, C. L. (1973) ‘‘Rotating blades and aerodynamic sound,’’ J. Sound Vib. 28, 587-617.

Nauhaus, L., Schulz, J., Neise, W, and Moser, M. (2003). “Active control of the aerodynamic performance and tonal noise of axial trubomachines,” Proc. Inst. Mech. Eng. Part A: J. Power and Energy 217, 375-383.

Quinlan, D. A. and Bent, P. H. (1998) ‘‘High frequency noise generation in small axial flow fans,’’ J. Sound Vib. 218, 177-204.

Quinlan, D. A. (1992) ‘‘Application of active control to axial flow fans,’’ Noise Control Eng. J. 39, 95-101.

Rao, N. M., Feng, J. E., Burdisso, R. A., and Ng, W. F. (2001). “Experimental demonstration of active flow control to reduce unsteady stator-rotor interaction,” AIAA J. 39, 458-464.

Sharland, I. J. (1964) ‘‘Sources of noise in axial flow fans,’’ J. Sound Vib. 1, 302-322

Simonich, J., Lavrich, P., Sofrin, T. and Topol, D. (1993), “Active aerodynamic control of wake-airfoil interaction noise –experiment,” AIAA J. 31, 1761-1768.

Thomas, R. H., Burdisso, R. A., Fuller, C. R., and O’Brien, W. F. (1993). “Preliminary experiments on active control of fan noise from a turbofan engine,” J. Sound Vib. 161(3), 532-537.

Thomas, R. H., Burdisso, R. A., Fuller, C. R., and O’Brien, W. F. (1994). “Active control of fan noise from a turbofan engine,” AIAA J. 32, 23-30.

Trunzo, R., Lakshminarayana, B. and Thompson, D. E. (1981) ‘‘Nature of inlet turbulence and strut flow disturbances and their effect on turbomachinery rotor noise,’’ J. Sound Vib. 76, 233-259.

Tyler, J. M. and Sofrin, T. G. (1962) ‘‘Axial flow compressor noise studies,’’ Soc. Auto. Eng. Trans. 70, 309-332.

Wang, J., Huang, L., and Cheng, L. (2005). “A study of active tonal noise control for a small axial flow fan,” J. Acoust. Soc. Am. 117(2), 734-743.

Wong, J. and Huang, L. (2003) ‘‘Identification and control of noise sources in a small axial-flow cooling fan,’’ Symp. Fan Noise 2003, Senlis, France, 23-25 September.

Wu, S. F., Su, S. G., and Shah, H. S. (1997). “Modeling of the noise spectra of axial flow fans in a free field,” J. Sound Vib. 200(4), 379-399.